IMPERIAL COLLEGE LONDON

TEMPO [(2,2,6,6-Tetramethylpiperidin-1-yl)oxyl]-Mediated Oxidation of Bacterial Cellulose Nanopaper

by

Yu Yang

A dissertation submitted in partial fulfilment of the requirements for the degree of

Doctor of Philosophy of Imperial College London

Department of Aeronautics

Imperial College London

London SW7 2AZ

March 2023

Statement of originality

I declare that this report and work presented hereafter are based on research carried out by the author at the Department of Aeronautics of Imperial College London. It is all the author's work except where otherwise acknowledged. No part of the present work has been submitted elsewhere for another degree or qualification.

Yu Yang

Copyright declaration

The copyright of this thesis rests with the author. Unless otherwise indicated, its contents are licensed under a Creative Commons Attribution – Non-Commercial 4.0 International Licence (CC BY-NC). Under this licence, you may copy and redistribute the material in any medium or format. You may also create and distribute modified versions of the work. This is on the condition that: you credit the author and do not use it, or any derivative works, for a commercial purpose. When reusing or sharing this work, ensure you make the licence terms clear to others by naming the licence and linking to the licence text. Where a work has been adapted, you should indicate that the work has been changed and describe those changes. Please seek permission from the copyright holder for uses of this work that are not included in this licence or permitted under UK Copyright Law.

Abstract

TEMPO [(2,2,6,6-tetramethylpiperidin-1-yl)oxyl] mediated oxidation of bacterial cellulose (BC) nanopaper has been explored. It was found that instead of forming a homogenous suspension of TEMPO-oxidised BC in water, the oxidation reaction produced robust and water stable TEMPO-oxidised BC (TOBC) hydrogels. This is discussed in detail in chapter 3 of this thesis, whereby a pristine BC pellicle was first press-dried into a dried and well-consolidated BC nanopaper, followed by TEMPO oxidation at various NaClO concentrations. The oxidation reaction introduced sodium carboxylate moieties onto the exposed segment of the BC nanofibrils within the nanopaper network structure. This then led to the swelling of the nanopaper into a hydrogel. A swelling ratio of up to 100 times the original thickness of BC nanopaper was observed upon TEMPO oxidation. Neat BC nanopaper, on the other hand, could not swell in water. The water retention value of the TOBC hydrogels was also found to increase with increasing carboxylate content. In chapter 4, this thesis reports that BC nanopaper heat-pressed from pristine BC pellicle at lower temperature is more susceptible towards TEMPO-mediated oxidation. The nanopaper swelling of up 120 times its original thickness when an NaClO concentration of 60 mmol g^{-1} and a heat-pressing temperature at 55°C was used. BC nanopaper heat-pressed from BC pellicle at 115°C achieved a swelling ratio of only 20 upon TEMPO-mediated oxidation at an NaClO concentration of 70 mmol g^{-1}. The strength of inter-fibril bonding of BC nanopaper was observed to increase with heat-pressing temperature. In chapter 5, self-standing TEMPO-oxidised nanocellulose films fabricated from TEMPO-oxidised BC hydrogel, as well as a homogenous suspension of BC-in-water were compared.

Content

Statement of originality **2**
Copyright declaration **3**
Abstract **4**
Acknowledgement **8**
List of Publications **9**
List of Figures **10**
List of Tables **15**
List of Abbreviations **16**
List of Symbols **19**
Chapter 1 - Introduction **21**
1.1 Background and motivation 21
1.2 Aim and objectives 23
1.3 Structure of this thesis 23
Chapter 2 - Literature review **25**
2.1 Cellulose 25
2.2 Bacterial cellulose 26
2.3 TEMPO-mediated oxidation of cellulose 27
2.4 TEMPO Oxidation of Bacterial Cellulose 35
2.5 Concluding remarks 66
Chapter 3 – TEMPO-mediated oxidation of bacterial cellulose nanopaper . 67
3.1 Introduction 67
3.2 Experimental 67
3.2.1 Materials 67
3.2.2 Preparation of BC nanopaper 68
3.2.3 TEMPO-mediated oxidation of BC nanopaper 68
3.2.4 Carboxylate content of TEMPO-oxidised BC hydrogels 69
3.2.5 Swelling Ratio (SR) and Water Retention Value (WRV) of TEMPO-oxidised BC hydrogels 70
3.2.6 Morphology of (TEMPO-oxidised) BC hydrogels 71
3.2.7 Crystallinity of (TEMPO-oxidised) BC. 72

3.2.8 Porosity of (TEMPO-oxidised) BC films. 72
3.2.9 Tensile Properties of (TEMPO-oxidised) BC films. 73
3.3 Results and discussion 74
3.3.1 The mechanism of hydrogel formation from BC nanopaper 74
3.3.2 Morphology of neat BC nanopaper and TEMPO-oxidised BC hydrogels .. 76
3.3.3 The carboxylate content of TEMPO-oxidised BC hydrogels 78
3.3.4 Swelling Ratio (SR) and Water Retention Value (WRV) of TEMPO-oxidised BC hydrogels 80
3.3.5 Crystallinity of (TEMPO-oxidised) BC 82
3.3.6 Is the TEMPO-mediated oxidation of BC nanopaper kinetically or diffusion limited? 83
3.3.7 Porosity of (TEMPO-oxidised) BC films 84
3.3.8 Tensile Properties of (TEMPO-oxidised) BC films 85
3.4 Conclusions 88
Chapter 4 – Susceptibility of BC nanopaper press-dried at different temperatures towards TEMPO-oxidation induced nanopaper swelling 89
4.1 Introduction 89
4.2 Experimental 90
4.2.1 Materials 90
4.2.2 Preparation of BC nanopaper 90
4.2.3 TEMPO-mediated oxidation of BC nanopaper 91
4.3 Characterisation of TOBC hydrogels produced from BC nanopaper heat-pressed at different temperatures 92
4.3.1 Carboxylate content of TOBC hydrogel 92
4.3.2 Swelling ratio of TOBC hydrogel 92
4.4 Characterisation of dried and well-consolidated BC nanopaper heat-pressed at different temperature 93
4.4.1 Determination of the residual moisture content of BC nanopaper 93
4.4.2 Specific surface area measurement of BC nanopaper 93
4.4.3 Porosity of the BC nanopaper heat-pressed at different temperature 94
4.4.4 Tensile properties of BC nanopaper heat-pressed at different temperatures 94
4.5 Results and discussion 95

4.5.1 Visual appearance of the TOBC hydrogels 95
4.5.2 Carboxylate content and swelling ratio of the TOBC hydrogels 97
4.5.3 Residual water content in the BC nanopaper 98
4.5.4 Influence of capillary force during the formation of BC nanopaper 100
4.5.5 Exposed surface area of BC nanopaper 101
4.5.6 Inter fibril bonding of BC nanopaper 105
4.6 Conclusions 109
Chapter 5 – Facile method to prepare self-standing TEMPO-oxidised nanocellulose films 110
5.1 Introduction 110
5.2 Experimental section 110
5.2.1 Materials 110
5.2.2 Preparation of neat BC nanopaper 111
5.2.3 TEMPO-mediated oxidation of BC nanopaper 111
5.2.4 Preparation of TOBC suspension 112
5.2.5 Preparation of TOBC film 113
5.3 Materials characterisation 113
5.3.1 Carboxylate content of TOBC and TOBCs 113
5.3.2 Porosity of (TEMPO-oxidised) BC films 114
5.3.3 Tensile Properties of (TEMPO-oxidised) BC films 115
5.3.4 Film Transmittance 115
5.3.5 Morphology of self-standing TOBC films 115
5.4 Results and discussion 116
5.4.1 Carboxylate content, internal morphology and porosity of TOBC films 118
5.4.2 Tensile properties of (PVA-doped) TOBC films. 119
5.4.3 Transmittance of (PVA-doped) TOBC films 122
5.5 Conclusions 126
Chapter 6 – Conclusions and future work 127
References 130

Acknowledgement

I am here to thank many people I have encountered during my PhD journey.

First and foremost, I to my supervisor, Dr. Koon-Yang Lee, for his tremendous support and tireless supervision. His scholarly advice, meticulous scrutiny, and rigorously scientific approach have inspired me greatly.

To the staff at the Department of Aeronautics that ensured my work went smoothly, mainly to Joseph Meggyesi and Keith Wolstenholme from DFF to Frank Gommer, Jon Cole, and Gary Senior from the Composite Suite, who provided great technical assistance, and to Clodagh Li and Ela Sapinsky, who offered great administrative support.

To past members of the *Future Materials Group*: Andre, Wenzhe, Diyang, and Alba, and to current members who are still battling in the field – Daniela, Grace, Joanne, Meredith, Yifang, Amy, and Dharu, who give me great help in my first year and during the covid-19 period. I appreciate your friendship over the years. I will cherish the good times, meals, and great conversations we had together. I wish you all the very best!

Most importantly, to my source of love and happiness: Mum, Dad, and my elder sister for their love, belief, and never-ending support, without which I could never have begun this journey.

List of Publications

Peer-reviewed journal papers

1. **K.Y. Yang**, D. Wloch, K.-Y. Lee, TEMPO-oxidised nanocellulose hydrogels and self-standing films derived from bacterial cellulose nanopaper, RSC Advances 11(45) (2021) 28352-28360.

2. **K.Y. Yang**, J. Li, K.-Y. Lee, Peculiar behaviour of TEMPO-mediated oxidation of bacterial cellulose nanopaper heat-pressed from pristine pellicle at different temperatures. *Submitted for peer-review publication at the time of the submission of this thesis.*

Conference presentations

1. **K.Y. Yang,** TEMPO-oxidised nanocellulose hydrogels and self-standing films derived from bacterial cellulose nanopaper. ACS Spring 2022 National Meeting.

2. **K.Y. Yang** & K.-Y. Lee, TEMPO-oxidised nanocellulose hydrogels and self-standing films derived from bacterial cellulose nanopaper. The 7th International Polysaccharide Conference of the European Polysaccharide Network of Excellence (EPNOE), 2021.

List of Figures

Figure 2-1: A BC pellicle 26

Figure 2-2: Scanning electron micrographs showing the fibrous network of cellulose in the BC [31] 27

Figure 2-3: Regioselective oxidation of C6 primary hydroxyls of cellulose to C6 carboxylate groups by TEMPO/NaBr/NaClO oxidation in water at pH 10–11 [1]. 29

Figure 2-4: A graph showing the carboxylate/aldehyde content and degree of polymerization about the amount of NaClO of the oxidised pulps in a TEMPO/NaBr/NaClO oxidation of bleached softwood kraft pulp at pH 10 and at room temperature [1] 31

Figure 2-5: TEM images (a–c) of a dried TEMPO-oxidised hardwood cellulose dispersion. The carboxylate and aldehyde contents of 0.8 and 0.0 mmol g^{-1}, respectively, are observed *via* the diffraction-contrast method in the bright-field mode using a low-dose exposure. (d) and (e) show a typical dispersion observed between cross polarizers [47]. 33

Figure 2-6: TEM images of dried TEMPO-oxidised hardwood cellulose dispersions with carboxylate contents of 1.0 and 1.5 mmol g^{-1}. The carboxylate contents are observed by negative staining with uranyl acetate. The insets show the corresponding aqueous dispersion [3]. 34

Figure 2-7: ATR-FTIR spectra of (a) BC, Periodate oxidised BC (POBC), TOBC and the (b) enlarged region of 3000 – 2800 cm^{-1} where typical peaks of acetal were observed [49] 36

Figure 2-8: XRD patterns of (a) BC, (b) POBC, and (c) TOBC [49]. 38

Figure 2-9: Photographs of (a) BC, (d) TOBC and (g) POBC, SEM images of (b) BC, (e) TOBC and (h) POBC, and fiber diameter distribution of (c) BC, (f) TOBC and (i) POBC (scale bar: 5 μm) [49]. 39

Figure 2-10: Neutralization of the sodium hypochlorite using ascorbic acid [19]. 40

Figure 2-11: SEM images of (a) pure BC, (b) C-TOCNs and (c) O-TOCNs. The scale bar for all three images corresponds to 500 nm [19]. 42

Figure 2-12: FTIR spectra of (a) pure BC, (b) C-TOCNs and (c) O-TOCNs [19]. 42

Figure 2-13: XRD patterns of (a) pure BC, (b) C-TOCNs and (c) O-TOCNs [19]. 43

Figure 2-14: (a) Changes in the contact angle of various concentrations of TOCNs in o/w emulsion over time and (b) images demonstrating the results of the washing experiments conducted to remove the carbon black from the surface [19]. 43

Figure 2-15：Photographs of the liquids for preparation of the films in the study performed by Wu *et al*. (a) turbidities of the 0.1% w/v BCF suspension and 0.1% w/v TOBCN2 dispersion; (b) images of the 0.1% w/v liquids with parallel or cross polarizers, demonstrating the birefringence properties of the material; note that all the liquids had the same cellulose weight content; (c) The maintenance times of birefringence of TOCN dispersion prepared from wood cellulose (top, 0—4 seconds) and TOBCN2 dispersion (bottom, 0—20 seconds) [21]..... 48

Figure 2-16：Photographs of the HDBCP (a), BCF (b), TOBCN1 (c) and TOBCN2 (d) films. e Light transmittances of the films from 300 to 800 nm in wavelength [21]. 49

Figure 2-17: Effects of carboxylate content of TOBCs on (a) the zeta potential and charge density of TOBC dispersions, and (b) zeta potential, charge density and (emulsion stability index) ESI of the corresponding TOBC emulsions (The fibril dosage was 0.35 wt.% and ratio of water to oil was 1:1) [50]. 51

Figure 2-18: Relationships between the ESI and fibril dosage-emulsifier ratio for BC (a) and 2-TOBC (b). The inset photographs show the appearance of the samples after being left to stand for 30 days with different fibril dosages (from left to right, 0.18, 0.35, and 0.70 wt.%). The volume ratio of water phase and oil phase was 1:1. The fibril dosage was indicated by the weight percentage ratio of the water phase [50]. 52

Figure 2-19: Droplet diameters of emulsions stabilized by 2-TOBC with different fibril dosages and storage time (The ratio of oil and water was 1:1) [50]. 54

Figure 2-20: Percent weight loss of BC/CTS scaffolds 6 weeks after incubation in ysozyme solution as a function of MFC content (scaffolds are prepared at −30 °C) [20]. 58

Figure 2-21: Specific capacitance and CV curves of TOBC-IL-G actuators according to scan rate: (a) 50 mV s^{-1}, (b) 100 mV s^{-1}, and (c) 200 mV s^{-1}; (d) current–voltage curves of TOBC-IL-G composite actuator at various scan rates [52]. 63

Figure 3-1：(a) BC pellicle containing *ca*. 99 wt.-% water; the press-drying of a BC pellicle produces (b) a dried and well-consolidated BC nanopaper. (c) BC nanopaper after immersion in water at room temperature for two weeks, showing that a BC nanopaper cannot be rehydrated to its original pellicle form. (d—f) The visual appearance of TEMPO-oxidised BC hydrogels produced from oxidation of BC nanopaper using (d) 10 mmol g^{-1} of NaClO, (e) 20 mmol g^{-1} of NaClO and (f) 30 mmol g^{-1} of NaClO, respectively. (g) A homogenous suspension of BC-in-water, followed by vacuum filtration and press-drying to produce BC nanopaper. (h) The outcome of TEMPO-mediated oxidation of BC nanopaper produced from a disintegrated BC pellicle using an NaClO concentration of 10 mmol g^{-1}..... 75

Figure 3-2: SEM micrographs of (a) a neat BC nanopaper, and (b—d) TEMPO-oxidised BC hydrogels modified with (b) 10 mmol g^{-1}, (c) 20 mmol g^{-1} and (d) 30 mmol g^{-1} of NaClO, as well as (e) a neat BC pellicle. Scale bar = 4 μm..... 78

Figure 3-3: Carboxylate content of the TEMPO-oxidised BC hydrogels..... 80

Figure 3-4: (a) swelling ratio, (b) water retention value of the TEMPO-oxidised BC hydrogels. 81

Figure 3-5: X-ray diffraction patterns of the (TEMPO-oxidised) BC. 82

Figure 3-6: Carboxylate content of the TEMPO-oxidised BC hydrogels as a function of reaction time. 84

Figure 3-7: Representative tensile stress-strain curves of the various (TEMPO-oxidised) BC films. 85

Figure 4-1 (a) BC pellicle, with a water content of 99 wt.-%, was heat-pressed at 55 ℃, 85 ℃ or 115 ℃ to produce (b) dried and well-consolidated BC nanopaper. (c) Exemplary BC nanopaper immersed in water for more than 2 weeks, indicating the stability of the BC nanofibril network in the nanopaper. The visual appearance of (d) the TOBC hydrogels produced from the oxidation of BC nanopaper heat-pressed at different temperature using 10 mmol, 30 mmol, 50 mmol and 70 mmol of NaClO per g of dry BC. 96

Figure 4-2 (a) Carboxylate content and (b) swelling ratio of the TOBC hydrogels made from BC pellicle heat-pressed at different temperature. 98

Figure 4-3 Thermal gravimetric measurement of BC nanopaper heat-pressed at different temperature. 99

Figure 4-4 N_2 adsorption-desorption isotherms of (a) BC-55, (b) BC-85 and (c) BC-115 nanopaper. 102

Figure 4-5 (a) $QPo - P$ vs P/Po and (b) BET plots of BC nanopaper heat-pressed at different temperature. The dashed lines correspond to the linear fit of the data within the BET range of $0.05 \leq P/Po \leq 0.35$ as validated from the $QPo - P$ vs P/Po plot. 103

Figure 4-6: Representative tensile stress-strain curves of BC nanopapers heat-pressed at different temperature. 105

Figure 4-7: (a) Tensile modulus, (b) tensile strength and (c) tensile strain-at-failure of BC nanopapers heat-pressed at different temperature. 106

Figure 5-1 (a) BC pellicle containing ca. 99 wt% water; (b) a dried and well-consolidated BC nanopaper; (c) The visual appearance of TEMPO-oxidised BC hydrogels produced from the oxidation of the BC nanopaper; (d) BC slurry made by blending the BC nanopaper; (e) TEMPO-oxidised BC hydrogels produced from the oxidation of the BC slurry; (f) TOBC film from TOBC hydrogel; (g) PVA-doped TOBC film from TOBC hydrogel; (h); TOBC film from TOBC suspension (i) PVA-doped TOBC film from TOBC suspension. 117

Figure 5-2 SEM micrographs of (a) PVA-doped TOBC film from TOBC hydrogel; (b)PVA-doped TOBC film from TOBC suspension. Scale bar = 10 μm. 119

Figure 5-3: Representative tensile stress-strain curves of neat BC, TOBC film from TOBC hydrogel, PVA-doped TOBC film from TOBC hydrogel, and PVA-doped TOBC film from TOBC suspension. 121

Figure 5-5: The visual appearance of (a) BC nanopaper; (b) TOBC film from TOBC hydrogel; (c) TOBC film from TOBC suspension; (d) PVA-doped TOBC film from TOBC hydrogel; (e) PVA-doped TOBC film from TOBC suspension. 124

Figure 5-6: (a) transmittance and (b) haze of the BC nanopaper; TOBC film from TOBC hydrogel; PVA-doped TOBC film from TOBC hydrogel and PVA-doped TOBC film from TOBC suspension as a function of wavelength. 125

List of Tables

Table 2-1: Summary of the material properties of the films prepared. [a]: The data were shown by mean ± standard deviation; [b]: No data [21]. 47

Table 2-2: Static contact angles and sizes of BC and TOBC samples [50]. 52

Table 2-3: Porosity of the BC/CTS scaffolds [20]. 60

Table 2-4: Electrochemomechanical properties of TOBC-G-IL composite membranes [52]. 64

Table 3-1: Tensile properties of the various (TEMPO-oxidised) BC films. ρA, P, E, σ, ε and UT denote the absolute density, porosity, Young's modulus, tensile strength, strain-at-failure and work of fracture of the films, respectively. 86

Table 4-1 Residual moisture content (Mc), BET surface area (As) and porosity (P) of BC nanopaper heat-pressed at different temperature. 104

Table 4-2: Normalised tensile properties of the BC nanopaper press-dried at different temperatures. The tensile modulus was normlaised against $(\rho B/\rho A)2$ and the tensile yield strength (σY) was normalised against $(\rho B/\rho A)1.5$. 107

Table 5-1 Carboxylate content of the various (TEMPO-oxidised) BC films. ρA and P denote the absolute density and porosity respectively. 118

Table 5-2: Tensile properties and transmittance of the various (TEMPO-oxidised) BC films. E, σ, ε and T denote the Young's modulus, tensile strength, strain-at-failure and transmittance of the films, respectively. 120

List of Abbreviations

TEMPO	(2,2,6,6-tetramethylpiperidin-1-yl)oxyl
NaBr	Sodium bromide
NaClO	Sodium hypochlorite
TOCNs	TEMPO-oxidised cellulose nanofibrils
BC	Bacterial cellulose
TOBC	TEMPO-oxidised bacterial cellulose
TOCN	TEMPO-oxidised cellulose nanofiber
TOBCs	TEMPO-oxidised bacterial cellulose slurry
PVA	Polyvinyl alcohol
pH	Acidity
NaOH	Sodium hydroxide
TEM	Transmission electron microscope
FTIR	Fourier transform infrared spectroscopy,
XRD	X-ray diffraction
SEM	Scanning electron microscope
ATR	Attenuated total reflection
PBS	Phosphate buffer saline
POBC	Periodate oxidised BC
BCNFs	Bacterial cellulose nanofibers
DPD	N/N-diethyl-p-phenylenediamine
O-TOCNs	TEMPO-oxidised cellulose nanofiber produced using the one-pot method

C-TOCNs	TEMPO-oxidised cellulose nanofiber produced using the conventional method
BCF	Bacterial cellulose fibers
TOBCNs	TEMPO-oxidised BC nanofibers
CSL-Fru	Corn steep liquor-fructose
H_2PO_4	Dihydrogen phosphate
$MgSO_4 \cdot 7H_2O$	Magnesium sulfate heptahydrate
$(NH_4)_2SO_4$	Ammonium sulfate
$FeSO_4 \cdot 7H_2O$	Iron (II) sulfate heptahydrate
$CaCl_2 \cdot 2H_2O$	Calcium chloride dihydrate
$Na_2MoO_2 \cdot 2H_2O$	Sodium molybdate dihydrate
$ZnSO_2 \cdot 7H_2O$	Zinc sulfate heptahydrate
$MnSO_4 \cdot 5H_2O$	Manganese (II) sulfate pentahydrate
$CuSO_4 \cdot 5H_2O$	Copper sulfate pentahydrate
HCl	Hydrochloric acid
$NaClO_2$	Sodium chlorite
BCP	Bacterial cellulose pellicle
HDBCPs	Heat dried bacterial cellulose pellicles
CTE	Coefficient of thermal expansion
DI	Deionized
TOBCPs	TEMPO-oxidised Bacterial cellulose pellicles
AgNPs	Silver nanoparticles
CTS	Chitosan

MFC	Microfibrillated cellulose
EDC	1-ethyl-3-(3-dimethyl-aminopropyl) carbodiimide hydrochloride
NHS	N-hydroxysuccinimide
GNs	Graphene nanoplatelets
HNO_3	Nitric acid
H_2SO_4	Sulfuric acid
IEC	Ion exchange capacity
IL	Ionic liquid
WRV	Water retention value
TGA	Thermal gravimetric analysis
BET	Brunauer-Emmett-Teller
RIs	Refractive indices
CNM	cellulose nanofibrous mats

List of Symbols

A_{a}	The areas of the XRD pattern ascribed to the amorphous part of the cellulose
A_{c}	The areas of the XRD pattern ascribed to the crystalline
A_{s}	BET surface area
E	Young's modulus
m_w	The wet mass of the TEMPO-oxidised BC hydrogel
m_d	The dry mass of the TEMPO-oxidised BC
M_{c}	Residual moisture content
n_R	Refractive indices of the resin
n_F	Refractive indices of the fiber
P	The porosity
r	Reflective coefficient
SR	Swelling ratio
T	Transmittance
U_{T}	Work of fracture
v	Volume
w	Weight
χ_{c}	The crystallinity
σ	Tensile strength
ε	Strain-at-failure
ρ_E	The envelope density

ρ_A	The absolute densities

Chapter 1 - Introduction

1.1 Background and motivation

TEMPO [(2,2,6,6-tetramethylpiperidin-1-yl)oxyl] mediated oxidation of cellulose is a regioselective oxidation of the C6 primary hydroxyl groups of native cellulose that uses sodium bromide (NaBr) and sodium hypochlorite (NaClO) as the regenerating oxidants [1]. The oxidation reaction introduces hydrophilic sodium carboxylate groups onto the surface of the individual cellulose fibrils in native cellulose; this then gives rise to strong electrostatic repulsions between the TEMPO-oxidised cellulose fibrils in water. Consequently, simple mechanical agitation of TEMPO-oxidised native cellulose in water is sufficient to individualise the cellulose fibrils, producing high aspect ratio TEMPO-oxidised cellulose nanofibrils (TOCNs) with a uniform lateral width of 3−4 nm and a length of several micrometres [2-4]. This simple and energy efficient method of producing cellulose nanofibrils has created a new wave of research in nanocellulose science and technology. Since the first report on the TEMPO-mediated oxidation of native cellulose [2], various research efforts have focused on the exploitation of TOCNs for packaging [5], wound dressing [6, 7], energy storage [8], filters for separation [9], as well as nano-reinforcement for polymers [1].

By far and large, the most used feedstock to produce TOCNs is bleached cellulose pulp. This is not surprising as they are widely available and can be easily sourced for research purposes. Typically, pressed bleached pulp sheets are first disintegrated in water to form a homogenous cellulose pulp suspension. To this suspension, sodium bromide (NaBr) or sodium hypochlorite (NaClO) is added along with catalytic amount of TEMPO. The addition of an oxidant, NaClO for the

TEMPO/NaBr system and $NaClO_2$ for the TEMPO/NaClO system, will oxidise the exposed C6 hydroxyl groups of cellulose into aldehydes and subsequently into carboxylates without disrupting the fibrillar and native cellulose-I crystal structure [10]. Other cellulose feedstock has also been investigated, albeit to a lesser extent compared to cellulose pulp in the literature. The TEMPO-mediated oxidation of a feedstock with a cellulose-II crystal structure, such as regenerated cellulose [11-13] or mercerised cellulose [12], showed a different behaviour. Instead of producing water-insoluble TOCNs with a cellulose-II structure, the TEMPO-mediated oxidation reaction typically produces water-soluble carbohydrates. Similar observations have also been reported for the TEMPO-mediated oxidation of amorphous cellulose [14].

Cellulose can also be synthesised microbially. Microbially synthesised cellulose, more commonly known as bacterial cellulose (BC), is an ultrapure form of cellulose synthesised by cellulose producing *Komagataeibacter* through the fermentation of low molecular weight sugars [15]. It is produced as a pellicle consisting of a three-dimensional network of cellulose nanofibrils with a typical lateral width and thickness of 30-50 nm and 6-10 nm, respectively [16]. TEMPO-mediated oxidation of BC presents an interesting scenario. Considering that BC is highly crystalline (~90%) [17] and possesses a cellulose-I crystal structure [18], the TEMPO-mediated oxidation of BC pellicle is expected to produce a pellicle consisting of nanofibrillar TEMPO-oxidised BC (TOBC). However, it has been reported that the oxidation reaction leads to the complete disintegration of the pellicle, producing a homogenous suspension of TOBC in water [19-21]. Based on current known literature about TEMPO-mediated oxidation of pulp, it is generally

assumed that the TEMPO-mediated oxidation of a dried and well-consolidated sheet of BC, i.e., a BC nanopaper, will also produce a homogenous suspension of TEMPO-oxidised BC in water. However, is this assumption true? No studies have been conducted to evaluate and this thesis sets out to investigate the validity of this assumption.

1.2 Aim and objectives

The aim of this thesis is to study the influence TEMPO-mediated oxidation reaction on a sheet of dried and well-consolidated BC nanopaper. The specific objectives are to:

- Derive the optimum TEMPO-mediation oxidation conditions of BC nanopaper.
- Quantify the effect of TEMPO-mediated oxidation reaction on the structure and properties of BC nanopaper.
- Compare TEMPO-oxidised BC with the state-of-the-art TEMPO-oxidised cellulose nanofibrils from a homogenous BC-in-water suspension.

1.3 Structure of this thesis

This thesis is divided into six chapters. Chapter 1 provides a brief introduction that covers the motivation and goal of the thesis. Chapter 2 reviews the background and state of the art of the various methods of achieving TEMPO [(2,2,6,6-tetramethylpiperidin-1-yl)oxyl]-mediated oxidation of bacterial cellulose. The subsequent chapters 3 – 5 are stand-alone articles that can be read independently. Chapter 3 introduces a simple approach to the production of TEMPO-oxidised

nanocellulose hydrogels and self-standing films derived from bacterial cellulose nanopaper. Chapter 4 reports on the peculiar behaviour of the TEMPO-mediated oxidation of dried and well-consolidated bacterial cellulose nanopapers that are heat-pressed at different temperatures. The effects of different drying temperatures on the carboxylate content, swelling ratio, specific surface area, residual moisture content, porosity, and mechanical properties are presented and discussed. Chapter 5 compares the properties of self-standing TEMPO-oxidised nanocellulose films made from the dewatering of a TEMPO-oxidised bacterial cellulose hydrogel and a homogenous TEMPO-oxidised BC-in-water suspension. The differences in the carboxylate content, porosity, transmittance, and mechanical properties are then discussed. Chapter 6 presents a summary of my findings, and suggestions for further study.

Chapter 2 - Literature review

2.1 Cellulose

Cellulose, a natural organic polymer, has held the scientific and industrial realms in thrall since its initial discovery by Anselm Payen as a primary constituent of plant cell walls. Constituting at least one-third of the terrestrial plant matter, it stands as the most abundant form of living terrestrial biomass [22]. Its near-pure existence in cotton fibers and its co-existence with other constituents like hemicellulose and lignin in various plant parts, accentuate its ubiquity and potential for diverse applications. Anselm Payen's recognition of cellulose as a significant component in plant cell walls marked the onset of numerous explorations into its structure, sources, and applications. The primary source of cellulosic is wood, owing to its abundance and the well-established infrastructure for its processing, especially in industries like pulp and paper, packaging, and pharmaceuticals [23, 24]. Additionally, agricultural crops and by-products like flax, sisal, hemp, kenaf, and residues from coconut, banana, sugar cane, and corn cultivation offer alternative sources of cellulose [25-27]. Another important source of cellulose is bacterial, a microbial source, *Gluconacetobacter xylinus*, has garnered attention for its ability to secrete cellulose microfibrils under specific culturing conditions [28-33]. Tunicates and algae also contribute to the microfibril cellulose pool [24].

Cellulose, a linear-chain polymer, comprises repeating units of β-D-glucose. These units covalently bond through an oxygen atom at the C1 and C4 positions, forming the β-1-4 glucosidic bond, which is stabilized by intrachain hydrogen bonding. The stacking of multiple chains, promoted by van der Waals and intermolecular hydrogen bonds, forms elementary fibrils which aggregate further

into microfibrils [23, 26, 34]. The microfibrils exhibit both crystalline and amorphous regions with different polymorphs of crystalline cellulose (I, II, III, and IV) exhibiting distinct properties [24]. Cellulose I can convert to cellulose II or III, while cellulose II, the most thermodynamically stable form, is synthesized via regeneration or mercerization processes [35, 36].

2.2 Bacterial cellulose

Bacterial cellulose (BC) (Figure 2-1) similar to wood-derived plant cellulose and even though they have distinct structural properties, their fundamental molecular structure, being polymerized glucose monomer units, remains the same. The structure of BC is organized in uniaxially oriented fibril bundles measuring 2-4 nm in diameter, with the nanofibrils being constructed from aligned smaller protofibrils [37, 38]. The nanofibrils then assemble into BC ribbons (Figure 2-2) a width of 50-100 nm in diameter and around 100 μm in length,[31, 33, 39] forming the biofilm.

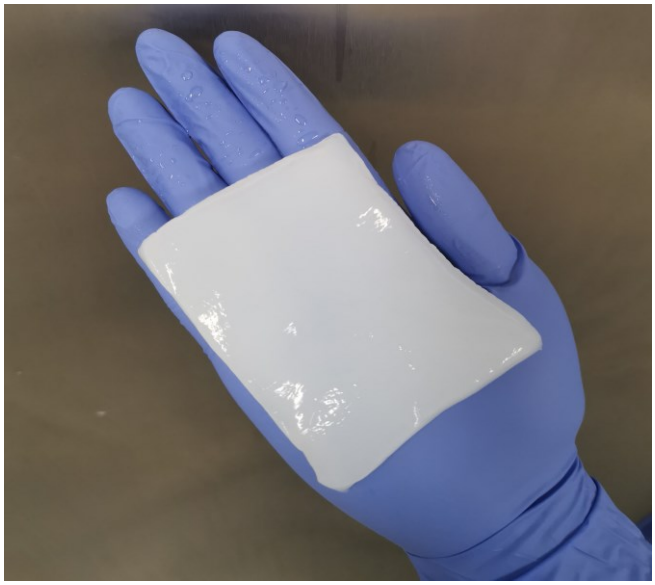


Figure 2-1: A BC pellicle

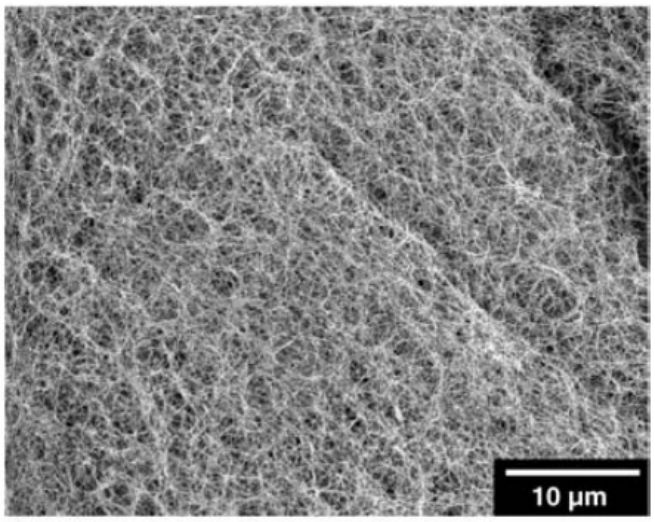


Figure 2-2: Scanning electron micrographs showing the fibrous network of cellulose in the BC [31]

2.3 TEMPO-mediated oxidation of cellulose

TEMPO-mediated oxidation is widely used in organic synthesis, particularly in the synthesis of pharmaceuticals and natural products. It has also found applications in the field of polymer chemistry, where it is used for the functionalisation of polymers and the preparation of various polymeric materials. TEMPO-mediated oxidation of cellulose is a chemical process that involves the oxidation of cellulose using a catalytic amount of TEMPO alongside a co-oxidant such as sodium hypochlorite or sodium bromide. This process is used to selectively oxidise the primary hydroxyl groups of cellulose to carboxyl groups, which increases its solubility in water and allows it to be used in a wider range of applications. TEMPO oxidation of cellulose is a relatively simple and environmentally friendly process that can be performed at room temperature and atmospheric pressure. The resulting oxidised cellulose can be used in a wide range of applications, including as a thickener, gelling agent, and stabilizer in food and cosmetic products, as well as in the production of paper and

textiles. It can also be used as a scaffold material for tissue engineering and regenerative medicine applications. These discoveries and applications are reviewed in the following sections.

High energy consumption and cellulose damage are inevitable when isolating fibrils from their wood and plant origins [1, 40]. These problems are typically solved by introducing charged functional groups to the fibril surfaces. Anionically charged groups form strong electrostatic repulsions between individual fibrils, resulting in easier fibrillation. Saito *et al.* expanded on this concept by oxidising cellulose fibers with TEMPO radicals; this eased the isolation of cellulose microfibrils without seriously damaging the fiber [2]. By leveraging catalytic oxidation with TEMPO, hydroxyl groups in native celluloses are respectively converted to aldehydes, ketones and carboxyl groups under mild conditions [1]. Moreover, TEMPO is commercially available and water-soluble [41].

The mechanism for TEMPO-oxidation of cellulose in water at pH 10—11 is shown in Figure 2-3. It is shown that at pH 10—11, when cellulose is subjected to TEMPO/NaBr/NaClO, C6 primary hydroxyl groups oxidise to C6 carboxylate groups; the pH is maintained by adding sodium hydroxide (NaOH). TEMPO/NaBr/NaClO oxidation largely maintains the native fibrous morphology of the native cellulose sources, including cotton linters, bacterial cellulose and bleached kraft pulps. It also produces little to no water-soluble products. These findings are independent of reaction times and oxidation conditions [12].

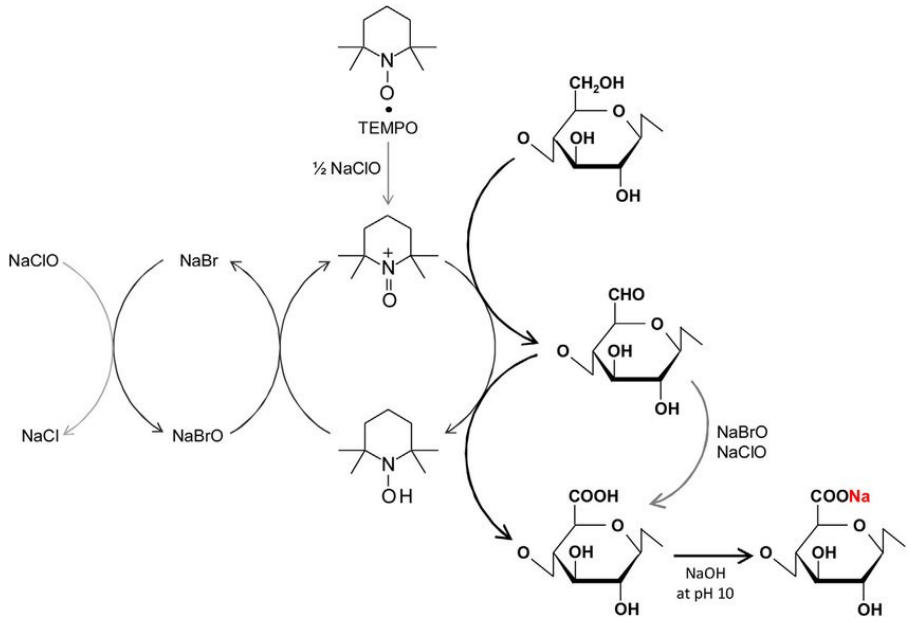


Figure 2-3: Regioselective oxidation of C6 primary hydroxyls of cellulose to C6 carboxylate groups by TEMPO/NaBr/NaClO oxidation in water at pH 10–11 [1].

TEMPO-oxidation has also been applied to other cellulose grades. These include regenerated and mercerised celluloses, ball-milled cellulose and liquid NH_3-treated native celluloses[10, 12, 14, 42]. When treated with TEMPO, these cellulose grades become transparent with hydration, indicating the creation of water-soluble oxidised products. These products, for example β-1,4-linked polyglucuronic acid sodium salt (cellouronic acid), have a homogeneous chemical structure. Unlike native celluloses, the C6 primary hydroxyls in the modified cellulose grades selectively convert to C6 sodium carboxylate groups during TEMPO-mediated oxidation [12, 14, 42]. It is important to note that during TEMPO-mediated oxidation with these cellulose grades, TEMPO does not play the only key role; the NaClO/NaBr in the TEMPO/NaBr/NaClO oxidation system is also responsible for the conversion [43].

Figure 2-4 shows the carboxylate/aldehyde content and degree of polymerisation about the amount of NaClO. A bleached softwood kraft pulp is oxidised using TEMPO/NaBr/NaClO at pH 10 and room temperature. Electric conductivity titration was used to determine the carboxylate and aldehyde contents, and the Mark-Houwink-Sakurada equation was used to roughly estimate the degree of polymerization *via* intrinsic viscosities [44]. The graph indicates an increase in sodium carboxylate content with increasing NaClO. By contrast, very few aldehyde groups form on the oxidised pulp.

While the sodium carboxylate group content increased with increasing NaClO concentrations, the degree of polymerisation decreased. This indicates an unavoidable decrease in degree of polymerisation when native cellulose is treated with TEMPO/NaBr/NaClO in water at pH 10 [1]. It was shown that the TEMPO/NaClO/$NaClO_2$ system partially suppresses depolymerisation of the oxidised pulp in water at pH 6.8 and 60°C [1]. Additionally, it was found that side reactions produce small quantities of C2 and C3 ketones depending on the oxidation conditions and reactivity of the TEMPO derivatives used. Furthermore, it has been shown that ketones and aldehydes discolour when heated despite their small quantities.

An additional investigation found that the maximum C6 oxidised ketones and aldehydes contents depends on the cellulose I crystal width [45]. In the study, Okita *et al.* identified native celluloses with various widths and treated them with an excess of NaClO during TEMPO-mediated oxidation. More oxidised groups formed on native celluloses with smaller microfibril widths. The study also showed

good agreement between the calculated and experimentally determined amount of surface C6 primary hydroxyl groups.

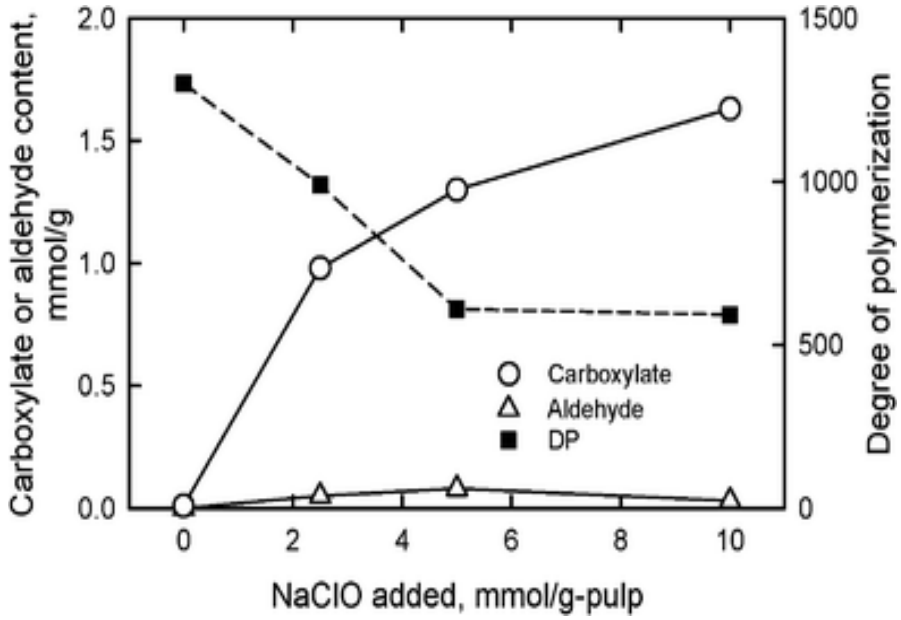


Figure 2-4: A graph showing the carboxylate/aldehyde content and degree of polymerization about the amount of NaClO of the oxidised pulps in a TEMPO/NaBr/NaClO oxidation of bleached softwood kraft pulp at pH 10 and at room temperature [1].

When treating lignin containing fibers (*e.g.,* softwood thermomechanical pulps) with TEMPO/NaBr/NaClO, the lignin and hemicellulose form water-soluble degraded fractions [46]. The remaining water-insoluble oxidised pulp can then be filtered out. TEMPO-mediated oxidation of native celluloses can yield carboxylate contents of 1—1.5 mmol g^{-1} and weight recovery ratios of up to 40%. The oxidised pulp produces a highly viscous and transparent gel in water. Upon oxidation, the disintegrated pulp consists of individual fibers with widths of 4—6 nm. From this study, it was proven that pulps containing lignin and hemicellulose (such as

softwood pulps) can produce pure TEMPO-oxidised cellulose. However, a higher NaClO content is required to achieve pure TEMPO-oxidised cellulose as compared to pure celluloses.

TEMPO-oxidised bleached hardwood and softwood kraft pulps can be dispersed in water *via* mechanical disintegration in household blenders, homogenizers, *etc*. When these pulps contain carboxylate contents in excess of 0.8 mmol g^{-1}, the resulting high viscosity dispersions are mostly transparent [47]. Transmission electron microscopy (TEM) images of dried TEMPO-oxidised hardwood cellulose dispersions are shown in Figure 2-5 [47]. The dispersions are revealed to contain mostly individual oxidised fibers. These fibers are a few microns long and 3—4 nm wide. Regardless of the wood species, the widths remain consistent while the lengths are widely distributed. The length variation is dependent on the oxidation and disintegration conditions, and the optimum oxidation conditions for high yield are largely dependent on the cellulose type.

The morphology and rheological properties of TEMPO-oxidised hardwood fibers are determined by their carboxylate contents. The TEM (Transmission electron microscopy) images of TEMPO-oxidised hardwood are shown in Figure 2-6. These images are taken at carboxylate contents of 1.0 and 1.5 mmol g^{-1}. At 1.0 mmol g^{-1} carboxylate content, the images exhibit low light transmittance, which would suggest fiber aggregation. At 1.5 mmol g^{-1} carboxylate content, the images show individualised nanofibers with consistent widths of 3—4 nm. The higher sodium carboxylate group content produces a higher anionic charge on the fiber surfaces. This in turn promotes electrostatic repulsion and/or osmotic effects in water [3]. The nanofiber yield, light transmittance and viscosity of the TEMPO-

oxidised cellulose dispersions are also affected by the apparatus and conditions employed during mechanical treatment [3].

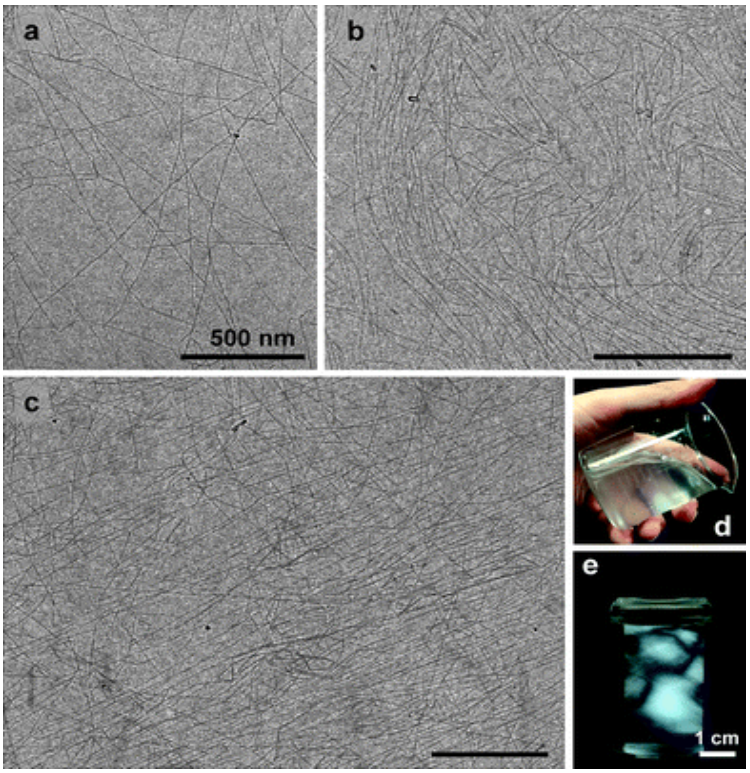


Figure 2-5: TEM images (a–c) of a dried TEMPO-oxidised hardwood cellulose dispersion. The carboxylate and aldehyde contents of 0.8 and 0.0 mmol g^{-1}, respectively, are observed *via* the diffraction-contrast method in the bright-field mode using a low-dose exposure. (d) and (e) show a typical dispersion observed between cross polarizers [47].

Industrial production of TEMPO-oxidised cellulose is attractive for several reasons. TEMPO-oxidation preserves the micron level fiber morphology of the treated cellulose. Despite the substantial increase in hydrophilic sodium carboxylate groups, the fibers do not excessively swell. Upon oxidation, the products can be

washed, filtered and squeezed. The resulting solids are less costly and more energy efficient to transport [1, 3]. TEMPO-oxidised cellulose can also be produced from multiple sources. Bleached kraft and sulfite pulps provide an inexpensive and efficient source for industrial TEMPO-oxidised cellulose production [1]. In general, the production of these pulps from wood chips leverage green, efficient, and low energy pulping and bleaching procedures; this leaves the catalyst as the costliest component of the oxidation process. However, the catalyst can be reclaimed and reused with desalination [48], meaning that it is possible to achieve cost effective TEMPO-oxidised cellulose production.

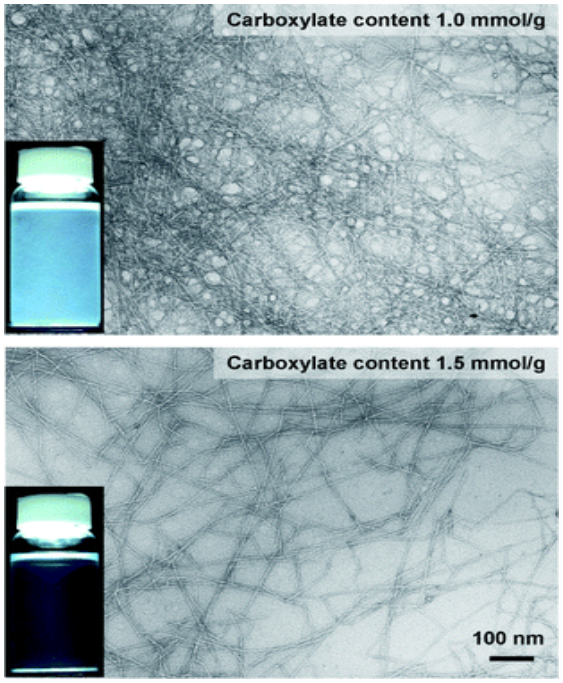


Figure 2-6: TEM images of dried TEMPO-oxidised hardwood cellulose dispersions with carboxylate contents of 1.0 and 1.5 mmol g^{-1}. The carboxylate contents are observed by negative staining with uranyl acetate. The insets show the corresponding aqueous dispersion [3].

2.4 TEMPO Oxidation of Bacterial Cellulose

TEMPO mediated oxidation is a commonly used method to modify the surface properties of cellulose. Bacterial cellulose, which is produced by certain species of bacteria such as *Gluconacetobacter xylinus*, can also be oxidised using TEMPO. The extent of TEMPO mediated oxidation can be controlled by adjusting the reaction conditions such as the concentration of NaClO, NaBr, and TEMPO, as well as the reaction time. The resulting material can be characterized using various techniques such as Fourier transform infrared (FTIR) spectroscopy, X-ray diffraction (XRD), and scanning electron microscopy (SEM).

There are only a few studies focussing on the TEMPO-oxidation of BC. Firstly, Luo *et al.* [49] compared two surface modifications on bacterial cellulose, TEMPO-mediated oxidation and periodate oxidation (PO). These oxidation methods were performed on BC pellicles to introduce aldehyde groups and to ensure that the BC nanofibers maintained their three-dimensional and nanoscale structural characteristics and produced TEMPO oxidised BC (TOBC) and periodate oxidised BC (POBC) respectively. Additionally, the team investigated how TEMPO-mediated oxidation influenced their macro- and micro- morphologies, tensile properties, and degradation behaviour, concluding that introducing aldehyde groups onto BC fibers through TEMPO-mediated oxidisation results in a new alternative nanofibrous BC material (TOBC) for tissue engineering research. In order to produce TOBC, BC pellicles were first produced using *Acetobacter xylinum* X-2. This bacterial strain was grown in culture media containing 0.3 wt% analytical grade green tea powder and 5 wt% analytical grade sucrose for 7 days. TOBC was produced by suspending about 50 g freeze dried BC pellicles in deionized water

with 0.13 g TEMPO and 1.3g sodium bromide under stirring. 0.267g of 10% sodium hypochlorite solution was then slowly added to this suspension and the pH value was maintained at 10.5 with 0.5M sodium hydroxide solution. The reaction continued at 30°C for 30 minutes, and 40 mL absolute ethanol was used to quench the oxidation. The resulting TOBC pellicles were washed with deionized water.

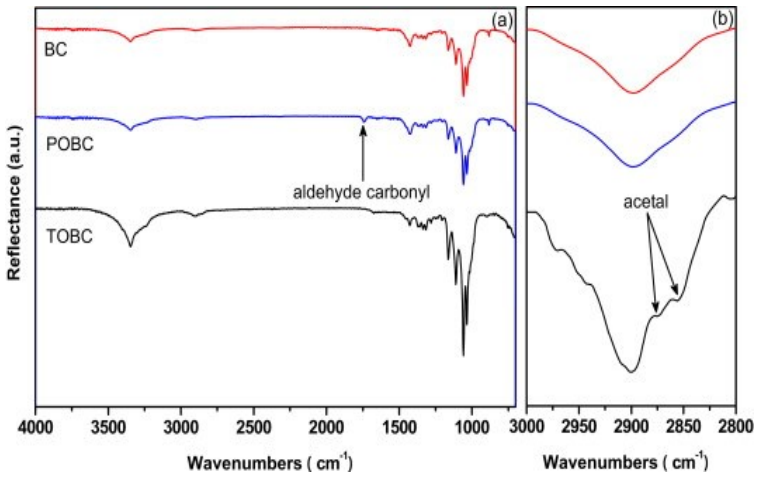


Figure 2-7: ATR-FTIR spectra of (a) BC, Periodate oxidised BC (POBC), TOBC and the (b) enlarged region of 3000 – 2800 cm^{-1} where typical peaks of acetal were observed [49].

Schiff base reactions were used to identify the existence of aldehyde groups on the BC molecules; a colour change was observed with TOBC. Using sodium hydroxide titration, the aldehyde content was found to be 0.15±0.05 mmol g^{-1}. These experiments confirmed that functional groups were indeed introduced. FTIR-ATR was used to further investigate the chemical structure of TOBC, and revealed that acetal groups, rather than aldehyde groups, were responsible for the observed colour change in the TOBC Schiff base reaction sample (Figure 2-7). In order for TO-BC to release free aldehyde groups, the conditions must be acidic. Using XRD,

it was shown that TOBC still belongs to the cellulose I structural class— however, the crystallinity differed strongly between samples. BC samples showed 88% crystallinity, while TOBC showed 94% crystallinity (Figure 2-8). TEMPO-mediated oxidation thus seems to increase crystallinity by generating aldehyde groups in disordered regions, forming acetal linkages with neighbouring hydroxyl groups. Comparing the macroscopic morphologies of BC and TOBC, it appeared that BC and TO-BC retain largely the same macromorphology. SEM and diameter analysis revealed that TOBC maintained a similar nanofiber structure and diameter to BC (Figure 2-9). The similarities between BC and TOBC samples extended to their tensile strength, approximately 0.60 ± 0.02 MPa. Finally, the specimens were placed in a phosphate buffer saline (PBS) solution to demonstrate in vitro degradation; both BC and TOBC remained stable in PBS. [49]

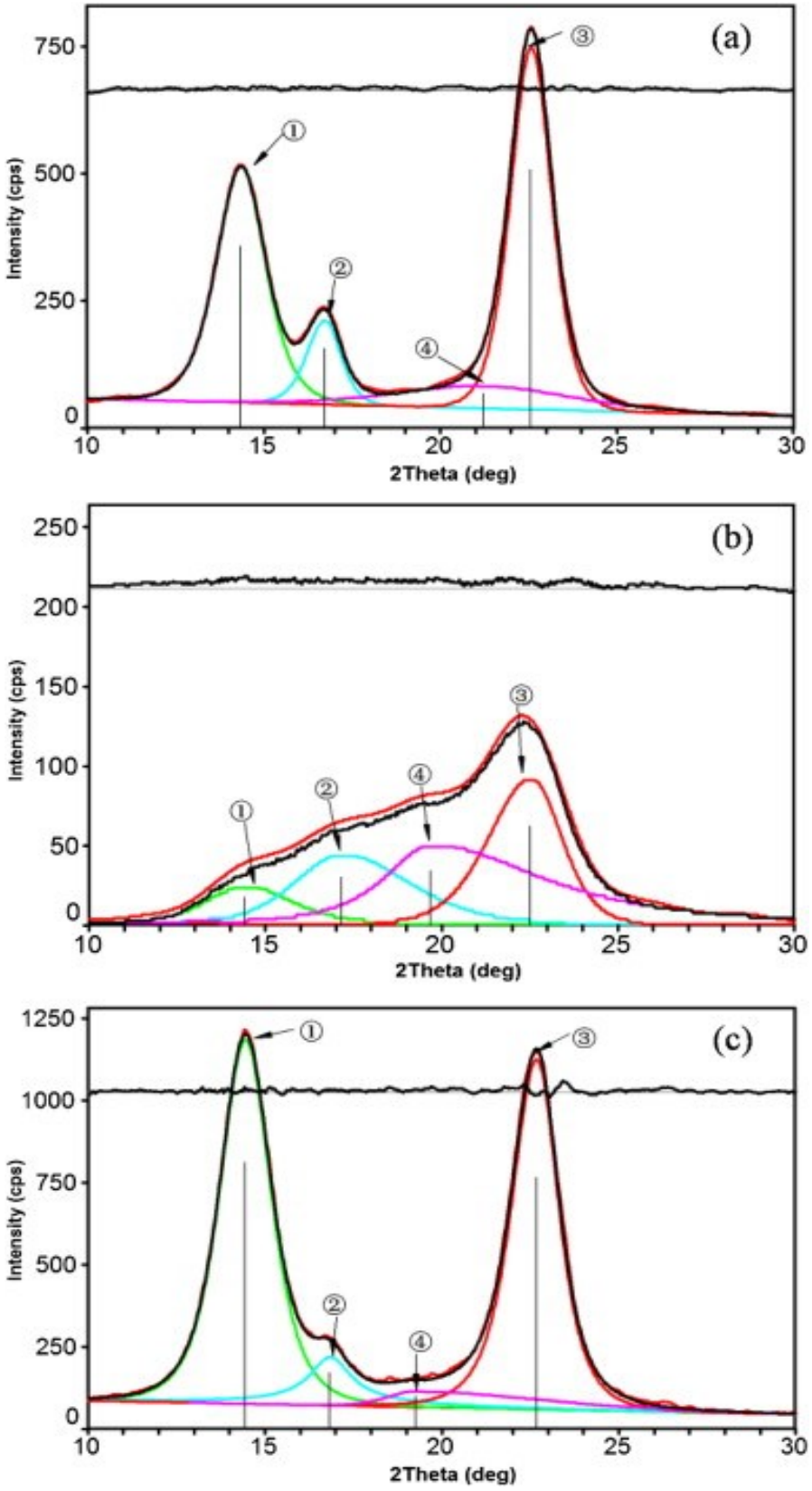


Figure 2-8: XRD patterns of (a) BC, (b) POBC, and (c) TOBC [49].

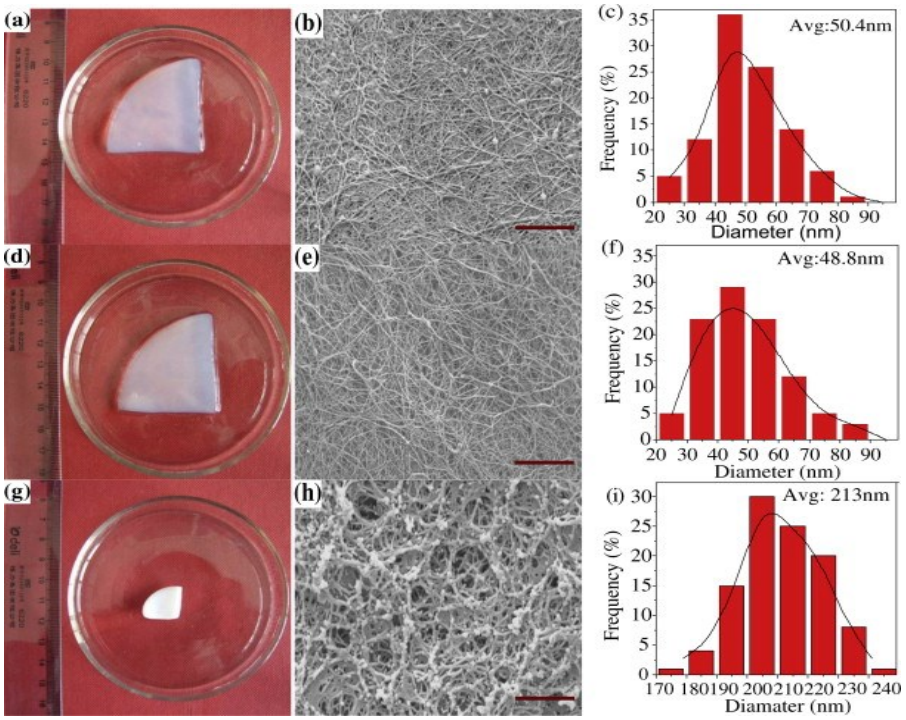


Figure 2-9: Photographs of (a) BC, (d) TOBC and (g) POBC, SEM images of (b) BC, (e) TOBC and (h) POBC, and fiber diameter distribution of (c) BC, (f) TOBC and (i) POBC (scale bar: 5 μm) [49].

Jun *et al.* [19] investigated the use of TEMPO-oxidation to create bacterial cellulose nanofibers (BCNFs) that could be dispersed in water. Using a novel one-pot synthesis method, the researchers demonstrated that TOCNs could be washed and dried without centrifugation and without residual chemicals. As such, the process was scalable, efficient, and more suited for skincare and biomedical research applications. To implement the one-pot synthesis method, sheets of bacterial cellulose (EZ Costec & Co. Ltd., Gyeonggi, Korea) were cut into small pieces. 20g of these BC pieces were suspended in 500 mL distilled water, dissolved sodium hypochlorite, and 20mg activated *SiliaCat-TEMPO* (SiliCycle Inc., Quebec, QC, Canada). *SiliaCat-Tempo*, a heterogeneous catalyst created with specialised

organosilica-silica entrapped radicals, was the key ingredient to this process and must be pre-treated to activate. To pre-treat the *SiliaCat-TEMPO* beads, they were first mixed with 4 M hydrochloride in dioxane and a 0.5 M solution of N-chlorosuccinimide in dichloromethane for 15 minutes. The beads were then washed in ethanol and vacuum dried before entering the bacterial cellulose suspension. The bacterial cellulose suspension was then stirred at pH 10 for the remainder of the oxidation period. To achieve a pure bacterial cellulose solution, ascorbic acid was added, and the *SiliaCat-TEMPO* beads were filtered through a nylon mesh in a vacuum decompression device. This left a pure nanofiber solution, leaving behind the *SiliaCat-TEMPO* beads. The paper concluded that the one-pot synthesis method was a simple and efficient way to create bacterial cellulose nanofibrous structures with water absorbing properties.

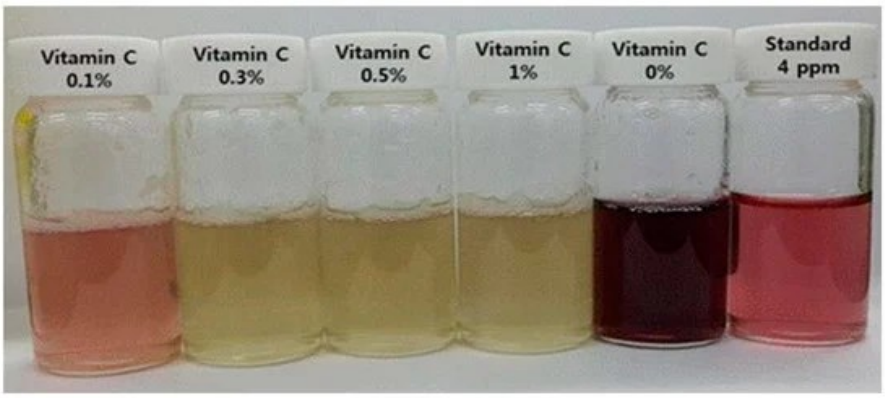


Figure 2-10: Neutralization of the sodium hypochlorite using ascorbic acid [19].

In order to test the efficacy of the one-pot process in removing residual chemicals, a free chlorine DPD method (phosphate buffer solutions and N/N-diethyl-p-phenylenediamine reagent) was used. It was confirmed that when >0.3%

ascorbic acid was used, the free residual chlorine was completely removed (Figure 2-10). This process also eliminates the need for washing. With the use of *SiliaCat-TEMPO*, a vacuum filtration process was used to remove the TOCN products from the reactants. This process could be done continuously, allowing for scalability. TOCNs produced using the one-pot method (O-TOCNs) and TOCNs produced using the conventional method (C-TOCNs) both exhibited increased carboxyl and aldehyde content using the conductivity titration method. SEM images of the original BC nanofibers confirmed that O-TOCNs retained a similar average fiber diameter (Figure 2-11). The hypothesis for this diameter difference was that the TEMPO catalyst could not fully solubilize when held in *SiliaCat-TEMPO* beads. As such, the TEMPO could only impact the fiber surface without penetrating the fiber bundle. FTIR spectra of BC nanofibers and O-TOCNs confirmed the successful conversion of hydroxyl groups to carboxyl groups (Figure 2-12), and XRD patterns of the two specimens indicated that both O-TOCNs retained their cellulose I crystal structure (Figure 2-14). O-TOCNs demonstrated similar and slightly improved crystallinity compared to BC (75.7% crystallinity in O-TOCNs *versus* 75.3% crystallinity for BC). Finally, the contact angles of the O-TOCNs were found to be greatly reduced, confirming increased water absorption, even when mixed with other materials (Figure 2-14).

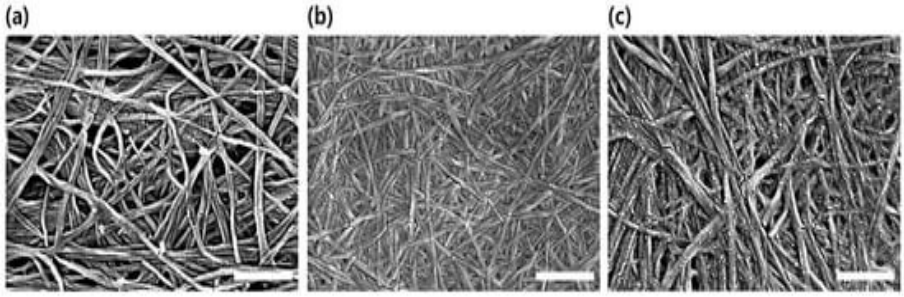


Figure 2-11: SEM images of (a) pure BC, (b) C-TOCNs and (c) O-TOCNs. The scale bar for all three images corresponds to 500 nm [19].

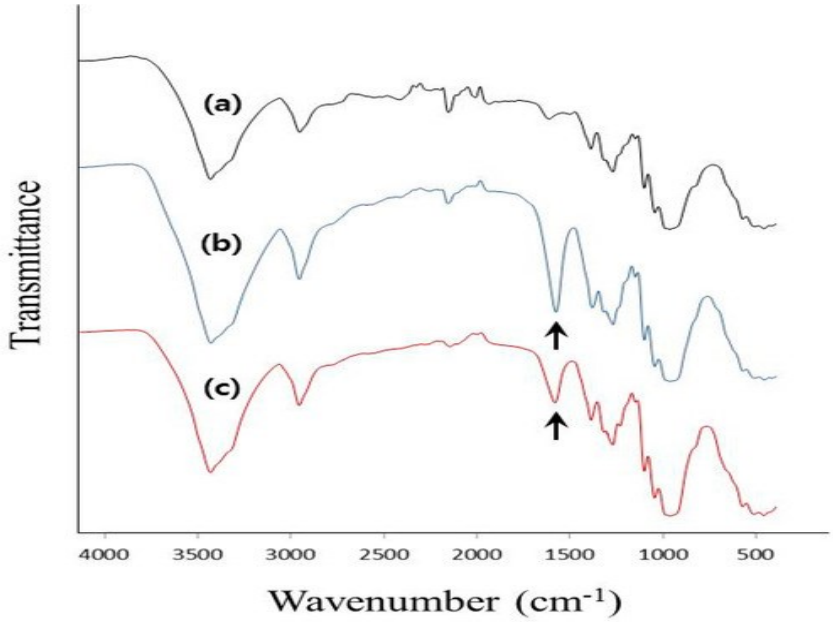


Figure 2-12: FTIR spectra of (a) pure BC, (b) C-TOCNs and (c) O-TOCNs [19].

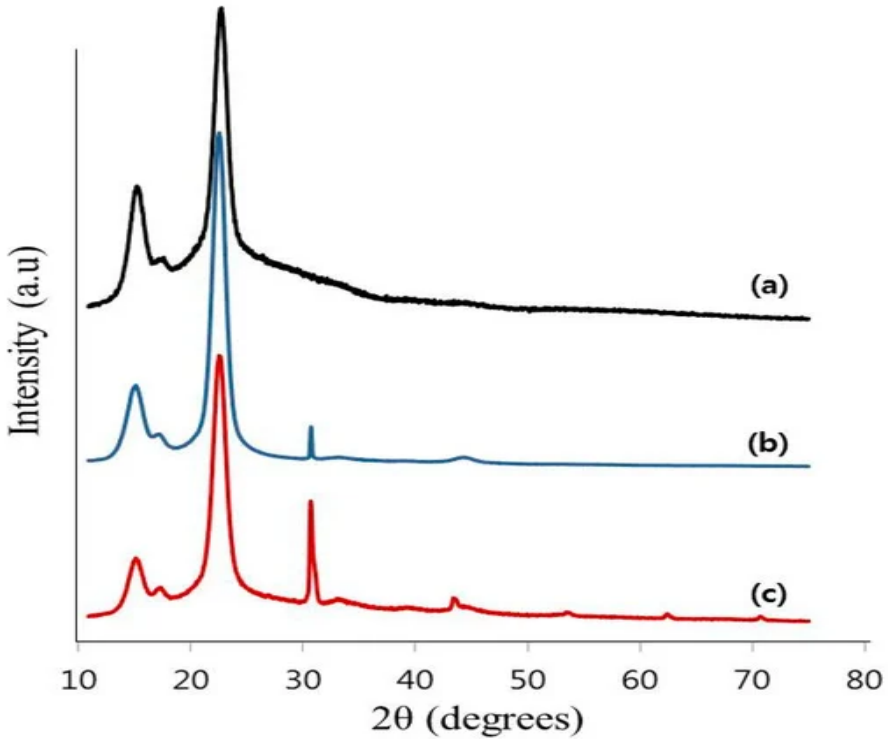


Figure 2-13: XRD patterns of (a) pure BC, (b) C-TOCNs and (c) O-TOCNs [19].

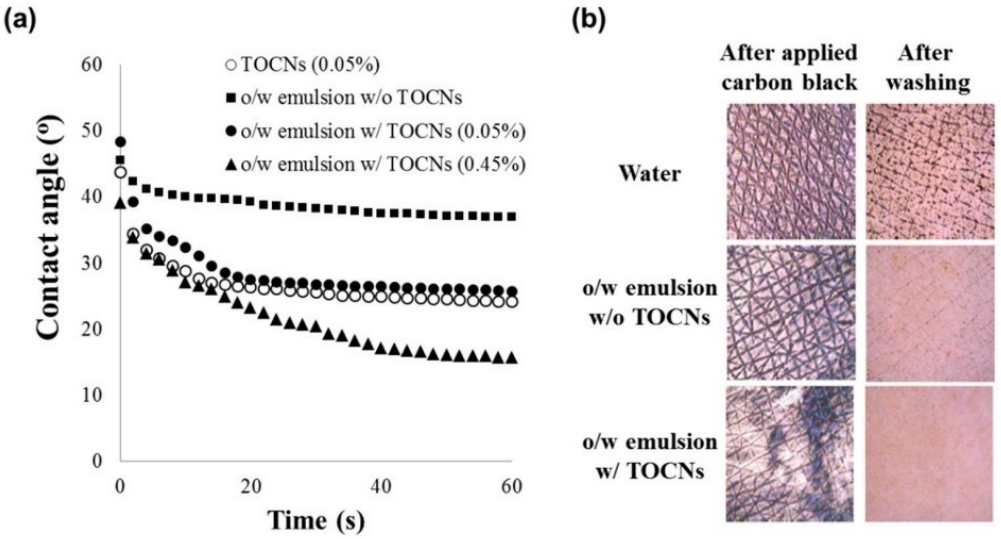


Figure 2-14: (a) Changes in the contact angle of various concentrations of TOCNs in o/w emulsion over time and (b) images demonstrating the results of the washing experiments conducted to remove the carbon black from the surface [19].

In another study, bacterial cellulose fibers (BCF) were treated with TEMPO and a mild mechanical treatment in order to create transparent film-forming suspensions [21]. This treatment increased the flowability of BCF and the mechanical and birefringence properties of the resulting films. To this end two TEMPO-oxidised BC nanofibers (TOBCNs) with middle or high carboxylate content were fabricated and cast-dried into films. *Gluconacetobacter xylinum* from the Bioresource Collection and Research Center in Hsinchu, Taiwan was cultivated. First, corn steep liquor with fructose (CSL-Fru) medium was prepared using the following ratios: corn steep liquor (20 mL), fructose (50 g), H_2PO_4 (1 g), $MgSO_4 \cdot 7H_2O$ (0.25g), $(NH_4)_2SO_4$ (3.3 g), $FeSO_4 \cdot 7H_2O$ (3.6 mg), $CaCl_2 \cdot 2H_2O$ (1.5 mg), $Na_2MoO_2 \cdot 2H_2O$ (2.4mg), $ZnSO_2 \cdot 7H_2O$ (1.7 mg), $MnSO_4 \cdot 5H_2O$ (1.4 mg), $CuSO_4 \cdot 5H_2O$ (0.05 mg), inositol (2 mg), pyridoxine/HCl (0.4 mg), p-amino-benzoic acid (0.2 mg), folic acid (0.002 mg), and biotin (0.002 mg). *G. xylinum* was then added to a 20% glycerol solution and frozen at -80°C. In a 250 mL flask, 1 mL of the frozen cell suspension was added to 50 mL of CSL-Fru medium and cultivated at 28°C for 5 days. Bacterial biomass formed on the medium surface and was hydrolysed by adding 1 mL of cellulase (Sigma-Aldrich) and the resulting mixture was then shaken at 120 rpm at a temperature of 28°C for 1 day. After shaking, the hydrolysed bacterial cellulose pellicles (BCP) fragments were carefully removed. The residual solution was centrifuged at 7830 rpm at 16°C for 10 min in a centrifuge (5430 R, Eppendorf Inc.) to wash and collect the bacterial biomass in the sediment. The solution was centrifuged three times to obtain *G. xylinum* pellets, which were thereafter resuspended in water and used as an inoculum.

To achieve BCPs, 0.12 mL *G. xylinum* was added to 20 mL CSL-Fru medium and incubated at 28°C for 10 days. The BCPs were obtained with a 9 cm diameter and immersed in a 1.0 M NaOH solution at 80°C for 1 hour for purification. This purification treatment was repeated until the BCPs appeared visibly white. Residual impurities were washed out of the BCPs using tap water for at least 2 days. The BCPs were then stored in water at 4°C. In order to prepare the TOBCNs, bacterial cellulose fiber (BCF) suspensions were first prepared. The BCPs were found to have a moisture content of approximately 99.40 ± 0.05% and a cellulose content of 0.06 g by weight. BCPs containing approximately 1 g cellulose were added to 200 mL water and homogenised at high speed for 3 min in a heavy-duty lab blender (7011HS, Waring Commercial Ltd.). The resulting suspension was washed and diluted using a glass filter until the liquid appeared transparent to the naked eye. Next, a BCF suspension containing ~1 g cellulose was poured into a 500 mL beaker. To ensure a homogeneous distribution of BCFs, water was added to the beaker until the total volume was ~350 mL. 0.018 g TEMPO and 0.1 g NaBr were added to this diluted suspension, and the solution was agitated for 30 min. Upon the addition of a NaClO solution (5 mmol g^{-1} cellulose), TEMPO-mediated oxidation began. The pH remained at 10 by adding 0.5 M NaOH solution with an autotitrator. The oxidation continued for 3 and 6 hours. The oxidation was quenched with ethanol until the pH remained stable. The oxidised solutions were highly viscous and milky. The newly TEMPO-oxidised bacterial celluloses (TOBCs) were washed by filtration five times and further oxidised in an acetate buffer using $NaClO_2$ (1.14 g g^{-1} cellulose) for 2 days at a pH of 4.8; this further oxidised any residual aldehyde groups.

In order to test properties of the TEMPO treated celluloses, two dispersions and two films were prepared. To prepare the dispersions, $NaClO_2$-treated TOBC gels were suspended in water to create 0.11% w/v TOBC suspensions. These were then sonicated for 2 min using 20 kHz ultrasonic waves and cooled in an ice bath five times. The aim of this sonication treatment was to separate anionic nanofibers while preventing crystal structure transitions from Iα to Iβ. After the sonication treatment, the unfibrillated fraction was separated from the TOBC suspensions by centrifuging at 12,000 rpm for 30 min. The supernatants of the centrifugation process were the TEMPO-oxidised bacterial cellulose nanoribbons (TOBCNs). The TOBCN dispersions were adjusted to 0.1% w/v using an evaporator at 40°C under reduced pressure. This process resulted in two separate dispersions. The TOBCN1s were then oxidised for 3 hours and were found to have a carboxylate content of 0.7 mmol per gram of cellulose, while TOBCN2s were oxidised for 6 hours and were found to have a carboxylate content of 1.1 mmol per gram of cellulose. To prepare the films, the TOBCN dispersions were poured into 25 mL petri dishes and oven dried for 2 days at 40°C. These films were then cut into 35×35 mm rectangles and stored at ~50% relative humidity.

Table 2-1: Summary of the material properties of the films prepared. [a]: The data were shown by mean ± standard deviation; [b]: No data [21].

Sample	HDBCPS	BCF	TOBCN1	TOBCN2
Thickness (μm)	13.2 ± 1.0[a]	10.8 ± 1.0	8.9 ± 0.6	7.6 ± 0.5
Density (g cm^{-3})	0.81	0.96	1.22	1.45
Porosity (%)	49	40	24	9
Crystallinity (%)	78	80	78	80
Crystal size (nm)	5.0	5.0	4.5	4.2
Carboxylate group content (mmol g^{-1})	_[b]	_	0.7	1.1
Light transmittance at 550 nm (%)	33	12	80	83
Young's modulus (GPa)	5.4 ± 1.4	2.3 ± 0.2	7.6 ± 1.3	9.0 ± 1.1
Tensile strength (MPa)	150 ± 5	48 ± 5	115 ± 10	163 ± 8
Strain at failure (%)	2.9 ± 0.6	3.9 ± 0.3	2.8 ± 0.6	2.8 ± 0.6
Work of fracture (MJ m^{-3})	2.2 ± 0.5	1.0 ± 0.1	1.8 ± 0.6	2.6 ± 0.7
Coefficient of thermal expansion (ppm K^{-1})	3.4 ± 0.1	3.6 ± 0.1	4.7 ± 0.4	3.2 ± 0.1

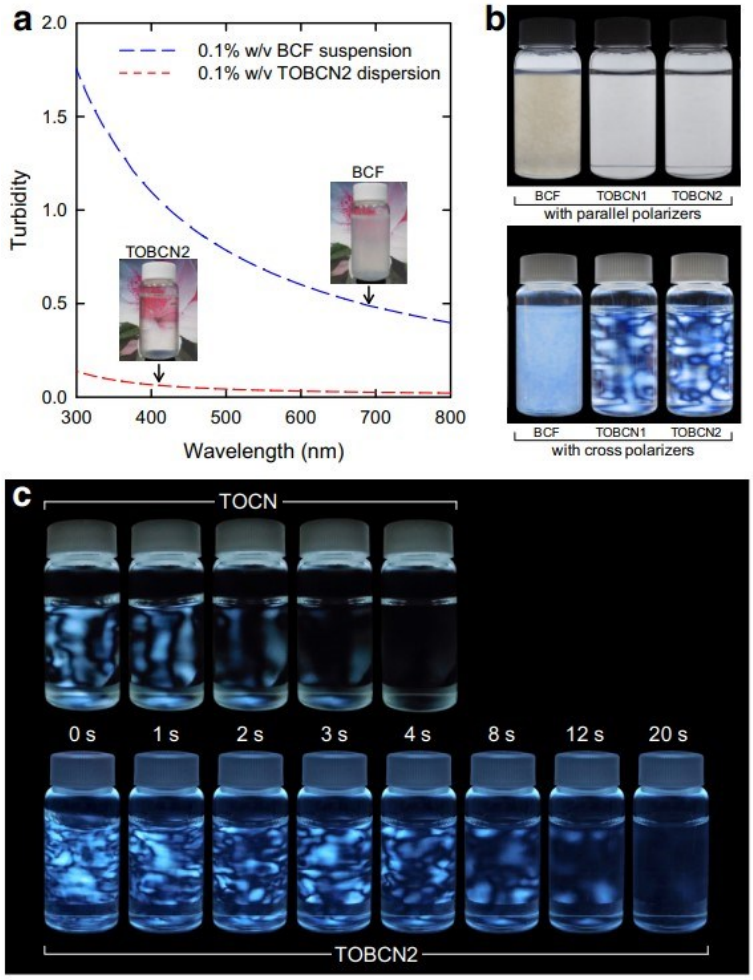


Figure 2-15：Photographs of the liquids for preparation of the films in the study performed by Wu *et al*. (a) turbidities of the 0.1% w/v BCF suspension and 0.1% w/v TOBCN2 dispersion; (b) images of the 0.1% w/v liquids with parallel or cross polarizers, demonstrating the birefringence properties of the material; note that all the liquids had the same cellulose weight content; (c) The maintenance times of birefringence of TOCN dispersion prepared from wood cellulose (top, 0—4 seconds) and TOBCN2 dispersion (bottom, 0—20 seconds) [21].

The material properties of the TOBCNs, as compared to the heat dried bacterial cellulose pellicles (HDBCPs) and bacterial cellulose fiber (BCFs), were

shown in Table 2-1. From this data, it showed that increasing the carboxylate content improves the corresponding material properties. TOBCN2 was found to be the most transparent, followed by TOBCN1. Additionally, the birefringence properties of the four material were displayed in Figure 2-15, with the corresponding photos and light transmittance data displayed in Figure 2-16. Of note is the coefficient of thermal expansion (CTE) of TOBCN2, which was found to be 3.2 ppm K^{-1}, the same value given by the monocrystalline silicon employed in solar cells. Industrial manufacture is still easier for TOCN (TEMPO-oxidised cellulose nanofiber from wood), however TOBCN had a higher crystallinity that improved its suitability of this material for film preparations, which were useful in applications such as flexible optoelectronic devices.

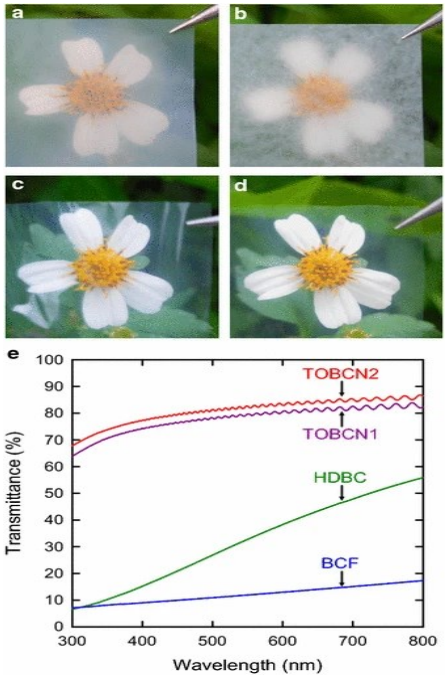


Figure 2-16：Photographs of the HDBCP (a), BCF (b), TOBCN1 (c) and TOBCN2 (d) films. e Light transmittances of the films from 300 to 800 nm in wavelength [21].

TEMPO oxidised bacterial cellulose also can be used as a safe, biodegradable, and sustainable solid stabiliser [50]. Specifically, researchers investigated the ability of TOBCs to stabilise an oil/water interface. First, bacterial cellulose pellicles were prepared. *Gluconacetobacter xylinus* screened from a traditional Chinese drink was stored in the China General Microbiological Culture Collection Center (registration No. 2955). Apart from analytical grade reagents, deionized (DI) water was used for all tests [50]. A medium was prepared using 25 g L^{-1} anhydrous dextrose, 10 g L^{-1} yeast powder, 7.5 g L^{-1} peptone, and 10 g L^{-1} disodium hydrogen phosphate. The pH was adjusted to 5.0 using acetic acid. *G. xylinus* was then activated in the medium for 24 hours at 30°C. *G. xylinus* was inoculated at 5% (v/v) in the same medium. After 5—8 days BC pellicles were found to have formed and were harvested. The gel-like membranes were washed in water and boiled in 0.1 M NaOH solution; this removed any residual medium and bacterial cells. Finally, the membranes were neutralised by washing in water. To disperse the BC pellicles, they were placed in a machine disintegrator (T-100, Adirondack Ltd.). They were then homogenised in a high-shear mixer (NS1001 L, Panda Ltd.) 10 times at 100 MPa until a nanoscale dispersion formed. To oxidise the resulting BCs, water (100 mL g^{-1} BC) was mixed with TEMPO (0.1 mmol g^{-1} dry BC) and sodium bromide (1 mmol g^{-1} dry BC). BC was then suspended in this solution and 10% NaClO was added to begin the oxidation reaction under continued stirring at ambient temperature. For this reaction, a pH of 10 ± 0.1 was maintained using a 0.1 M NaOH solution; the reaction continued until the pH no longer decreased. At that point, the reaction was quenched with 10 mL ethanol. The product was then centrifuged for 10 min at 10,000 rpm, and the supernatant was removed. Finally, the precipitate

was cleaned repeatedly, and residual ions were removed from the oxidised TOBC with water [50].

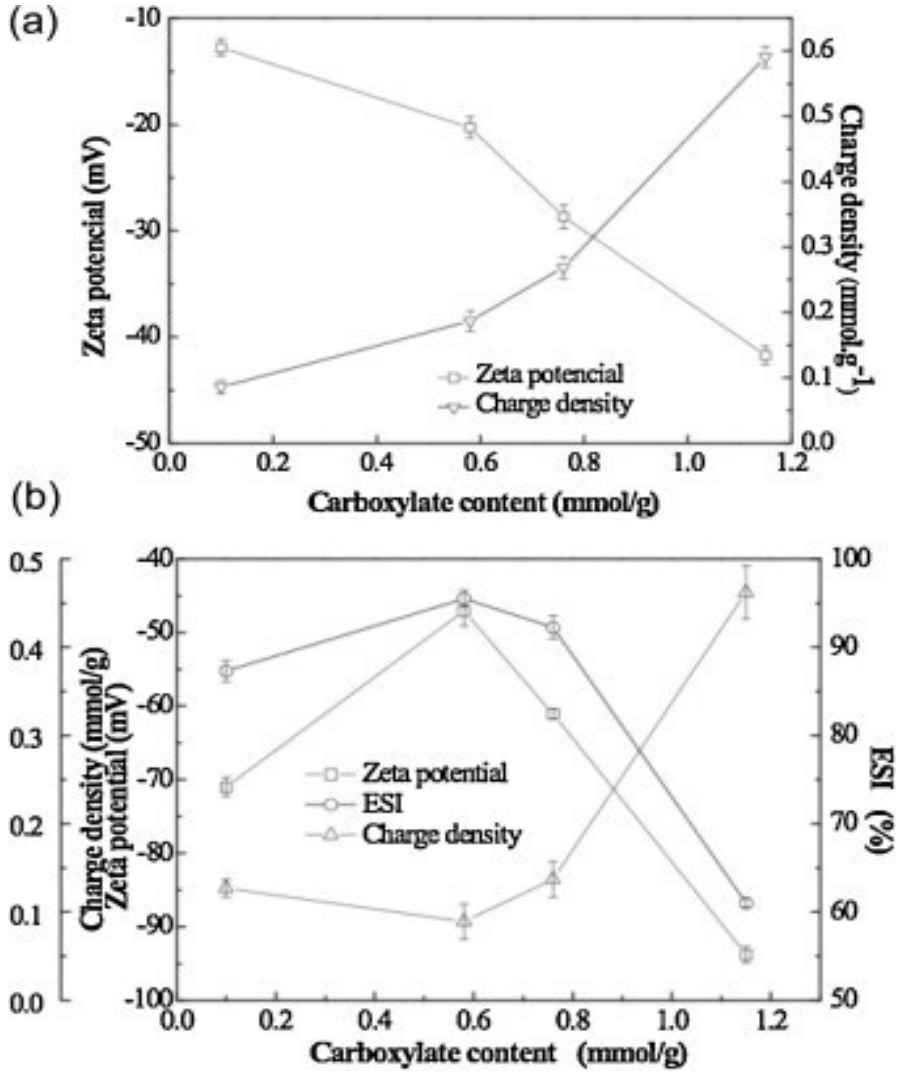


Figure 2-17: Effects of carboxylate content of TOBCs on (a) the zeta potential and charge density of TOBC dispersions, and (b) zeta potential, charge density and (emulsion stability index) ESI of the corresponding TOBC emulsions (The fibril dosage was 0.35 wt.% and ratio of water to oil was 1:1) [50].

Table 2-2: Static contact angles and sizes of BC and TOBC samples [50].

Samples	BC	2-TOBC	6-TOBC	10-TOBC
Contact angle (°)	56.6 ± 2.75	42.7 ± 1.35	41.9 ± 2.05	<5
Size (nm)	> 20,000[a]	4580.4 ± 220	3173.0 ± 150	2993 ± 140

[a] BC length was beyond the detect limit of particle sizer. 20μm were estimated from optical graph of BC (data not shown).

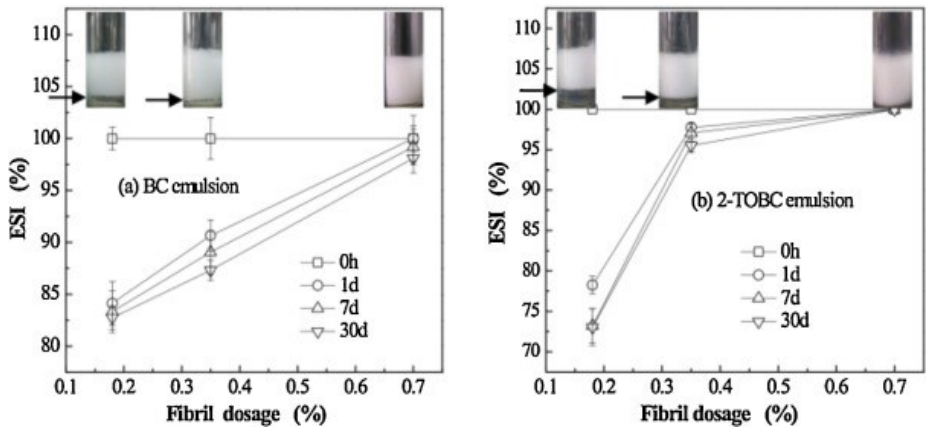


Figure 2-18: Relationships between the ESI and fibril dosage-emulsifier ratio for BC (a) and 2-TOBC (b). The inset photographs show the appearance of the samples after being left to stand for 30 days with different fibril dosages (from left to right, 0.18, 0.35, and 0.70 wt.%). The volume ratio of water phase and oil phase was 1:1. The fibril dosage was indicated by the weight percentage ratio of the water phase [50].

It was shown that the degree of oxidation increased with the amount of oxidising agent used. Using the above protocol, TOBC samples containing 2 mmol g^{-1} (2-TOBC), 6 mmol g^{-1} (6-TOBC), and 10 mmol g^{-1} (10-TOBC) NaClO were created. The carboxyl group contents ranged from 0.58 mmol g^{-1} in 2-TOBC to 1.15

mmol g^{-1} in 10-TOBC. 2-TOBC was shown to be the best particle stabiliser. As seen in Figure 2-17, the absolute value of the zeta potential and charge density increased. The absolute value of wettability also seemed to improve, although this was counterbalanced by the fibril size when producing emulsions. Fibril sizes and contact angles of each of the TOBC sample were given in Table 2-2. Increasing the number of carboxyl groups increases the fibril hydrophilicity and so increases its wettability. This reduced the detach energy of TOBCs from the interface, creating unstable emulsions. This said, the size-reducing effects of oxidation create smaller fibrils that also lower the detach energy at the interface. 2-TOBC was counterbalanced by both wettability and fibril size for stabilising particles. The carboxylation of the TOBC samples was confirmed by FTIR, and the size reduction of the fibrils was confirmed by SEM and AFM. The emulsion was also shown to improve with increasing fibril dosage. This could be seen in Figure 2-18 where the oil: water ratio was given as 1:1, and the fibril dosage was tested at 0.18, 0.35, and 0.70 wt.%. The droplet size was shown to increase with increasing fibril dosage as shown in Figure 2-19. This disagrees with the author's hypothesis and may because of the increased fibril dosage leading to fibril aggregates due to hydrogen bonding. However, increasing the fibril dosage forms a dense cellulose film that resisted coalescence and maintained particle distribution from 0—7 days with little change after 30 days [50].

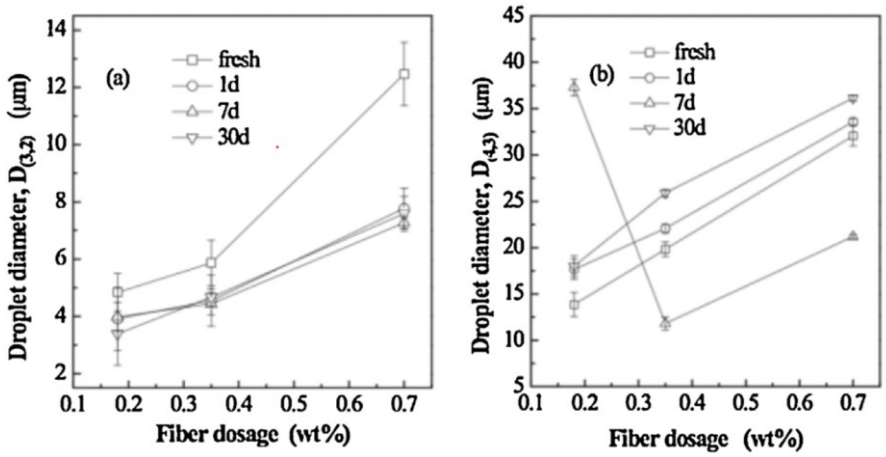


Figure 2-19: Droplet diameters of emulsions stabilized by 2-TOBC with different fibril dosages and storage time (The ratio of oil and water was 1:1) [50].

In addition, Wu *et al.* [51] used TEMPO-oxidised BC pellicles with silver nanoparticles for wound dressing applications. The aim of this study was to synthesise a biocompatible, antibacterial material for wound dressing using bacterial cellulose pellicles. To this end, bacterial cellulose was subjected to TEMPO-mediated oxidation followed by thermal reduction to synthesise silver nanoparticles. Bacterial cellulose pellicles (BCP) were synthesised using *G. xylinu*s. Upon creation of the BCP, one sample was freeze dried for 2 days and cut to a dimension of 15×15 mm. These freeze-dried pieces (~0.2g cellulose) were added to 300 mL water in a 500 mL beaker. 0.018 g TEMPO and 0.1g NaBr were added to the beaker, and the total solution was agitated for 1 hour. NaClO solution (10 mmol g^{-1} cellulose) was added to the solution, triggering the oxidation reaction. The pH for this reaction was maintained at 10 using auto titration with a 0.5 M NaOH solution. The oxidation was allowed to continue for 1 hour followed by quenching with ethanol until the pH no longer changed. The TEMPO-oxidised BCPs (TOBCPs) were then washed 10 times in water. The carboxylate content of the

TOBCP after 1 hour was given as 1.1 mmol g^{-1} cellulose *via* electric conductivity titration using a 0.05 M NaOH solution. This sample was selected for further experiments because the material retained the structure of the original BCP. To synthesise the silver nanoparticles onto the TOBCP surface, TOBCP was immersed in an $AgNO_3$ (1.5 mmol Ag^+ g^{-1} cellulose) solution for 24 hours in the dark. This immersion started an ion exchange between sodium ions at the C6 carboxylate groups with silver ions (Ag+). Once the ion exchange had completed, the newly formed TOBCP/Ag^+ was washed 10 times in water to remove any residual ions. Next the pellicles were placed in a water bath at 100°C for 2 hours to initiate thermal reduction of the TOBCP/Ag^+. As the silver nanoparticles (AgNPs) formed, the pellicle colour shifted, becoming a deeper yellow with increasing reduction time. The newly formed TOBCP with AgNPs is referred to as TOBCP/AgNP.

As previously stated, the carboxyl group content of the TOBCP was 1.1 mmol g^{-1} cellulose, as assayed using electrical conductivity titration. The researchers continued testing with TOBCPs oxidised for 1 hr due to its structural stability and retained density. It was found that increasing oxidation time increased the carboxylate group content. Increasing the carboxylate content results in increasing repulsive forces between the TOBC nanofibers and thus a higher swelling capacity in water. The success of the AgNP synthesis on the TOBCP/AgNP was confirmed by the colour change of the nanofibers to deeper yellow and the appearance of peaks at 2θ values 38.1°, 44.2°, 64.5°, and 77.3° in the corresponding XRD patterns, confirming the FCC structure of the AgNPs. FE-SEM of 200 AgNPs showed an average diameter of 16.5 ± 4.0 nm. XPS confirmed that the ratio of AgNPs on the nanofiber surface:interior was approximately 18:7. AgNPs from thermal reduction

produced larger crystals than those made by $NaBH_4$, and the release rate of Ag^+ from thermal reduction was 12.2% per day over 3 days. To demonstrate biocompatibility, *in vitro* cytotoxicity was performed over 48 hrs in incubation and the NIH3T3 cell viability was shown to be 95.2 ± 3.0% in the presence of TOBCP/AgNP. The antibacterial activity of TOBCP/AgNP was shown to be 100% against *E. coli* and 99.21% against *S. aureus* using growth inhibition zones (GIZ). The water retention value (WRV) of TOBCP/AgNP was shown to be 169%, similar to untreated BCs. BC on its own has a high WRV because of its 3D network and because of the large surface area of the NC nanofibers. Plain TOBCP showed a WRV of 194% due to the carboxylate groups, but it reduces upon the introduction of Ag^+ and AgNPs due to ionic radius effects. AgNPs further slowed down the attraction of water to the carboxylate groups on TOBCP. Nevertheless, TOBCP/AgNP can maintain a moist, antibacterial, and biocompatible environment for promoting wound healing.

In addition, bacterial cellulose (BC) and chitosan (CTS) porous scaffolds were created as potential biomaterials for wound healing in 2010 by Nge *et al*. [20] The microfibrillated BC (MFC) underwent a TEMPO-mediated oxidation followed by integration within a chitosan matrix. The polysaccharides were then crosslinked to create covalent amide bonds, and the porosity and material properties of this final material were tested for biomaterial suitability. To start, BC pellicles were produced using *Acetobacter Aceti* (AJ 12368) and *Hestrin-Schramm* (HS) medium according to the protocol described in Nge and Sugiyama. The pellicles were kept hydrated after purification and fibrillated with a Physcotron NS 50 homogenizer (Microtech Nichion Inc.). To set up the TEMPO-mediated oxidation, 3 g of microfibrillated

cellulose (MFC) was suspended in a mixture of 0.075 g TEMPO, 0.375 g NaBr, and 1 L water. The reaction began once NaClO (4.84 mmol g^{-1} cellulose) was added with stirring. The reaction continued at room temperature and a pH of 10.5 was maintained using 0.5 M NaOH. Once it was observed that no more alkali was being consumed, 5 mL ethanol was added to quench the reaction and the pH was adjusted to 7 with 0.1 M HCl. The TEMPO-oxidised BC suspension underwent several centrifugal washes before being stored at 4°C. From conductometric titration, the carboxylate content of the BC suspension was measured as 0.74 mmol g^{-1} cellulose.

Once the TEMPO-oxidised BC suspension (now referred to as BC) was prepared it was cross-linked to CTS using EDC (1-ethyl-3-(3-dimethyl-aminopropyl) carbodiimide hydrochloride) mediated amide binding. The resulting slurry was then frozen and lyophilized to create the scaffolds. To begin with, a 1% (w/v) chitosan solution was prepared by dissolving Chitosan 100 (MW 150,000 with a degree of deacetylation of ~80%) from Wako Pure Chemicals (Japan), in 0.1 M HCl. This mixture was then filtered through 8 layers of nylon cloth with a mesh size of 50 µm. The authors tried five different ratios of BC/CTS from 20/80 to 60/40 w/w%. In addition, a key molar ratio, specifically the CTS: EDC: NHS (N-hydroxy succinimide) ration, was maintained at 1:1:1 with each shifting BC/CTS ratio. At room temperature, NHS was added to BC under stirring to begin the coupling reaction. CTS was then slowly introduced, and the pH of the mixture was adjusted to 5.5—6.0 with 0.5 M NaOH. The mixture stirred for 30 minutes, and an aqueous EDC solution was added dropwise. The mixture was then left to stir overnight. The next day the mixture underwent dialysis at a pore size of 50 Å to remove excess EDC, NHS, and any residual by-products. After 3 days, the dialysis medium was

exchanged with fresh water multiple times, and the dialysis tubes were immersed in aqueous poly (ethylene glycol), MW 20,000, for 3—4 days. Once this was completed, a concentrated BC/CTS (6—7 mg/mL) slurry was obtained. The BC/CTS slurries were degassed for 2 hrs and distributed into tissue culture plates (48 well, 1 mL/well or 60 mm polystyrene dishes with a volume of 10 mL/dish). The culture plates were then placed in two separate freezer conditions at -30°C and -80°C. The mixtures were allowed to solidify, inducing solid-liquid phase separation between the solvent and the BC/CTS. The mixtures were maintained for 24 hrs at freezing temperatures and then sublimated at 0°C under vacuum (approximately 15 Pa) for 3 days.

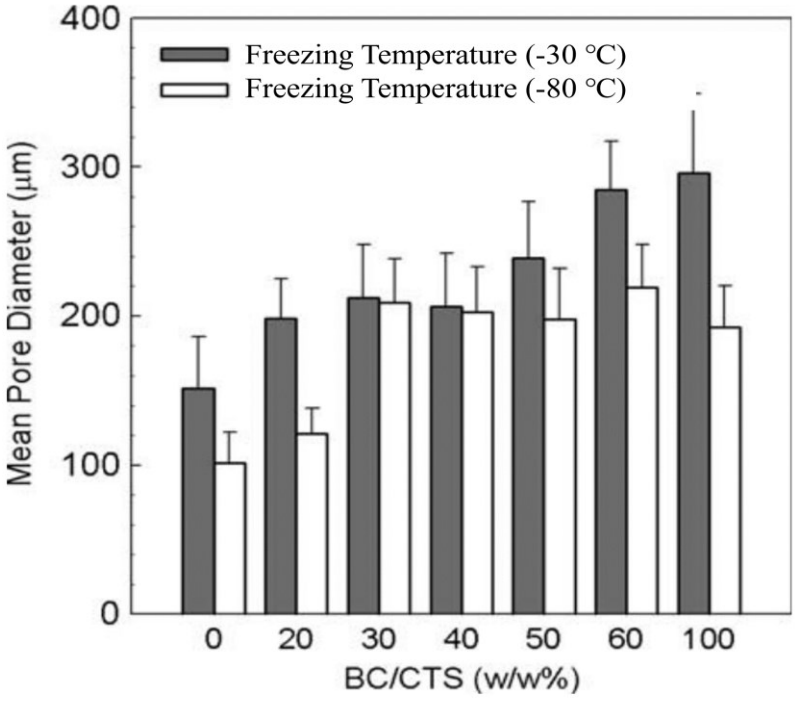


Figure 2-20: Percent weight loss of BC/CTS scaffolds 6 weeks after incubation in 58 ysozyme solution as a function of MFC content (scaffolds are prepared at −30 °C) [20].

The resulting scaffolds were found to have interconnecting pores with mean pore diameters ranging from 198(±26)—284(±32) μm for the BC/CTS scaffolds solidified at -30°C, and 121(±17)—219(±29) μm for the BC/CTS solidified at -80 °C (Figure 2-20). The compressive mechanical properties of the -30 °C and -80°C BC/CTS scaffolds were summarised in Table 2-3. In general, the scaffolds solidified at -80 °C showed less desirable mechanical properties as compared to the BC/CTS scaffolds frozen at -30 °C because of structural non-uniformities and ill-defined pore microstructure. In their dry state, BC/CTS 20/80 and 0/100 solidified at -80°C showed a significantly smaller pore diameter than their counterparts, the 20:80 BC/CTS and 0:100 BC/CTS samples solidified at -30 °C. This resulted in an improvement in the mechanical properties and demonstrated the significant effect of the freezing temperature on the mean pore size of scaffolds containing <20% MFC. The trend in improved compressive mechanical properties with increasing MFC content is observed in the hydrated state. That said, the mechanical properties of both the -30 °C BC/CTS and the -80 °C BC/CTS degraded significantly between the dry and hydrated states.

Table 2-3: Porosity of the BC/CTS scaffolds [20].

MFC content (wt%)	Mean pore size (μm)	Dry state (room temperature)		Hydrated state (in PBS, at 37°C)	
		E^* (kPa)	σ^* (kPa)	E^* (kPa)	σ^* (kPa)
BC/CTS-30 ℃ group [a]					
0	152 ± 34	ND	ND	ND	ND
20	198 ± 26	248 ± 74	4.01 ± 0.28	6.33 ± 1.46	0.31 ± 0.02
30	212 ± 36	363 ± 34	4.76 ± 0.22	14.24 ± 3.16	0.25 ± 0.04
40	206 ± 36	383 ± 74	4.87 ± 0.53	19.97 ± 0.94	0.36 ± 0.03
50	239 ± 38	583 ± 95	7.16 ± 1.46	21.29 ± 1.82	0.50 ± 0.18
60	284 ± 32	702 ± 142	8.41 ± 1.59	32.22 ± 16.13	0.67 ± 0.10
100	296 ± 53	384 ± 73	5.48 ± 0.71	6.13 ± 0.13	0.21 ± 0.08
BC/CTS-80 ℃ group [b]					
0	101 ± 21	ND	ND	ND	ND

20	121 ± 17	450 ± 127	5.39 ± 0.19	5.49 ± 0.80	0.12 ± 0.05
30	209 ± 29	345 ± 51	4.74 ± 0.20	7.49 ± 0.47	0.17 ± 0.06
40	203 ± 30	347 ± 3	5.02 ± 0.43	13.55 ± 2.88	0.29 ± 0.05
50	198 ± 34	406 ± 18	5.39 ± 0.91	17.20 ± 5.08	0.41 ± 0.08
60	219 ± 29	505 ± 80	7.82 ± 2.39	19.64 ± 5.28	0.40 ± 0.16
100	192 ± 28	225 ± 99	4.22 ± 0.43	6.31 ± 2.43	0.28 ± 0.06

*The data were shown by mean ± standard deviation.

[a, b] The BC/CTS scaffolds with various MFC content are prepared at freezing temperature of -30 and -80°C.

Additionally, Kim *et al.* [52] developed a muscular actuator using TEMPO oxidised bacterial cellulose, ionic liquid, and graphene. The idea was to make a bioelectronic muscular actuator with biofriendly, biodegradable, and biocompatible functionalities for human-related bioengineering, biomimetic robots, and biomedical active devices.

The bioelectronic actuator was produced in four phases. First, BC pellicles were produced *via* a static culture using a Hestrin and Shramm medium. 1 g BC pellicles were then stirred into a mixture of 100 mL deionized water, TEMPO (0.016g, 0.1 mmol), and NaBr (0.1g, 1 mmol). To begin the TEMPO-mediated oxidation, 12% NaClO solution (3.1 g, 5.0 mmol) was agitated into the BC slurry at room temperature. A 0.5 M NaOH solution was used to adjust the pH of the slurry to ~10. Upon completion of the reaction, the TOBC was washed in deionized water several times. A TOBC dispersion was created by stirring 0.45 g TOBC into 100 mL deionized water. Once the dispersion was created, preparation of chemically modified graphene began. Graphene nanoplatelets (GNs, AO-2) with a specific surface area of 100 $m^2 g^{-1}$ and a purity of 99.9% were purchased from a commercial supplier (Graphene Supermarket, USA). The graphene was then modified by using 63% nitric acid (HNO_3) and 98% sulfuric acid (H_2SO_4) (1:3 v/v). The chemically modified graphene and the TOBC dispersion were then combined with an ionic liquid to prepare the TPBC-IL-G films. Chemically modified graphene and TOBC were stirred together at mixing ratios of 0.05 and 0.1%. After stirring for 24 hrs, 0.5 g [EMIM][BF_4] (1-ethyl-3-methylimidazolium tetrafluoroborate, >98%), purchased from Ionic Liquids Technologies (IOLITEC, Germany), was added to the dispersion. The resulting TOBC-IL-G dispersion was ultrasonicated for 1 hour,

drop cast, and dried at 65°C for 24 hrs in a vacuum oven. To complete the actuator, the now dried TOBC-IL-G films were dipped into a PEDOT: PSS solution and dried at 65°C for 3 hours in a vacuum oven.

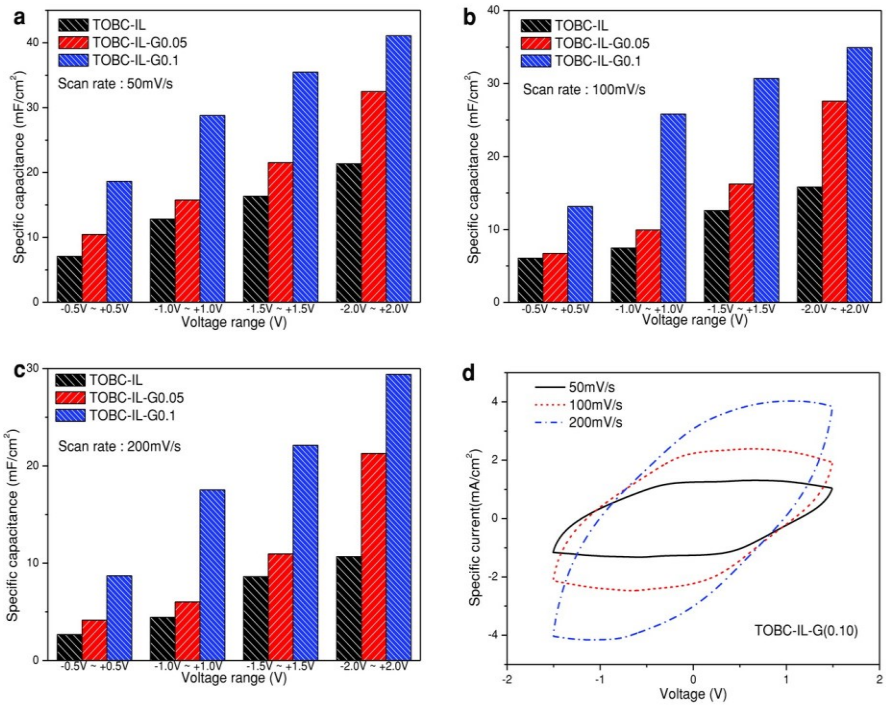


Figure 2-21: Specific capacitance and CV curves of TOBC-IL-G actuators according to scan rate: (a) 50 mV s^{-1}, (b) 100 mV s^{-1}, and (c) 200 mV s^{-1}; (d) current–voltage curves of TOBC-IL-G composite actuator at various scan rates [52].

Table 2-4: Electrochemomechanical properties of TOBC-G-IL composite membranes [52].

Membrane	IEC ($meq.g^{-1}$)	IL uptake/swelling ratio	Capacitance ($\mu F\ cm^{-2}$ /mF g^{-1})	Tensile modulus (Gpa)	Tensile strength (Mpa)	Elongation (%)	Ionic conductivity ($S\ cm^{-1}$)
BC	1.15			3.145 ± 0.182	283.04 ± 42.67	11.04 ± 0.56	8.14×10^{-6}
BC-IL	-	27.34/11.63		-	-		1.04×10^{-4}
TOBC	1.51	38.82/17.97		0.469 ± 0.031	39.68 ± 4.94	14.82 ± 1.33	1.59×10^{-3} a)
TOBC-G (0.05 wt%)	1.56	40.95/20.97		-	-		2.26×10^{-3} a)
TOBC-G (0.10 wt%)	1.63	48.47/24.49		-	-		3.72×10^{-3} a)
TOBC-IL	-	50.0	37.13/0.975	0.353	43.36	18.81	2.04×10^{-4}
TOBC-IL-G (0.05 wt%)	-	50.0	43.32/1.356	0.479	62.02	19.37	3.10×10^{-4}
TOBC-IL-G (0.10 wt%)	-	50.0	72.48/2.115	0.576	69.46	19.73	4.50×10^{-4}

a) These values were measured in fully hydrated condition.

The carboxylate group content of the TOBC was given as 1.3 mmol g^{-1}. SEM analysis confirmed the effective and strong binding between nanofibrous TOBC, ionic liquid, and chemically modified graphene. The ionic liquid was found to first anchor onto the nanofibers, and then the chemically modified graphenes were randomly dispersed onto the resulting composite. Better dispersion of the TOBC-IL-G membranes resulted in increased nanocomposting between the TOBC and chemically modified graphene, resulting in an immediately apparent colour change from grey to black. The intensity of the colour increased with graphene loading, whilst the presence of ionic interactions was confirmed using FTIR. In particular, a characteristic peak at 1605 cm^{-1}, which indicates C=O stretching of the carboxylic group, confirmed the presence of ionic interactions between the TOBC and the ionic liquid. This was further supported by the presence of additional peaks at 3165 and 3120 cm^{-1}. A peak at 750 cm^{-1} corresponded to the C-H and BF_4 groups of neat [EMIM][BF_4]. These results demonstrated the formation of anionic membranes that exhibited both carboxyl group and ionic interactions. The strong ionic interactions of the hydroxyl groups with chemically modified graphene appeared at 3410 cm^{-1}. XRD confirmed that the characteristic BC crystalline and amorphous regions were maintained by TOBC-IL-G. Additionally, (0 0 2) peaks and (0 0 4) peaks were observed at respective 2θ values of 26.5 and 54.6 degrees, confirming the presence of graphene nanoplatelets on the surface of the TOBC nanofibers. The electromechanical properties of TOBC-IL-G were summarised in Table 2-4. In particular, TOBC-IL exhibited a superior elongation of ~20%, whilst TOBC-IL-G (at 0.10wt%) and TOBC-IL exhibited tensile modulii of 63% and 60%, respectively. As the mixing proportions of TOBC and chemically modified graphene increased

(0.05 wt% to 0.1 wt%) the IEC and ionic liquid uptake values increased. Of the samples produced, TOBC-IL-G (0.1 wt%) demonstrated the largest specific capacitance of 72.45 μF cm^{-2} (2.115 mF g^{-1}). It was shown that the TOBC-IL-G actuators exhibited much larger bending actuations and faster response times than those of pure TOBC. The specific capacitance and CV curves of the TOBC-IL-G actuators were given in Figure 2-21. Peak to peak displacement of the TOBC-IL-G actuators at ±1 V reached 4.0 mm and the actuator maintained durable actuation for 3 hours under a continuous sinusoidal electrical oscillation of ±1V at a frequency of 0.5 Hz.

2.5 Concluding remarks

It is evident from the literature review of this thesis that the TEMPO-mediated oxidation of BC pellicle directly will lead to the complete disintegration of the pellicle, producing a homogenous suspension of TOBC in water, which can then be subsequently processed into various advanced nanocellulosic materials. However, an important question still remains unanswered in the literature: "*What happens if a sheet of dried and well-consolidated BC nanopaper undergoes TEMPO-mediated oxidation reaction?*" Will the BC nanopaper swell into a TOBC hydrogel or will it disintegrate, forming a suspension of TOBC in water? This remainder of this thesis will close this missing knowledge gap.

Chapter 3 – TEMPO-mediated oxidation of bacterial cellulose nanopaper

3.1 Introduction

This chapter reports what the TEMPO-mediated oxidation of a dried and well-consolidated sheet of BC nanopaper. A high grammage BC nanopaper was first manufactured and TEMPO-oxidised under the NaClO/NaBr system at different NaClO concentrations.

3.2 Experimental

3.2.1 Materials

BC pellicles (dry grammage ~100 g m^{-2}) with a water content of 99 wt.-% were purchased from a commercial retailer (Vietcoco International Co. Ltd., Ho Chi Minh City, Vietnam) and were purified prior to subsequent use following the previously described protocol [53]. Sodium hydroxide pellets (AnalaR NORMAPUR, purity > 99%), sodium hypochlorite solution (GPR RECTAPUR, 12 % Cl2), hydrochloric acid (AnalaR NORMAPUR, 37%) and sodium borohydride (BioXtra, purity ≥ 99%) were purchased from VWR International Ltd. (Lutterworth, UK). (2,2,6,6-Tetramethylpiperidin-1-yl)oxyl (TEMPO) (Aldrich, purity ≥ 98%), sodium bromide (BioXtra, purity ≥ 99%) and sodium chloride (Riedel-de-Haën, purity ≥ 99%) were purchased from Sigma-Aldrich (Dorset, UK). These chemicals were used as received without further purification.

3.2.2 Preparation of BC nanopaper

To produce the BC nanopaper, a purified BC pellicle (80 mm × 80 mm × 10 mm) was first gently pressed between filter papers (Qualitative filter paper 413, VWR, Lutterworth, UK) to remove excess water on the surface of the pellicle. It was then sandwiched between fresh filter and blotting papers (Whatman Qualitative filter paper, Grade 3, GE Health Care, Buckinghamshire, UK), followed by press-drying at 55°C with a compaction force of 100 N for 10 min. The pressed BC pellicle was carefully removed, and the press-drying step was repeated with fresh filter and blotting papers until the weight of the press-dried BC remained constant. At this stage, the press-dried BC— now in its dried and well-consolidated nanopaper form with a nominal thickness of ca. 80 μm— was trimmed to dimensions of 70 mm × 70 mm prior to subsequent use.

3.2.3 TEMPO-mediated oxidation of BC nanopaper

The TEMPO-mediated oxidation of BC nanopaper was performed following the protocol for the TEMPO-oxidisation of cellulose pulp, described previously by Saito *et al.* [3] Briefly, 49.5 mg of TEMPO and 275 mg of NaBr were first dissolved in 825 mL of deionised water under magnetic stirring. BC nanopaper (0.55 g) was then suspended in this solution. To this, the desired amount of NaClO solution, corresponding to 10, 20 and 30 mmol of NaClO per gram of dry BC, respectively, was then added slowly to initiate the oxidation of the BC nanopaper. The pH of the reaction was monitored (HI-2550, Hanna Instruments, UK) and maintained at a value of 10 through the titration of a 0.5 M sodium hydroxide solution. The oxidation reaction was conducted for 5 hours at room temperature. After the

reaction, the TEMPO-oxidised BC, now in the form of a swollen hydrogel, was carefully removed from the reaction medium and rinsed with fresh deionised water until a neutral pH was attained. The TEMPO-oxidised BC hydrogel was then reduced with $NaBH_4$ (0.1 g of $NaBH_4$ per g of dry BC) by suspending the TEMPO-oxidised BC hydrogel in a solution of $NaBH_4$ in deionised water (825 mL) for 3 h at room temperature with magnetic stirring to convert any remaining aldehydes and ketones to hydroxyl groups [54]. This reduction step was carried out to prevent the heat-induced discolouration of the TEMPO-oxidised BC hydrogel. After this reduction reaction, the TEMPO-oxidised BC hydrogel was rinsed with deionised water until a neutral pH was attained. The reduced, TEMPO-oxidised BC hydrogel was then subjected to an ion-exchange treatment to convert the sodium carboxylate groups to free carboxyl groups. The ion-exchange treatment was performed by suspending the reduced TEMPO-oxidised BC hydrogel in 825 mL of HCl solution at a pH of 1 for 1 h under magnetic stirring [55]. Thereafter, the ion-exchanged TEMPO-oxidised BC hydrogel was rinsed thoroughly with deionised water until a neutral pH was attained. In some experiments, the TEMPO-oxidised BC hydrogels were press-dried under a force of 9 kN at 105°C for 5 min between filter and blotting papers in a heated hydraulic press (4122CE, Carver Inc., Wabach, IN, USA).

3.2.4 Carboxylate content of TEMPO-oxidised BC hydrogels

The carboxylate content of the TEMPO-oxidised BC was determined using the conductometric titration method as described by Saito and Isogai [2], and Katz *et al.* [56]. Briefly, 0.1 g (dry basis) of the TEMPO-oxidised BC hydrogel was blended (Optimum 9400, Froothie Ltd., Cranleigh, UK) in 200 mL of deionized water to

first produce a homogenous TEMPO-oxidised BC-in-water suspension. 10 mL of 0.01 M NaCl solution was then added to this suspension. The pH of the suspension was adjusted to a value of 3 through the titration of 0.1 M HCl. A 40 mM NaOH solution was then pipetted at a rate of 0.2 mL min^{-1} until the pH of the TEMPO-oxidised BC suspension reached a value of 11. Throughout the NaOH titration process, the conductivity of the suspension was recorded (HI-2550, Hanna Instruments, UK) and the carboxylate content of the TEMPO-oxidised BC hydrogel was calculated based on the conductivity of the weak acid groups. All measurements were duplicated.

3.2.5 Swelling Ratio (SR) and Water Retention Value (WRV) of TEMPO-oxidised BC hydrogels

The swelling ratio of the BC nanopaper press-dried into a TOBC hydrogel was quantified using simple thickness gain measurement. Prior to the TEMPO oxidation, a micrometer was used to measure the thickness of the BC nanopaper (t_{d}). TOBC hydrogels were immersed in excess deionised water for 800 h (first 5 h was reaction time of TEMPO oxidation) to ensure that the hydrogels have swelled to their equilibrium state. Prior to measuring the thickness of wet TOBC hydrogel (t_{w}), the surface excess water was removed by dabbing with filter paper (Qualitative filter paper 413, VWR, Lutterworth, UK). The thicknesses of TOBC hydrogels were measured frequently during the immersion period. The swelling ratio of the BC nanopaper into a TOBC hydrogel upon TEMPO-mediated oxidation was calculated as:

$$\mathrm{SR} = \left(\frac{t_\mathrm{w} - t_\mathrm{d}}{t_\mathrm{d}}\right) \tag{3.1}$$

The Water Retention Value of the TEMPO-oxidised BC hydrogel was determined using a simple mass gain measurement. To determine the wet mass of the TEMPO-oxidised BC hydrogel (m_w), the hydrogel was immersed in excess deionised water for 72 hours until an equilibrium was reached. Vacuum filtration was then used to drain away the excess liquid until dripping from the TEMPO-oxidised BC hydrogel was no longer observed. The TEMPO-oxidised BC hydrogel was then sandwiched between filter papers and press-dried with a force of 9 kN at 105°C for 30 min using a heated hydraulic press (4122CE, Carver Inc., Wabach, IN, USA) to obtain the dry mass of the TEMPO-oxidised BC (m_d) in the hydrogel. The WRV was calculated using the formula:

$$\mathrm{WRV} = \frac{m_w - m_d}{m_d} \tag{3.2}$$

3.2.6 Morphology of (TEMPO-oxidised) BC hydrogels

Scanning electron microscopy (SEM) was used to investigate the internal morphologies of the BC hydrogels. SEM micrographs were obtained using a large chamber scanning electron microscope (Hitachi S-3700N, Tokyo, Japan) operating at an accelerating voltage of 10 kV. Prior to SEM analysis, the hydrogels were frozen in liquid nitrogen for 15 mins and freeze-dried using a laboratory-grade freeze-drier (Alpha 1-2 LDplus, Martin Christ, Osterode, DE). The samples were then mounted onto aluminium stubs using carbon tabs and sputter coated with Au (Agar^{TM} auto sputter coater, Stansted, UK) for 20 seconds with a coating current of

40 mA. SEM was conducted by Daniela Wloch due to Covid-19 imposed laboratory access restrictions.

3.2.7 Crystallinity of (TEMPO-oxidised) BC.

X-ray diffraction (XRD) patterns of the TEMPO-oxidised BCs were obtained from film samples using an X-ray diffractometer (PANalytical X'pert Pro, PANalytical Ltd., Cambridge, U.K.). The measurements were taken between 2θ =10—28° using a step size of 0.05° and a scan speed of 0.1° s^{-1}. The diffractometer was equipped with a 1.54 Å Cu Kα X-ray source. The crystallinity ($\boldsymbol{\chi_c}$) of the samples was calculated based on the area under the XRD curve after baseline correction and peak deconvolution using the following equation.

$$\chi_{\mathrm{c}} = \frac{A_{\mathrm{c}}}{A_{\mathrm{c}} + A_{\mathrm{a}}} \times 100 \tag{3.2}$$

where A_c and A_{a} are the areas of the XRD pattern ascribed to the crystalline and the amorphous part of the cellulose, respectively. XRD was conducted by Daniela Wloch due to Covid-19 imposed laboratory access restrictions.

3.2.8 Porosity of (TEMPO-oxidised) BC films.

The absolute densities (ρ_A) of the TEMPO-oxidised BCs was determined using He pycnometry (Accupyc II 1340, Micromeritics Ltd., Hexton, UK). The ρ_A of the neat BC was taken 1.60 g cm^{-3} based on data presented in the literature [57]. To evaluate the envelope density of the (TEMPO-oxidised) BC films (ρ_E), a micrometer was used to first measure the thickness of the films. With the thickness known, the

envelope volume was determined and ρ_E was calculated by taking the ratio between the mass and envelope volume of the films. The porosity (P) of the film was then obtained using the following equation:

$$P = 1 - \frac{\rho_E}{\rho_A} \tag{3.3}$$

3.2.9 Tensile Properties of (TEMPO-oxidised) BC films.

Tensile testing of the TEMPO-oxidised BC films was conducted in accordance with ASTM D632-14. Rectangular shaped test specimens were cut from the films using a manual cutting press (ZCP 020, Zwick Roell Ltd., Herefordshire, UK); the test specimens had overall lengths of 40 mm and widths of 5 mm. Tensile tests were conducted using a micro-tensile tester (model MT-200, Deben UK Ltd., Woolpit, UK) equipped with a 200 N load cell. After mounting a test specimen onto the micro-tensile tester, the exposed specimen length was 25 mm. Prior to loading the specimen under uniaxial tension, the surface of the test specimen was marked with a speckle pattern; the strain of the test specimens was evaluated by monitoring the movement of this pattern using a noncontact video extensometer (iMetrum Ltd., Bristol, UK). All test specimens were loaded with a crosshead displacement speed of 0.5 mm min^{-1}, which corresponded to a strain rate of 3×10^{-4} % s^{-1}. A total of 5 specimens were tested for each sample.

3.3 Results and discussion

3.3.1 The mechanism of hydrogel formation from BC nanopaper

Press-drying of BC pellicles (Figure 3-1a) produced a dried and well-consolidated network of BC nanofibrils, more commonly known as a BC nanopaper (Figure 3-1b). When the BC nanopaper was immersed in water, it did not rehydrate into its original pellicle form (Figure 3-1c). This can be attributed to (i) the highly crystalline nature of BC [58, 59], which prevents intra-fibril swelling and (ii) inter-fibril hornification (*i.e.*, the irreversible hydrogen bond formation between adjacent cellulose fibrils upon drying) [60, 61]. For the latter, the high surface area of BC nanofibrils (measured at 41 m^2g^{-1}) [62] leads to a large number of contact or physical crosslinking points between adjacent BC nanofibrils *via* hydrogen bonding, meaning that the BC nanopaper remains stable in water. When the BC nanopapers were subjected to TEMPO-mediated oxidation, they swelled into hydrogels (Figure 3-1(d—f), corresponding to TEMPO-mediated oxidation of BC nanopapers using 10, 20 and 30 mmol of NaClO per g of dry BC, respectively). These TEMPO-oxidised BC hydrogels were found to be robust and water stable as they did not disintegrate under prolonged (> 1 month) magnetic stirring in water.

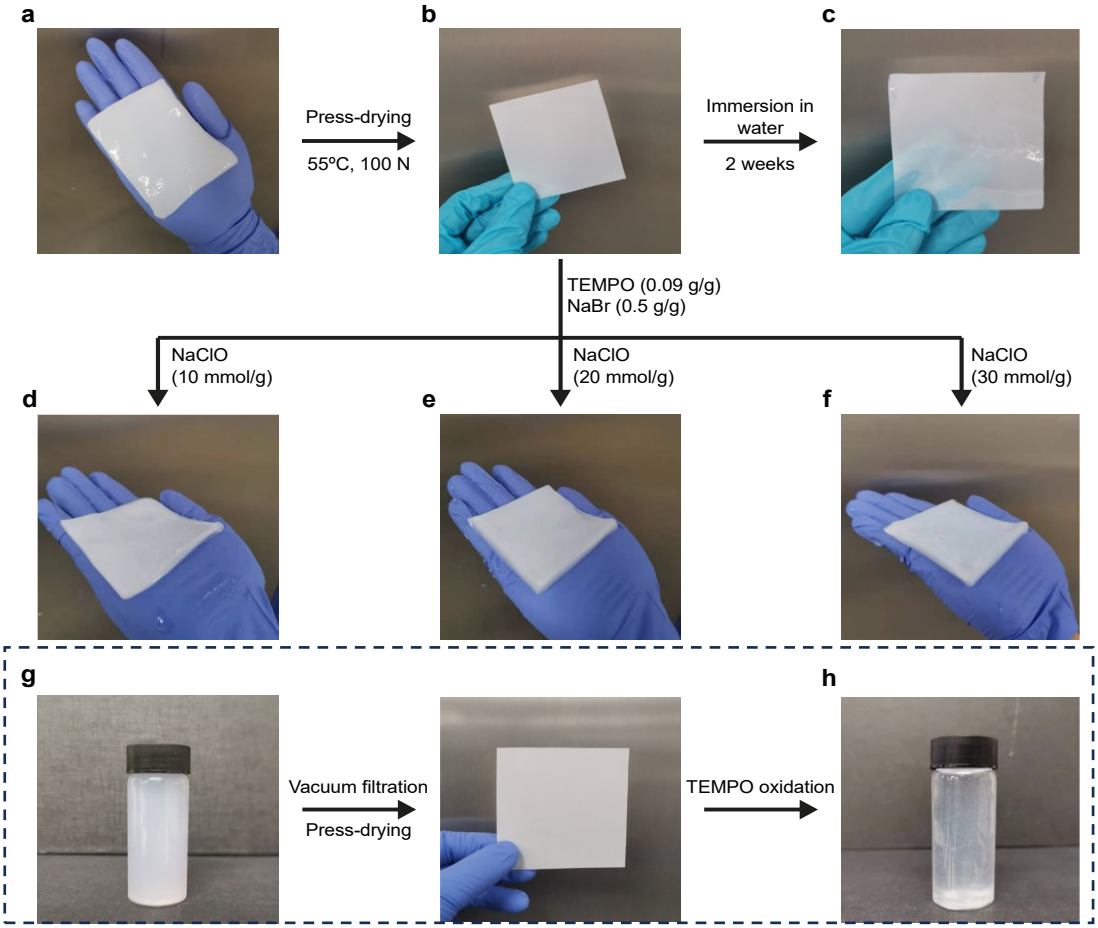


Figure 3-1：(a) BC pellicle containing *ca*. 99 wt.-% water; the press-drying of a BC pellicle produces (b) a dried and well-consolidated BC nanopaper. (c) BC nanopaper after immersion in water at room temperature for two weeks, showing that a BC nanopaper cannot be rehydrated to its original pellicle form. (d—f) The visual appearance of TEMPO-oxidised BC hydrogels produced from oxidation of BC nanopaper using (d) 10 mmol g^{-1} of NaClO, (e) 20 mmol g^{-1} of NaClO and (f) 30 mmol g^{-1} of NaClO, respectively. (g) A homogenous suspension of BC-in-water, followed by vacuum filtration and press-drying to produce BC nanopaper. (h) The outcome of TEMPO-mediated oxidation of BC nanopaper produced from a disintegrated BC pellicle using an NaClO concentration of 10 mmol g^{-1}.

To ascertain whether TEMPO-mediated oxidation was necessary to cause the BC nanopaper to swell into a hydrogel, a BC nanopaper was immersed in NaClO/NaBr, TEMPO/NaBr and NaClO/TEMPO solutions under magnetic stirring for 5 h. No swelling of the BC nanopaper was observed in these solutions, confirming that TEMPO-mediated oxidation is indeed required to swell the BC nanopaper to a hydrogel. In addition to the direct press-drying of a BC pellicle, nanopapers can also be produced by first disintegrating a BC pellicle using a blender to produce a homogenous suspension of BC-in-water, followed by filtration and press-drying [57, 63-65] (Figure 3-1g). Therefore, this chapter investigated whether the same swelling effect could also be achieved by the TEMPO-mediated oxidation of a BC nanopaper produced *via* this method. To our surprise, the BC nanopaper disintegrated during the oxidation reaction instead of swelling into a water stable hydrogel (Figure 3-1h), even at the lowest NaClO concentration used in this work. These results suggest the importance of the starting BC network.

3.3.2 Morphology of neat BC nanopaper and TEMPO-oxidised BC hydrogels

To further investigate the mechanism behind the swelling of the BC nanopaper made from pristine BC pellicle into a hydrogel upon TEMPO-mediated oxidation, SEM analysis was performed. Morphologically, BC nanopapers possess a layered structure consisting of thin nanocellulose sheets (Figure 3-2a); a similar layered structure has also been observed by numerous researchers [33, 66, 67]. The internal morphology of the TEMPO-oxdised BC hydrogels, on the other hand, contains both thin nanocellulose sheets as well as loose BC nanofibrils in between the sheets (Figure 3-2b-d). It is well-known that at the contact or physical crosslinking points

between adjacent BC nanofibrils, the hydroxyl groups remain inaccessible [68-70]. Therefore, the oxidation reaction of the BC nanopaper made from pristine BC pellicles can only proceed from the accessible hydroxyl groups in the exposed nanofibrils within the nanopaper network structure, which are found in between the thin nanocellulose sheets. As the reaction progresses, water molecules penetrate the nanopaper structure as its sodium carboxylate groups are hydrophilic. This then gives rise to electrostatic repulsions between the TEMPO-oxidised BC nanofibrils, causing the nanopaper to swell into a hydrogel. Pristine BC pellicles consist of a *pseudo*-continuous network of BC nanofibrils, hypothesised to be a result of continuous fibril synthesis during cell division [71-73] (Figure 3-2e). As a result, the TEMPO-oxidation of BC nanopapers made from pristine BC pellicles produces water stable TEMPO-oxidised BC hydrogels; disintegrating the BC pellicles disrupts this continuity [57]. Consequently, the BC nanopaper made from disintegrated BC pellicles disintegrated upon TEMPO-oxidation.

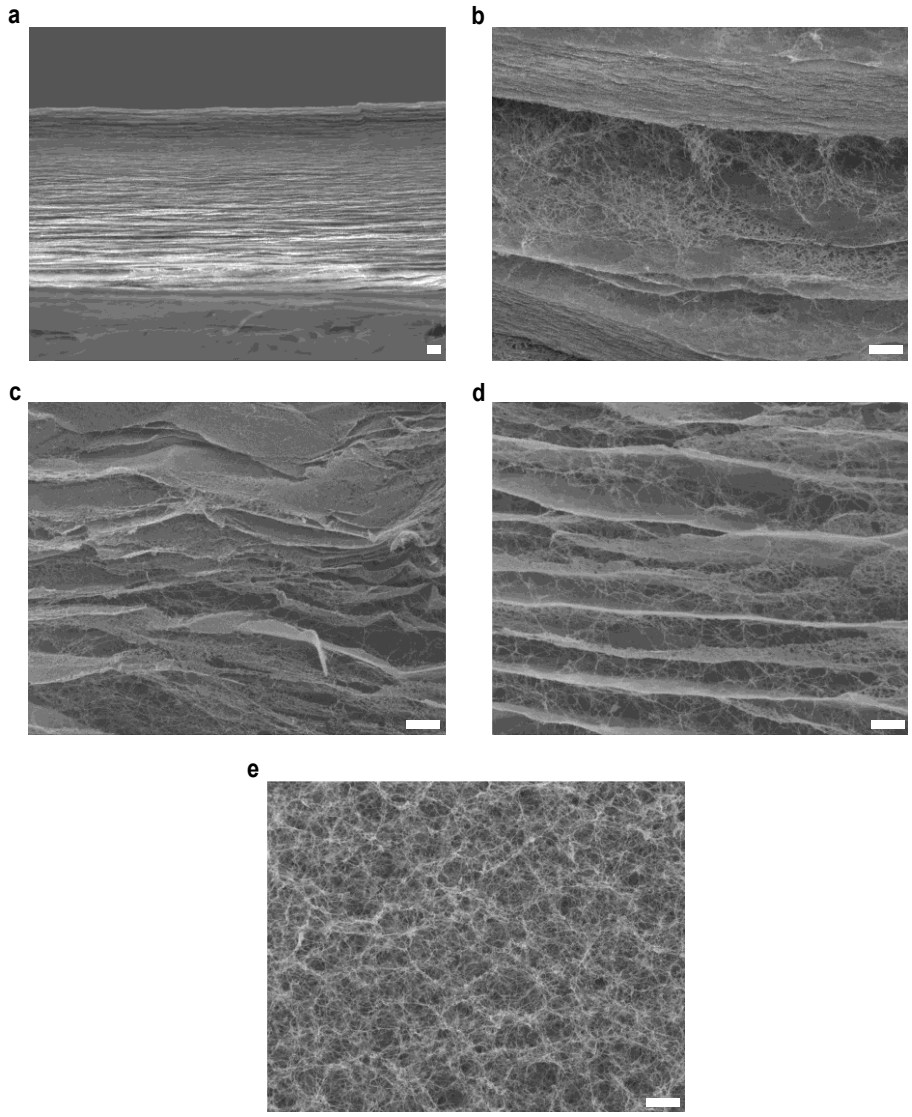


Figure 3-2: SEM micrographs of (a) a neat BC nanopaper, and (b—d) TEMPO-oxidised BC hydrogels modified with (b) 10 mmol g^{-1}, (c) 20 mmol g^{-1} and (d) 30 mmol g^{-1} of NaClO, as well as (e) a neat BC pellicle. Scale bar = 4 μm.

3.3.3 The carboxylate content of TEMPO-oxidised BC hydrogels

Figure 3-3 summarises the carboxylate content of TEMPO-oxidised BC hydrogels as a function of NaClO concentration added. A carboxylate content of 0.72 mmol g^{-1} was achieved for BC nanopapers that were TEMPO-oxidised using 10 mmol g^{-1} NaClO. Increasing the concentrations of NaClO to 20 mmol g^{-1} and 30 mmol g^{-1}

increased the carboxylate content to 1.24 mmol g^{-1} and 1.45 mmol g^{-1}, respectively. Wu *et al.* [51] studied the efficiency of TEMPO-mediated oxidation of freeze-dried BC at NaClO concentrations of 10 mmol g^{-1} as a function of reaction time. At reaction times similar to this study, the authors obtained a carboxylate content of 1.6 mmol g^{-1}, double that of what this study has obtained at the same NaClO concentration. As a reference, this study also performed TEMPO-oxidation directly on never-dried BCs at an NaClO concentration of 10 mmol g^{-1}. A carboxylate content of 1.32 mmol g^{-1} was obtained. However, the resulting TEMPO-oxidised BC hydrogel was not robust and disintegrated in water. Nonetheless, these results agree both with the reduced accessibility of BC nanopaper's hydroxyl groups due to interfibril hornification, and with proposed mechanism in this study, which assumes that the oxidation reaction can only proceed from the exposed BC nanofibrils [47, 74]. The efficiency of TEMPO-oxidation of cellulose is a function of pH, reaction time and NaClO-to-cellulose concentration used, however the influence of the accessible hydroxyl groups on the resulting carboxylate content has rarely been commented on. Saito *et al*. [3] previously reported that both never-dried and once-dried cellulose pulp are equally susceptible to TEMPO-oxidation reactions. However, this does not seem to be the case for dried and well-consolidated nanocellulose networks, presumably due to strong interfibril hornification between the nanofibrils compared to cellulose pulps.

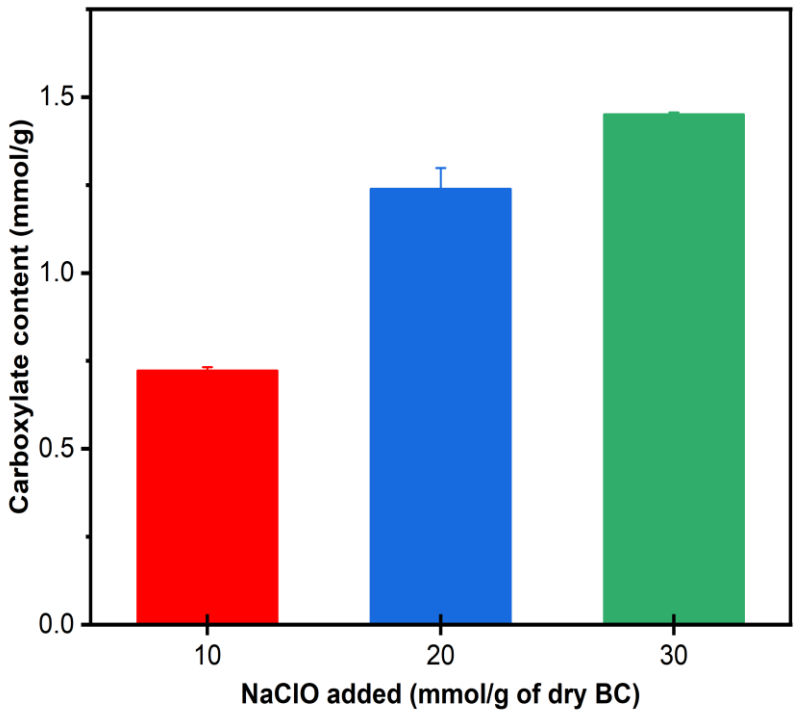


Figure 3-3: Carboxylate content of the TEMPO-oxidised BC hydrogels.

3.3.4 Swelling Ratio (SR) and Water Retention Value (WRV) of TEMPO-oxidised BC hydrogels

Figure 3-4a and b show the swelling ratio of the BC nanopaper due to TEMPO-mediated oxidation and the water retention value (WRV) of the TEMPO-oxidised BC hydrogels with different carboxylate contents, respectively. It can be seen from these figures that both the swelling ratio and WRV increase with increasing carboxylate content. The WRV reflects the swelling of the BC nanopaper into water stable TEMPO-oxidised BC hydrogels and is influenced by charge density. It should be noted however that both the swelling ratios and WRVs did not recover to the values the BCs possessed in their original pellicle forms.

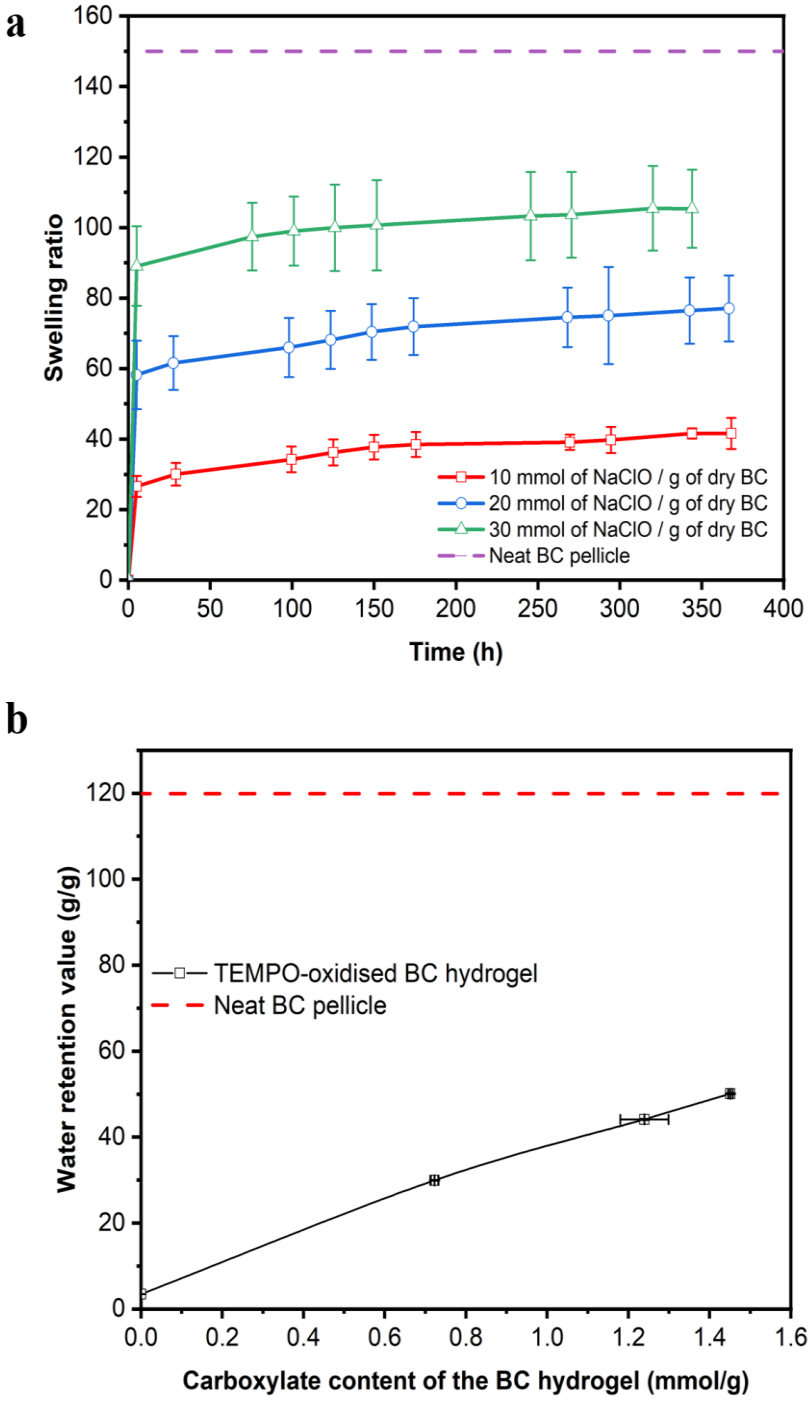


Figure 3-4: (a) swelling ratio, (b) water retention value of the TEMPO-oxidised BC hydrogels.

3.3.5 Crystallinity of (TEMPO-oxidised) BC

The X-ray diffraction patterns of the (TEMPO-oxidised) BCs are shown in Figure 3-5. The peaks at 2θ = 14.5°, 16.5° and 22.5° correspond to the (100), (010) and (110) lattice planes of cellulose-Iα [75]. No peak shift or the appearance of new peaks was observed. The degree of crystallinity for all three of the (TEMPO-oxidised) BCs were calculated to be ~88%, which implies that the TEMPO-oxidation of BC occurs essentially only on the surface of the BC nanofibrils, consistent with the findings by Saito *et al*. [2, 47]

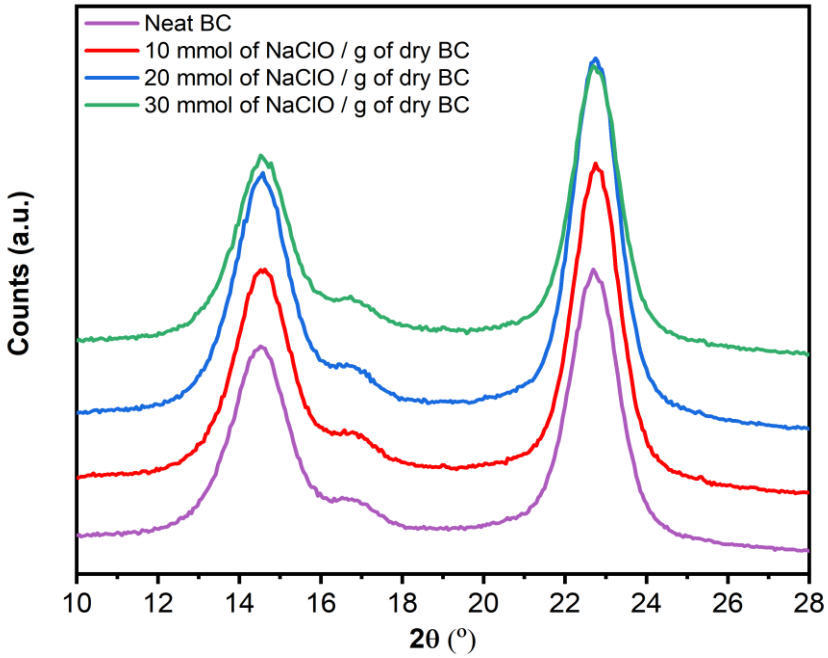


Figure 3-5: X-ray diffraction patterns of the (TEMPO-oxidised) BC.

3.3.6 Is the TEMPO-mediated oxidation of BC nanopaper kinetically or diffusion limited?

This study further ascertains whether the TEMPO-mediated oxidation of BC nanopaper is kinetically or diffusion limited at the start of the oxidation reaction. This is because BC nanopapers possess low water permeances [76]. As BC nanopaper is essentially a stack of thin nanocellulose sheets (Figure 3-2a), the oxidation reaction may first proceed from the surface of the BC nanopaper. This then causes an initial swelling, exposing the hydroxyl groups in subsequent nanocellulose sheets to oxidation until the whole nanopaper structure swells into a TEMPO-oxidised BC hydrogel. If the TEMPO-mediated oxidation of BC nanopaper is diffusion limited at the start of the oxidation reaction, the initial rate of reaction will not be a function of NaClO concentrations added. On the other hand, if the TEMPO-mediated oxidation of BC nanopaper is kinetically limited at the start, the initial rate of reaction will be influenced by the concentration of NaClO added. Therefore, the TEMPO oxidation reaction was conducted as a function of reaction time at various NaClO concentrations (Figure 3-6). It was found that the initial carboxylate content of the TEMPO-oxidised BC was a function of NaClO concentration used; this implies that the initial rate of reaction is kinetically limited.

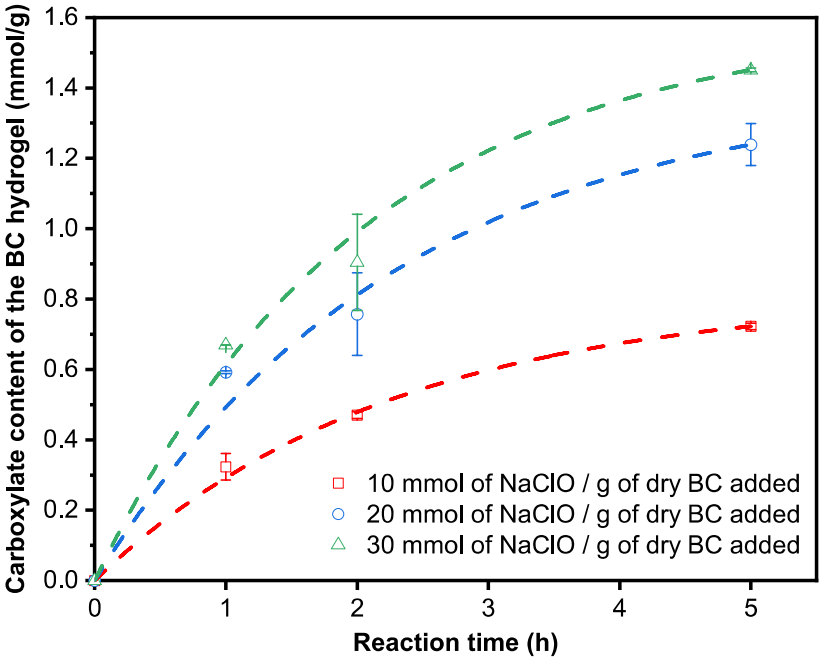


Figure 3-6: Carboxylate content of the TEMPO-oxidised BC hydrogels as a function of reaction time.

3.3.7 Porosity of (TEMPO-oxidised) BC films

The robust and water-stable TEMPO-oxidised BC hydrogels were then press-dried into self-standing TEMPO-oxidised BC films. In general, the production of self-standing TOCN film starts with a suspension of TOCN-in-water; this is then followed by vacuum filtration [4, 77, 78]. However, due to small diameters of the nanofibrils, their poor stability in water, and viscosifying effects, filtering a suspension of TOCNs remains a challenge. Multivalent salts can be added to reduce the Debye length of TOCNs, forcing their aggregation in water to reduce filtration time [79]. Water evaporation is also a commonly used technique to fabricate self-standing TOCN films [55, 80, 81]. However, long drying times are required as low drying temperatures are necessary to produce high quality uniform TOCN films. As a result, the grammage of TOCN films is typically low. Here, the possibility of first

producing a robust and water stable TOCN hydrogel allowed for the production of self-standing TOCN films from a simple press drying process without the need for vacuum assisted filtration or water evaporation. The porosity of the TEMPO-oxidised BC films was found to be ~20% (Table 3-1); by contrast, neat BC films possess a higher porosity of ~35%.

3.3.8 Tensile Properties of (TEMPO-oxidised) BC films

Figure 3-7 presents representative stress-strain curves of the (TEMPO-oxidised) BC films tested under uniaxial tension. After the initial elastic response, all samples yielded prior to catastrophic failure, characterised by a sudden load drop to zero once peak stress was reached.

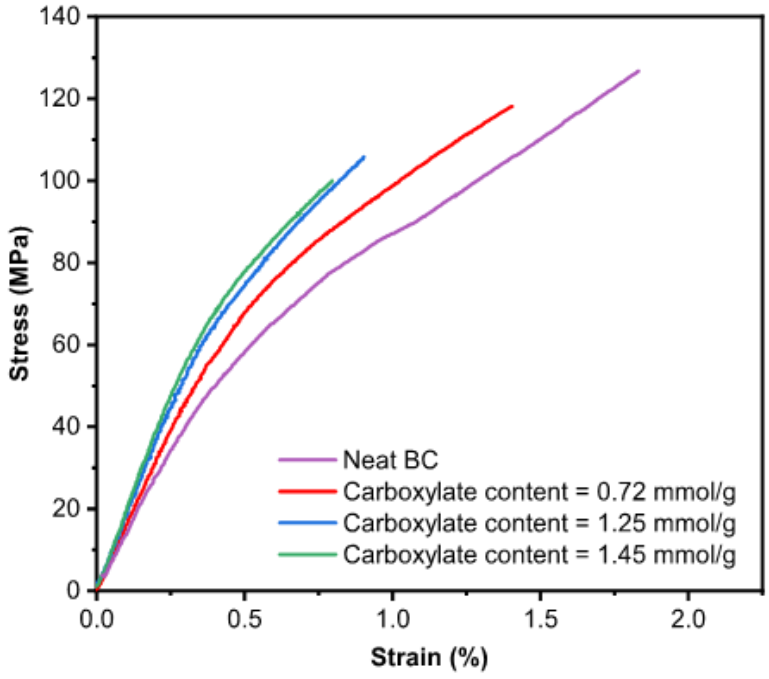


Figure 3-7: Representative tensile stress-strain curves of the various (TEMPO-oxidised) BC films.

Table 3-1: Tensile properties of the various (TEMPO-oxidised) BC films. ρ_A, P, E, σ, ε and U_T denote the absolute density, porosity, Young's modulus, tensile strength, strain-at-failure and work of fracture of the films, respectively.

Film	Carboxylate content [mmol g^{-1}]	ρ_A [g cm^{-3}]	P [%]	E [GPa]	σ [MPa]	ε [%]	U_T [MJ m^{-3}]
Neat BC	-	1.60 ± 0.01†	35.3 ± 3.1	15.4 ± 0.8	122 ± 9	1.60 ± 0.4	1.15 ± 0.32
TEMPO-oxidised BC	0.72 ± 0.01	1.47 ± 0.01	23.5 ± 0.8	15.9 ± 1.0	119 ± 10	1.48 ± 0.2	1.05 ± 0.26
	1.24 ± 0.06	1.50 ± 0.01	20.7 ± 0.4	18.5 ± 0.9	102 ± 12	0.89 ± 0.3	0.57 ± 0.23
	1.45 ± 0.01	1.50 ± 0.01	19.5 ± 0.8	18.9 ± 0.9	91 ± 9	0.79 ± 0.1	0.40 ± 0.12

†Data obtained from Santmarti *et al.*[57]

The neat BC film possesses a tensile modulus of 15.4 GPa (Table 3-1). By increasing the carboxylate content of the resulting TEMPO-oxidised BC films, the tensile modulus increases from 15.9 GPa for a TEMPO-oxidised BC film with a carboxylate content of 0.72 mmol g^{-1} to nearly 19 GPa for a TEMPO-oxidised BC film with a carboxylate content of 1.45 mmol g^{-1}. However, this increase is at the expense of the tensile strength of the TEMPO-oxidised BC films. The tensile strength of TEMPO-oxidised BC films decreased from 120 MPa to only 96 MPa when the carboxylate content is increased from 0.72 mmol g^{-1} to 1.45 mmol g^{-1}. In contrast, the neat BC film possesses a tensile strength of 122 MPa. The strain-at-failure of the neat BC film was found to be 1.60% (Table 3-1). TEMPO-oxidised BC films were found to be brittle: with increasing carboxylate content, the strain-at-failure of the TEMPO-oxidised BC film decreased progressively to only 0.78%. Correspondingly, the work-of-fracture of the (TEMPO-oxidised) BC films decreased with increasing carboxylate content. These results can be attributed to the differences in interfibrillar bond strength between the (TEMPO-oxidised) BC nanofibrils. For TEMPO-oxidised BC nanofibrils, a pair of carboxyl moieties form two hydrogen bonds with each other; however, a pair of hydroxyl groups in neat BC nanofibrils can only form one hydrogen bond with each other. As a result, the tensile modulus of the TEMPO-oxidised BC films is higher than that of neat BC film and increases with increasing carboxylate content. This also reduces the plasticity of the (TEMPO-oxidised) BC films, increasing their brittleness and reduces their tensile strength.

3.4 Conclusions

In summary, this chapter demonstrated that the TEMPO-mediated oxidation of BC nanopaper leads to a robust and water stable TOCN hydrogels. This study found that this observation is unique only to nanopapers that are press-dried from pristine BC pellicles. The direct TEMPO-mediated oxidation of BC nanopaper produced from disintegrated BC pellicles, however, leads to the destruction of the nanopaper, forming homogenous TEMPO-oxidised BC nanofibril-in-water suspension. The initial rate of TEMPO-mediated oxidation of BC nanopaper was observed to be kinetically limited. The tensile properties of the TEMPO-oxidised BC films produced from the press drying of TEMPO-oxidised BC hydrogels were found to be a strong function of carboxylate content. Increasing the carboxylate content of a TEMPO-oxidised BC film leads to an increase in tensile modulus (from 15 GPa to nearly 19 GPa) but at the expense of tensile strength (from 122 MPa to only 90 MPa) and strain-at-failure (~1.6% to 0.8%). This is a result of the increased strength of hydrogen bonding within the TEMPO-oxidised BC films due to the presence of carboxyl functionalities.

Chapter 4 – Susceptibility of BC nanopaper press-dried at different temperatures towards TEMPO-oxidation induced nanopaper swelling

4.1 Introduction

If the BC pellicle is first heat-pressed into a sheet of dried and well-consolidated BC nanopaper, the previous chapter showed that TEMPO-mediation oxidation reaction will lead to nanopaper swelling, producing a TOBC hydrogel that can be further dewatered into a self-standing high grammage TOBC film [82]. Whilst the resulting self-standing TOBC film possesses equally high mechanical performance as those made from cellulose pulp derived TOCNs, it lacked the transparency typical of a TOCN film. Therefore, attempts were made to increase the carboxylate content of the TOBC in the resulting hydrogels in an effort to produce optically transparent TOBC film. Unfortunately, it was observed that the BC nanopaper disintegrated during TEMPO-mediated oxidation at high oxidant concentration. It was further observed that the heat-pressing temperature of the BC pellicle used to produce the BC nanopaper also influenced the degree of swelling of the nanopaper during TEMPO-mediated oxidation reaction. BC nanopaper produced by the heat-pressing of BC pellicle at higher temperature was observed to be more resistant to TEMPO-mediated oxidation induced nanopaper swelling. In this chapter, the

influence of press-drying temperature on the susceptibility towards TEMPO-oxidated induced nanopaper swelling is discussed.

4.2 Experimental

4.2.1 Materials

All the materials used for the experiments in this chapter have been reported in section 3.2.1.

4.2.2 Preparation of BC nanopaper

The purified BC pellicle was first cut into dimensions of 80 mm × 80 mm × 10 mm and gently dabbed with filter paper (Qualitative filter paper 413, VWR, Lutterworth, UK) to remove excess water on the pellicle surface. It was then placed between two sheets of filter paper, followed by two additional sheets of blotting paper (Whatman Qualitative filter paper, Grade 3, GE Health Care, Buckinghamshire, UK) and heat-pressed between two parallel aluminium plates under a compaction force of 100 N for 10 min. Three different heat-pressing temperatures were used, namely 55℃, 85℃ and 115℃, respectively. After 10 min of heat-pressing at the selected temperature, the partially dried BC pellicle was carefully removed from the used sheets filter and blotting paper. The heat-pressing step was then repeated with fresh sheets of filter and blotting paper each time until successive weight measurements of the heat-pressed BC pellicle remained constant, *i.e.*, a BC nanopaper was formed. All BC nanopaper possessed a nominal thickness of *ca.* 80 μm and were trimmed to 70 mm × 70 mm prior to subsequent use. BC nanopapers produced by press-drying the BC

pellicle at 55℃, 85℃ and 115℃ are herein termed BC-55, BC-85 and BC-115, respectively.

4.2.3 TEMPO-mediated oxidation of BC nanopaper

TEMPO-mediated oxidation of BC nanopaper was performed following the previously described protocol in chapter 3. Briefly, BC nanopaper (0.4 g) was first immersed in 600 mL of aqueous solution containing dissolved TEMPO (0.23 mmol) and NaBr (1.94 mmol). To this, 12% Cl_2 aqueous NaClO solution was slowly pipetted to initiate the oxidation reaction. The pH of the TEMPO/NaBr/NaClO solution was maintained at a value 10 through the titration of 0.5 M sodium hydroxide and the oxidation reaction was conducted for 5 h at room temperature under magnetic stirring. The reaction was terminated through the addition of 10 mL of ethanol and the resulting TEMPO-oxidised BC (TOBC) was rinsed with deionised water until neutral pH was attained. TOBC was then reduced with $NaBH_4$ to convert the C6-aldehydes and C2/3-ketones into -OH groups [54]. It was performed by suspending the TOBC in 600 mL of deionised water with $NaBH_4$ dissolved (0.1 g per g of dry BC) for 3 h at room temperature under magnetic stirring. After this step, the TOBC was purified by rinsing with deionised water until neutral pH was attained. Finally, the reduced TOBC was subjected to an ion exchange treatment to convert the sodium carboxylate groups to free carboxyl groups [55]. This was conducted by suspending the reduced TOBC in 600 mL of aqueous HCl solution at a pH = 1 for 1 h under magnetic stirring, prior to thorough rinsing with deionised water until neutral pH was attained.

4.3 Characterisation of TOBC hydrogels produced from BC nanopaper heat-pressed at different temperatures

4.3.1 Carboxylate content of TOBC hydrogel

The carboxylate content of the TOBC hydrogel was determined using conductometric titration as described by Saito and Isogai [2], as well as Katz and Beatson [56]. Briefly, the TOBC hydrogel was first dried in an oven at 55 °C overnight to obtain an accurate dry mass of TOBC needed for subsequent carboxylate content calculation. It was then blended in deionised water to produce a homogenous TOBC-in-water suspension with a consistency of 0.05% (g mL^{-1}). To this suspension, 10 mL of 0.01 M NaCl solution was added. The pH of the TOBC-in-water suspension was adjusted to 3 through the titration of 0.1 M HCl solution. A 40 mM NaOH solution was then pipetted at a rate of 0.2 mL min^{-1} until the pH of the suspension reached a value of 11. Throughout the titration process, the pH and the conductivity of the suspension were monitored and recorded (HI-2550, Hanna Instruments, UK). The carboxylate content of the TOBC hydrogel was calculated based on the conductivity of the weak acid groups. All carboxylate content measurements were duplicated.

4.3.2 Swelling ratio of TOBC hydrogel

The swelling capacity of the BC nanopaper press-dried at different temperatures into a TOBC hydrogel was quantified using simple weight gain measurement. Prior to the measurement, all TOBC hydrogels were immersed in excess deionised water for 120 h to ensure that the hydrogels have swelled to their equilibrium state. Prior to measuring the wet mass of the TOBC hydrogel (m_w), the surface excess water

was removed by dabbing with filter paper (Qualitative filter paper 413, VWR, Lutterworth, UK). The hydrogel was then press-dried (4122CE Carver Inc., Wabach, IN, USA) using a compaction force of 9 kN at 105℃ for 30 min to obtain its dry mass (m_{d}). The swelling capacity of the BC nanopaper into a TOBC hydrogel upon TEMPO-mediated oxidation was calculated as:

$$\mathrm{SR} = \left(\frac{m_{\mathrm{w}} - m_{\mathrm{d}}}{m_{\mathrm{d}}}\right) \tag{4.1}$$

4.4 Characterisation of dried and well-consolidated BC nanopaper heat-pressed at different temperature

4.4.1 Determination of the residual moisture content of BC nanopaper

Thermal gravimetric analysis (TGA) was conducted to accurately quantify this residual moisture content in the BC nanopaper. A sample mass of ~8 mg was used. Prior of test, the initial weight of each BC nanopaper sample was measured. All samples were dried at 55℃ overnight prior to heating (Discovery TGA, TA Instruments, Elstree, UK) from 30℃ to 180℃ at a rate of 1℃ min^{-1} under 50 mL min^{-1} of dry nitrogen flow. The TGA instrument will record the weight loss of the BC nanopaper sample as a function of temperature.

4.4.2 Specific surface area measurement of BC nanopaper

Volumetric N_2 Adsorption/Desorption isotherms of BC nanopaper at −196°C were performed using 3Flex adsorption analyser (Micromeritics Ltd., Hexton, UK). Prior to the measurement, the BC nanopaper was degassed (VacPrep 061, Micromeritics Ltd., Hexton, UK) at 80°C for 18 h under vacuum to remove any adsorbed water molecules. A BC nanopaper sample mass of 20 mg was used for this measurement.

This measurement was conducted by Joanne Li due to COVID-19 imposed laboratory access restrictions.

4.4.3 Porosity of the BC nanopaper heat-pressed at different temperature

The absolute density (ρ_A) of BC was measured using He pycnometry (Accupyc II 1340, Micrometrics Ltd., Dunstable, UK). To obtain the envelope density (ρ_E) of the BC nanopaper, it was first cut into rectangular sample with dimensions of 40mm in length and 5mm in width. The thickness of the sample was then measured using a digital micrometer (Mitutoyo MDC Lite, RS Components Ltd., Northants, UK). With the dimensions known, $\rho_E$was calculated by dividing the mass of the sample by its envelope volume. The porosity (P) of the BC nanopaper was obtained using:

$$P, \% = \left(1 - \frac{\rho_E}{\rho_A}\right) \tag{4.2}$$

4.4.4 Tensile properties of BC nanopaper heat-pressed at different temperatures

Tensile testing of the BC nanopaper was conducted using a micro-tensile tester (model MT-200, Deben UK Ltd., Woolpit, UK) equipped with a 200 N load cell. Before the test, rectangular test specimen was cut from the fabricated BC nanopaper using a manual cutting press (ZCP020, Zwick Roell Ltd. Herefordshire, UK) and dried overnight at 55 ℃. The rectangular test specimen possessed an overall length of 40 mm and a width of 5 mm. A speckle pattern was marked on the surface of the rectangular test specimen prior to mounting it onto the micro-tensile tester. After mounting, the exposed length of the specimen was 25 mm. The test specimen was then loaded with a crosshead displacement speed of 0.5 mm min^{-1} (corresponding

to a strain rate of 2×10^{-4}% s^{-1}). The strain of the specimen was recorded using a non-contact video extensometer (iMetrum Ltd., Bristol, UK) by monitoring the changes in the speckled pattern. A total of 5 specimens were tested for each type of BC nanopaper.

4.5 Results and discussion

4.5.1 Visual appearance of the TOBC hydrogels

The heat-pressing of a pristine BC pellicle (Figure 4-1a) directly produces a sheet of dried and well-consolidated BC nanopaper (Figure 4-1b) that remains stable in water and does not swell or rehydrate into its original pellicle form (Figure 4-1c). This can be attributed to (i) the highly crystalline nature of BC, with a degree of crystallinity of *ca.* 90% [59], that prevented intra-fibril swelling, as well as (ii) the high specific surface area of BC, measured to be 41 m^2 g^{-1} [62] that promoted strong interfibril hornification between adjacent BC nanofibrils. Figure 4-1d shows the influence of NaClO concentration on the swelling of the BC nanopaper heat-pressed directly from pristine BC pellicle at different temperatures into TOBC hydrogels. Up to an NaClO concentration of 50 mmol g^{-1}, BC nanopaper could be oxidised into TOBC hydrogels, independent of the temperature used to heat-press the pristine BC pellicle. At an NaClO concentration of 70 mmol g^{-1} however, only BC-85 and BC-115 nanopaper could be oxidised into a TOBC hydrogel. At this NaClO concentration, the structural integrity of the TOBC hydrogel made from BC-55 nanopaper was lost, leading to the disintegration of the hydrogel into a homogenous suspension of TOBC-in-water.

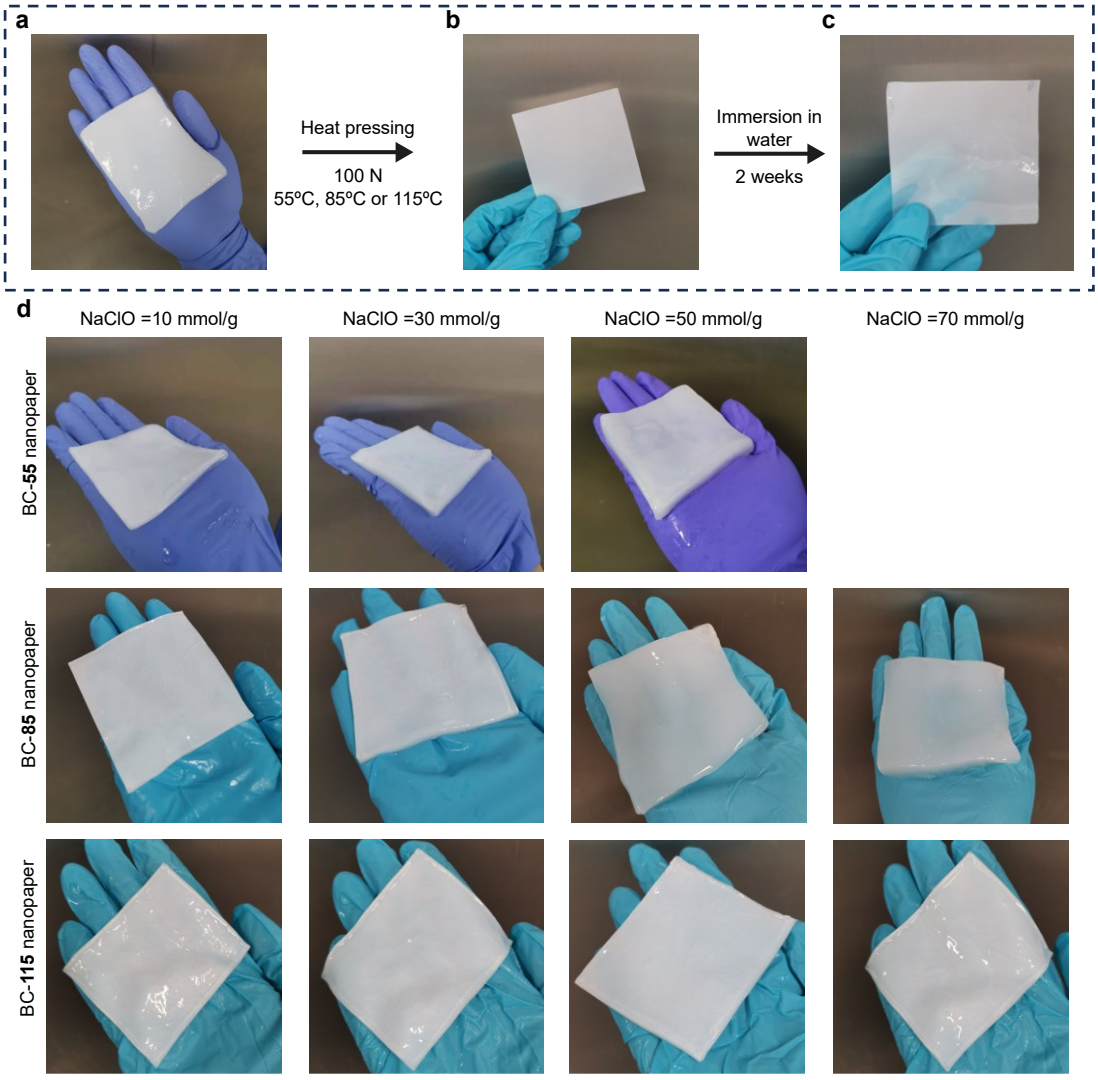


Figure 4-1 (a) BC pellicle, with a water content of 99 wt.-%, was heat-pressed at 55 °C, 85 °C or 115 °C to produce (b) dried and well-consolidated BC nanopaper. (c) Exemplary BC nanopaper immersed in water for more than 2 weeks, indicating the stability of the BC nanofibril network in the nanopaper. The visual appearance of (d) the TOBC hydrogels produced from the oxidation of BC nanopaper heat-pressed at different temperature using 10 mmol, 30 mmol, 50 mmol and 70 mmol of NaClO per g of dry BC.

4.5.2 Carboxylate content and swelling ratio of the TOBC hydrogels

The carboxylate content and the swelling ratio of the TOBC hydrogels are summarised in Figure 4-2. As a stable TOBC hydrogel could not be produced from BC-55 nanopaper oxidised with an NaClO concentration of 70 mmol g^{-1}, a TOBC hydrogel oxidised with 60 mmol g^{-1} of NaClO was produced from BC-55 nanopaper instead. It can be seen from Figure 4-2a that the carboxylate content of the TOBC hydrogel increases with increasing NaClO concentration used and plateaued at ~1.4 mmol g^{-1}, ~1.0 mmol g^{-1} and ~0.8 mmol g^{-1} for TOBC hydrogels produced from BC-55, BC-85 and BC-115 nanopaper, respectively. The low carboxylate content of the TOBC hydrogel produced from BC-55 nanopaper oxidised at an NaClO concentration of 60 mmol g^{-1} can be attributed to its high mass loss (*ca.* 15 wt.-%). This signifies that even at this NaClO concentration, the integrity of the TOBC hydrogel was poor. The swelling ratio (Figure 4-2b) also corroborates with the carboxylate content of the TOBC hydrogels as higher charge density is expected to lead to higher degree of swelling if no significant mass loss occurred. TOBC hydrogels produced from BC-55 nanopaper was found to possess the highest swelling ratio, followed by TOBC hydrogels produced from BC-85 and BC-115 nanopaper. In fact, the swelling ratio of the TOBC hydrogel produced from BC-55 nanopaper oxidised with 60 mmol g^{-1} of NaClO concentration approaches the swelling ratio of pristine BC pellicle.

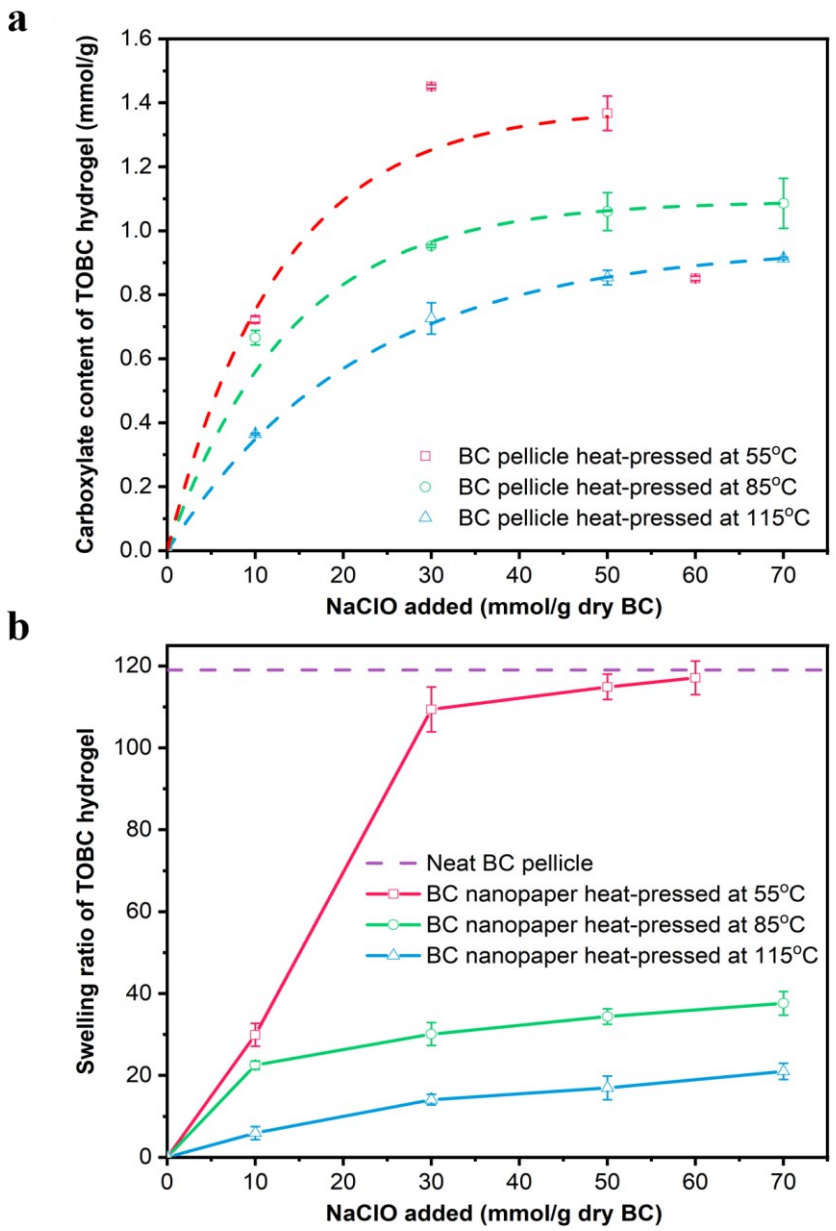


Figure 4-2 (a) Carboxylate content and (b) swelling ratio of the TOBC hydrogels made from BC pellicle heat-pressed at different temperature.

4.5.3 Residual water content in the BC nanopaper

Even though all the prepared BC nanopaper possess excellent water stability (see Figure 4-1a), the residual water content in the different BC nanopaper. This is because cellulose is hydrophilic and lower heat-pressing temperature may not be

sufficient to remove the water adsorbed on the BC nanofibrils completely. Consequently, this may reduce interfibril hornification, causing the observed susceptibility of the different BC nanopaper to TEMPO-oxidation induced swelling. This study therefore first used thermal gravimetric analysis to ascertain whether BC nanopaper heat-pressed from pristine BC pellicle at different temperatures possess significantly different residual moisture content. Figure 4-3 shows the evaporation of residual water from the BC nanopaper. The weight of all the prepared BC nanopaper decreased with increasing temperature and plateaued at ~98 wt.-%. Whilst there is a slight variation in the residual moisture content across the different BC nanopaper (see Table 4-1), this variability is minor and does not account for the observed large variation in the TEMPO-oxidation induced swelling of the different nanopaper into a hydrogel.

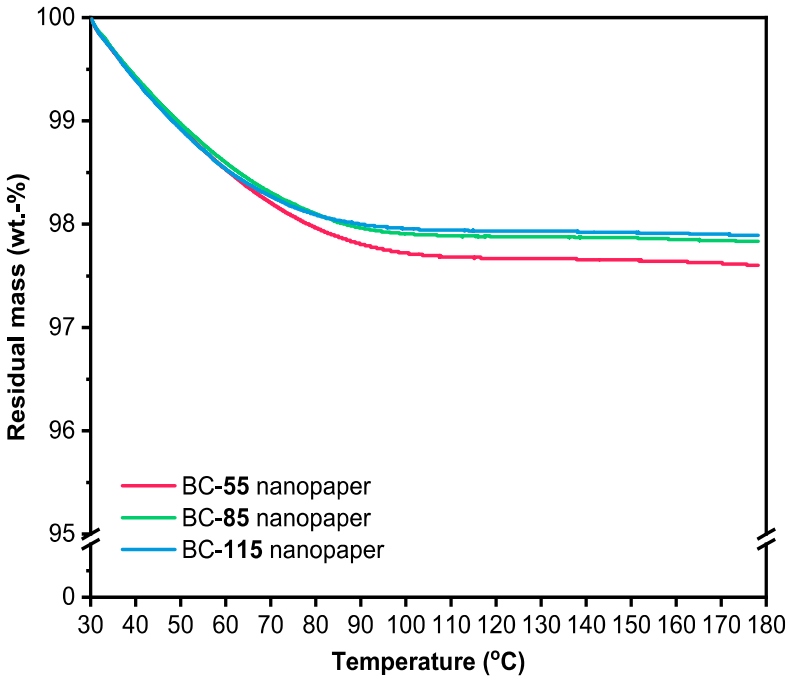


Figure 4-3 Thermal gravimetric measurement of BC nanopaper heat-pressed at different temperature.

4.5.4 Influence of capillary force during the formation of BC nanopaper

The formation of a self-standing, dried and well-consolidated network of nanocellulose, *i.e.*, cellulose nanopaper, can be attributed to capillary force [83]. After the removal of the bulk of the water from a network of nanocellulose, capillary bridges are created between adjacent cellulose nanofibrils. Further removal of water leads to a decrease in the radius of meniscus in the capillaries. This increases the capillary force that pulls the cellulose nanofibrils together and consequently, increases the bond energy between the cellulose nanofibrils [84]. As capillary force is proportional to the surface tension of the liquid, liquids with lower surface tension will lead to the formation of a more porous cellulose nanopaper with a looser hydrogen bonding network. Such results have been reported by various authors, whereby cellulose nanopaper made from methanol, ethanol and acetone solvents was found to possess higher porosity and lower mechanical properties than those made from water as the dispersing medium for the cellulose nanofibrils [85]. Nevertheless, it should be noted that the surface tension of water decreases with increasing temperature [86-88]. The surface tension of water at 25°C is 72 mN m^{-1} but at an elevated temperature of 80°C, water surface tension decreases to 63 mN m^{-1}. This implies that the BC-115 nanopaper should possess the loosest hydrogen bonding network and therefore most susceptible to TEMPO-mediated oxidation, as well as TEMPO-oxidation induced nanopaper swelling. However, this contradicts with the results presented in Figure 4-1 and Figure 4-2, whereby BC-115 nanopaper is the least susceptible to TEMPO-oxidation induced nanopaper swelling.

4.5.5 Exposed surface area of BC nanopaper

This thesis previously postulated that the oxidation reaction introduced carboxylate moieties onto the exposed BC nanofibrils within the nanopaper network structure and this led to the swelling of the nanopaper into a hydrogel. It can be anticipated that a nanopaper network with larger exposed surface area should be more susceptible to TEMPO-oxidation induced swelling. Therefore, Brunauer-Emmett-Teller (BET) surface area measurement was conducted. Figure 4-4 presents the volumetric N_2 adsorption-desorption isotherms of BC nanopaper heat-pressed from pristine BC pellicle at different temperatures. It can be seen from these figures that the N_2 adsorption isotherms of BC nanopaper are Type IVa, characterised by a reversible Type II isotherm at low relative pressure (P/P_o < 0.4) and a hysteresis at high relative pressure (P/P_o > 0.4) due to capillary condensation with hysteresis [89].

It was proposed that BET surface area analysis should be conducted over a range of $0.05 \leq P/P_o \leq 0.35$, with the implicit assumption that a monolayer is formed within this P/P_o range [90]. However, a recent study showed that the BET range for BC should be selected with care due to the high surface energetics of highly crystalline BC [91]. Therefore, a plot of $Q(P_o - P)$ vs P/P_o was first plotted (see Figure 4-5a) to select a suitable P/P_o range for subsequent BET analysis. Here, the selection is based on the work of Rouquerol *et al.* [92], whereby (i) the selected BET range must yield a positive c-value, (ii) the calculated monolayer capacity, Q_m, must be within the selected P/P_o range and (iii) $Q(P_o - P)$ must increase with increasing P/P_o. Based on this analysis, that a P/P_o range of 0.05 and 0.35 was

confirmed to be suitable and the subsequent BET surface area calculation is based on this P/P_o range.

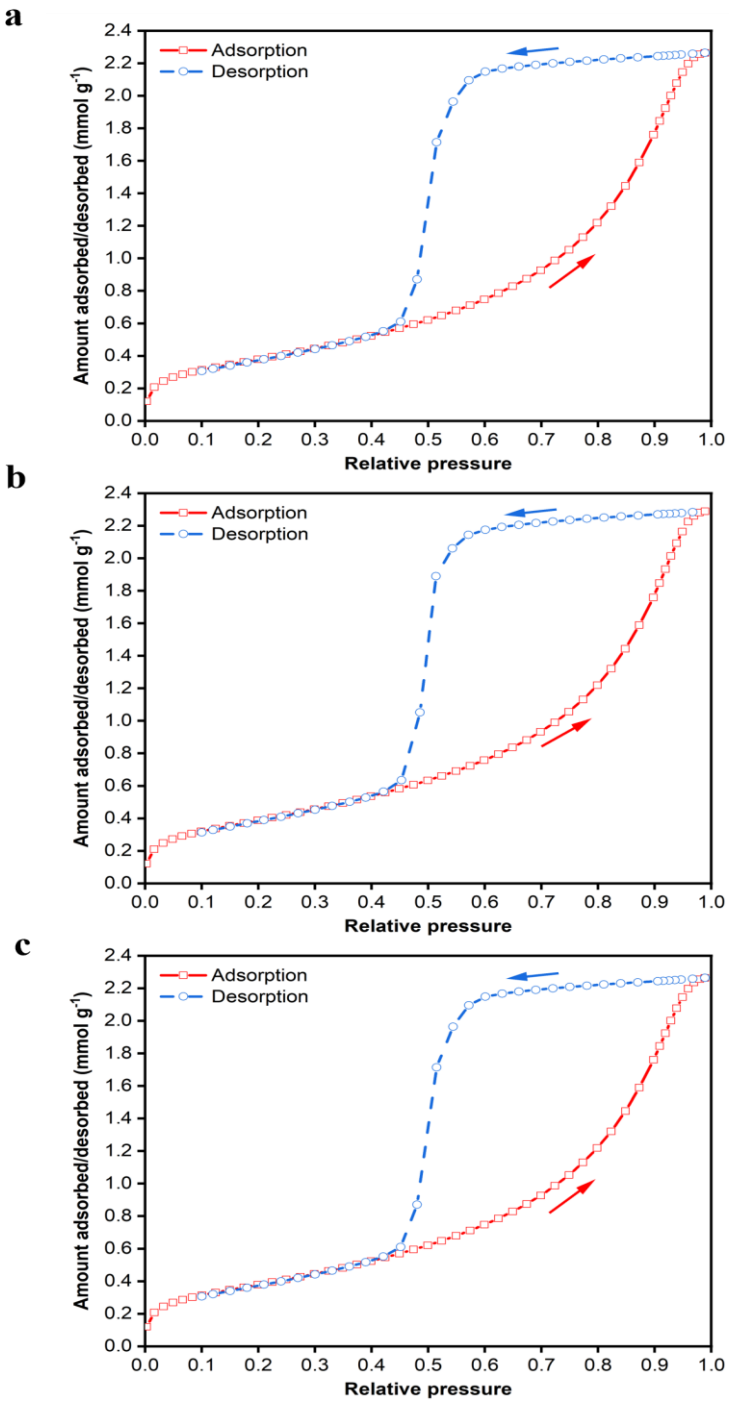


Figure 4-4 N_2 adsorption-desorption isotherms of (a) BC-55, (b) BC-85 and (c) BC-115 nanopaper.

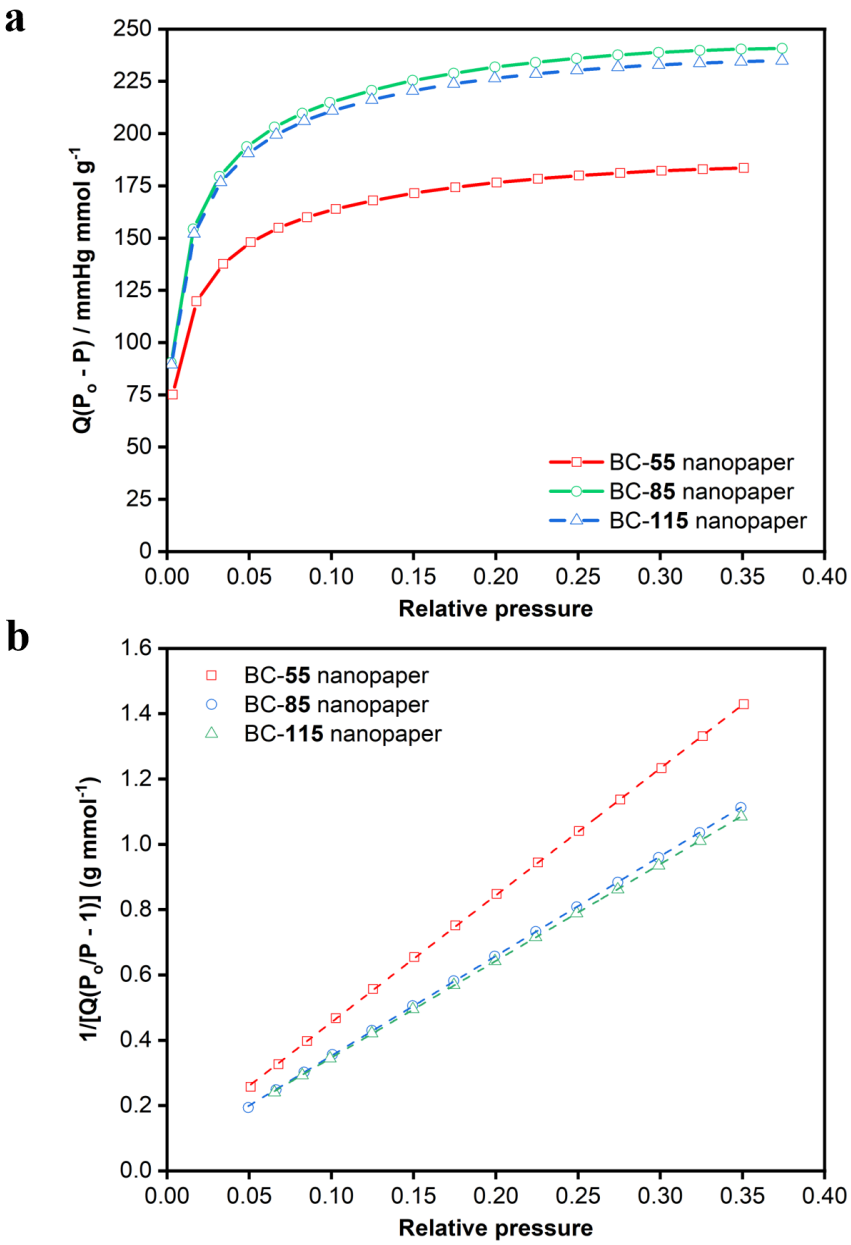


Figure 4-5 (a) $Q(P_o - P)$ vs P/P_o and (b) BET plots of BC nanopaper heat-pressed at different temperature. The dashed lines correspond to the linear fit of the data within the BET range of $0.05 \leqslant P/Po \leqslant 0.35$ as validated from the $Q(P_o - P)$ vs P/P_o plot.

The BET plots of the BC nanopaper are presented in Figure 4-5b and the calculated BET surface areas are summarised in Table 4-1. BC-85 and BC-115 nanopaper were found to possess a higher surface area of 36 m^2 g^{-1} compared to BC-55 nanopaper, which possessed 35% lower surface area of 27 m^2 g^{-1}. The porosity of the BC nanopaper was found to decrease with increasing heat-pressing temperature of the pristine BC pellicle (also see Table 4-1). This implies that BC nanopaper produced from pristine BC pellicle heat-pressed at higher temperature possesses smaller BC nanofibril aggregates leading to higher specific surface area. The smaller nanofibril aggregates also leads to better packing of the nanofibrils, resulting in BC nanopaper with a lower porosity. It is postulated that higher water evaporation rate prevented the nanofibrils from forming larger aggregates as the pellicle dries out faster, locking in the structure. Nonetheless, the BET surface area results contradict the observation of higher susceptibility of BC-55 nanopaper, which possesses a lower surface area, towards TEMPO-mediated oxidation. The reason for this observation is not clear but it implies that the exposed surface area of the BC nanopaper is not solely responsible for the TEMPO-mediated oxidation induced swelling of the BC nanopaper.

Table 4-1 Residual moisture content (M_c), BET surface area (A_s) and porosity (P) of BC nanopaper heat-pressed at different temperature.

Nanopaper	A_s (m^2 g^{-1})	c-value	ρ_T (g cm^{-3})	ρ_E (g cm^{-3})	P (%)	M_c (wt.-%)
BC-55	27.2 ± 3.6	58 ± 2	1.49 ± 0.03	1.12 ± 0.03	21 ± 4	2.40 ± 0.10
BC-85	36.3 ± 5.5	58 ± 3	1.48 ± 0.02	1.23 ± 0.02	17 ± 2	2.13 ± 0.01
BC-115	36.8 ± 7.5	64 ± 2	1.48 ± 0.02	1.27 ± 0.01	14 ± 1	2.06 ± 0.01

4.5.6 Inter fibril bonding of BC nanopaper

Uniaxial tensile testing was conducted as an indirect measure to quantify the degree of interfibril bonding of the BC nanopaper heat-pressed from pristine BC pellicle at different temperatures. The representative tensile stress-strain curves of the BC nanopapers are presented in Figure 4-6. After the initial linear elastic response, the BC nanopaper yielded, followed by plastic deformation prior to catastrophic fracture. Such brittle behaviour is typical of both nanopaper made from bacterial and plant origin and can be attributed to the large number of contact or physical crosslinking between adjacent cellulose nanofibrils due to their high specific surface area [53, 57, 93].

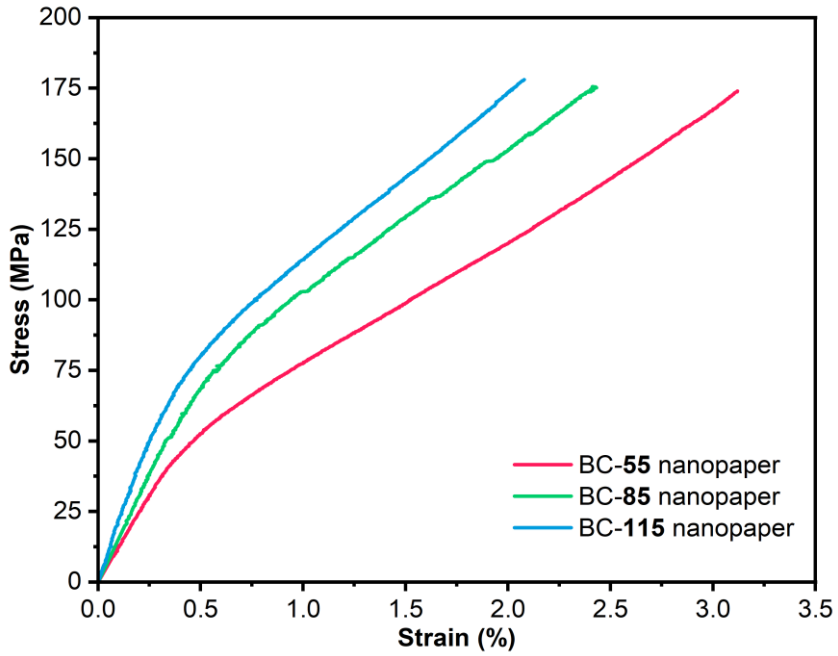


Figure 4-6: Representative tensile stress-strain curves of BC nanopapers heat-pressed at different temperature.

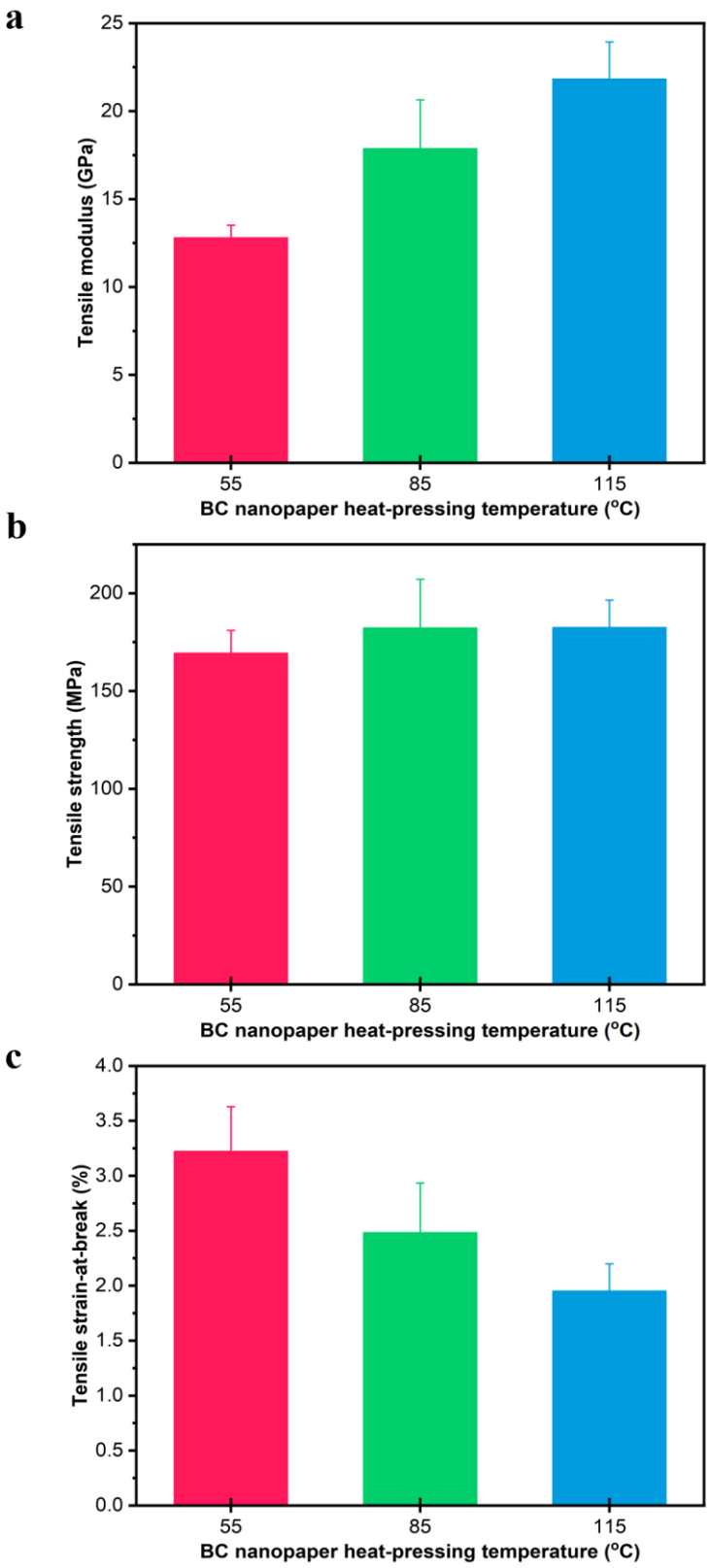


Figure 4-7: (a) Tensile modulus, (b) tensile strength and (c) tensile strain-at-failure of BC nanopapers heat-pressed at different temperature.

Nevertheless, it can be seen from Figure 4-7a that the tensile modulus of the BC nanopaper was found to increase with increasing heat-pressing temperature of the pristine BC pellicle. Similar results were also obtained for the tensile strength of the BC nanopaper, whereby BC-55 nanopaper possessed a lower tensile strength of 170 MPa whilst both BC-85 and BC-115 nanopaper was found to possess a tensile strength of ~185 MPa. As the porosity of the different BC nanopaper differs from each other (see Table 4-1), both the tensile modulus and strength of the BC nanopaper were normalised against their respective relative densities (see Table 4-2). Similar trend, i.e., increasing press drying temperature leads to BC nanopaper with higher normalised tensile properties, was still observed.

Table 4-2: Normalised tensile properties of the BC nanopaper press-dried at different temperatures. The tensile modulus was normalised against $(\rho_B/\rho_A)^2$ and the tensile yield strength (σ_Y) was normalised against $(\rho_B/\rho_A)^{1.5}$.

Sample	$E/(\rho_B/\rho_A)^2$ (GPa)	$\sigma_Y/(\rho_B/\rho_A)^{1.5}$ (MPa)
BC-55 nanopaper	22.66 ± 0.11	61.38 ± 0.10
BC-85 nanopaper	25.88 ± 0.16	65.99 ± 0.14
BC-115 nanopaper	29.64 ± 0.10	70.45 ± 0.08

The tensile properties of a network of cellulose fibrils are governed by the mechanical properties of the fibrils themselves, the fibril length and the degree of interfibril bonding [94, 95]. As both the mechanical properties and the length of the BC nanofibrils are the same for all BC nanopaper, the observed increase in tensile

modulus and strength must be due to an increase in the degree of interfibril bonding when higher heat-pressing temperature was used, especially when the residual moisture content of the BC nanopaper was found to be similar (see Table 4-1). The decreasing strain-at-failure of the BC nanopaper with increasing heat-pressing temperature used (see Figure 4-7c) is also consistent with the increase in interfibril bonding. These results corroborate with the observations in this study that BC nanopaper heat-pressed from pristine BC pellicle at lower temperature is more susceptible to TEMPO-oxidation induced swelling. However, this raises another question: why should a network of BC nanofibrils, when heat-pressed at different temperatures, produce nanopaper with different degrees of interfibril hornification? In the pulp and paper literature, the relationship between drying temperature used to produce paper sheets from cellulose pulp and their respective properties have been reported by numerous authors. However, there has not been any consensus as the results appear to be contradictory. Giacomozzi and Joutsimo [96] reported that when higher drying temperature was used, the tensile properties of the paper sheet decreased. However, Wahlström [97] showed that the tensile properties of a paper sheet is independent of drying temperature and time. Whilst no exact reasons were given in these publications, it is speculated by Salmén and Stevanic [98] that hornification or aggregation of cellulose microfibrils could be related to the mobility of the cellulose chains, which was found to be higher at elevated temperatures under moist conditions.

4.6 Conclusions

This chapter observed that BC nanopaper heat-pressed from pristine BC pellicle at lower temperature is more susceptible towards TEMPO-mediated oxidation. When heat-pressed at 55°C, the TEMPO-mediated oxidation reaction led to significant nanopaper swelling of up 120 times its original weight when an NaClO concentration of 60 mmol g^{-1} was used, before disintegrating into a homogenous TOBC suspension at an NaClO concentration of 70 mmol g^{-1}. BC nanopaper heat-pressed from BC pellicle at 115°C achieved a swelling ratio of only 20 upon TEMPO-mediated oxidation at an NaClO concentration of 70 mmol g^{-1}. Whilst there was a slight variation in the residual moisture of the BC nanopaper heat-pressed at different temperature, the variability was minor and does not account for the observed large variation in TEMPO-oxidation induced swelling of the different BC nanopaper into a hydrogel. The strength of capillary force is expected to decrease with increasing temperature. Consequently, BC nanopaper heat-pressed from BC pellicle at higher temperature should possess the "loosest" hydrogen bonding network but this contradicts with our experimental observations. BET surface area measurements were also found to disagree with our experimental observations as BC nanopaper heat-pressed from BC pellicle at higher temperature was found to possess higher surface area. Tensile testing showed that BC nanopaper heat-pressed from BC pellicle at higher temperature possess better tensile modulus and strength, which indicates stronger inter-fibril bonding. Whilst this could explain our experimental observation, it also raises another question: why is the strength inter-fibril bonding of BC nanopaper affected by heat-pressing temperature?

Chapter 5 – Facile method to prepare self-standing TEMPO-oxidised nanocellulose films

5.1 Introduction

The biggest challenge in the production of self-standing TEMPO-oxidised nanocellulose films is the long dewatering time [21, 80, 81] (usually to produce a 15-30 gsm TOCN film, the dewatering time is in the order of hours or days) [79]. It has been reported in chapter 3 that a robust and water stable TEMPO-oxidised BC hydrogel is produced from the TEMPO-mediated oxidation of BC nanopaper press-dried from pristine BC pellicle. This opens up a simple method to produce self-standing TEMPO-oxidised nanocellulose film as the TOBC can be directly press-dried without the need of long vacuum filtration time to produce a TEMPO-oxidised nanocellulose film. This then raises another question: Is the self-standing TEMPO-oxidised nanocellulose film produced from press-drying a TOBC hydrogel perform equally well as those made from the vacuum filtration of a suspension of TEMPO-oxidised nanocellulose? This chapter sets out to address this question.

5.2 Experimental section

5.2.1 Materials

Instead of using a high dry grammage BC pellicle, a BC pellicle with a low dry grammage ~16 g m^{-2} was used (water content of 99 wt.-%). It was purchased from

a commercial retailer (Qihong Technology Co. Ltd., Guilin City, China), and was purified following the previously described protocol prior to subsequent use [53]. A low dry grammage BC pellicle was used in this chapter as high grammage (80 gsm) self-standing TOBC film cannot be produced from a suspension of TOBC-in-water due to the aforementioned dewatering challenge. Poly (vinyl alcohol) (PVA, Mw = 31,000–50,000, 98%-99% hydrolysed) was purchased from Sigma Aldrich and used as an additive for self-standing TOBC film making [99]. Sodium hydroxide, sodium hypochlorite solution (GPR RECTAPUR, 12% Cl_2), hydrochloric acid (AnalaR NORMAPUR, 37%), sodium borohydride (BioXtra, purity ≥99%), (2,2,6,6-Tetramethylpiperidin-1-yl)oxyl (TEMPO) (Aldrich, purity ≥98%), sodium bromide (BioXtra, purity ≥99%) and sodium chloride (Riedel-de-Haën, purity ≥99%) were purchased as previously reported in chapter 3.

5.2.2 Preparation of neat BC nanopaper

The low grammage BC nanopaper used in this chapter was prepared following the same procedure previously described. Briefly, the BC pellicle was gently pressed between filter papers (Qualitative filter paper 413, VWR, Lutterworth, UK) and press-dried at 55°C with a compaction force of 100 N for 10 min. The low grammage BC nanopaper produced has a nominal thickness of *ca.* 16 μm).

5.2.3 TEMPO-mediated oxidation of BC nanopaper

The TEMPO-mediated oxidation of the low grammage BC nanopaper was performed following the previously described protocol but modified to account for the lower weight of BC in the reaction. Briefly, 7.65 mg of TEMPO and 42.5 mg

of NaBr were first dissolved in 127.5 mL of deionised water under magnetic stirring. BC nanopaper (85.0 mg) was then suspended in this solution. To this, 30 mmol of NaClO per gram of dry BC was slowly added to initiate the oxidation of the BC nanopaper. The pH of the reaction was monitored with a pH probe (HI-2550, Hanna Instruments, UK) and maintained at a value of 10 by the titrating in a solution of 0.5 M sodium hydroxide. The oxidation reaction was conducted for 5 hours at room temperature and quenched with ethanol, reduced with NaBH4 and ion-exchanged as previously described to produce a low dry grammage TEMPO-oxidised BC hydrogel. The hydrogels were stored at 4°C before further treatment.

5.2.4 Preparation of TOBC suspension

BC nanopaper (0.085 g, dry mass) was blended using a kitchen blender (Optimum 9400, Froothie Ltd, Cranleigh, UK) in deionized water (127.5 mL) and TEMPO (7.65 mg), as well as sodium bromide (42.5 mg) were added. The oxidation was conducted at room temperature with stirring and was initiated by adding an NaClO solution (30 mmol NaClO per gram of BC). The pH was monitored using a pH meter and was maintained at a value of 10 by adding 0.5 M NaOH. The reaction was quenched after 5 hours by adding 10 mL of ethanol. The resulting suspension was thoroughly washed with deionized water and adjusted to a pH value of 7 by centrifugation. Subsequently, the TEMPO-oxidised BC suspension was blended with deionized water again to yield a consistency of 0.25% (g mL^{-1}). Finally, the TOBC suspension (TOBCs) was stored at 4 ◦C prior to further treatment or analysis.

5.2.5 Preparation of TOBC film

Self-standing TOBC films were prepared using an evaporative method instead of the hot-pressing method described in chapter 3 due to the low dry grammage of BC used. The previously produced TEMPO-oxidised BC hydrogels or TOBC suspensions were transferred onto a polystyrene petri dish and dried at 55°C in an oven for 3 hours. Thereafter, the TEMPO-oxidised BC hydrogels were further dried at room temperature for another 3 to 5 days to produce the self-standing TEMPO-oxidised BC films. All samples were stored in a desiccator prior to subsequent use. PVA was also used as additive as it is common to add PVA to TOCN film making [100]. Briefly, PVA was first dissolved in water under constant stirring at 90°C to obtain a 5% (w/w) solution. The PVA solution was allowed to cool to room temperature. The TEMPO-oxidised BC hydrogels were immersed in the PVA (mass ratio of dry BC: PVA = 3:1) under mechanical stirring at 2000 rpm for 1 hour prior to transferring to a polystyrene petri dish and dried at 55°C in an oven for 3 hours, followed by room temperature drying for another 3-5 days. In the case of TOBC-in-water suspension, the 5% (w/w) PVA solution was added into the TOBC suspension (mass ratio of dry BC: PVA = 3:1) prior to the aforementioned drying steps.

5.3 Materials characterisation

5.3.1 Carboxylate content of TOBC and TOBCs

The carboxylate content of the TEMPO-oxidised BC was determined using conductometric titration method as described by Saito and Isogai [2], and Katz *et al*. [56] Briefly, 0.1 g (dry basis) of the TEMPO-oxidised BC was blended using a

kitchen blender (Optimum 9400, Froothie Ltd., Cranleigh, UK) with 200 mL of deionized water to first produce a homogenous TEMPO-oxidised BC-in-water suspension. 10 mL of 0.01 M NaCl solution was then added to this suspension. The pH of the suspension was adjusted to a value of 3 through the titration of 0.1 M HCl. A 40 mM NaOH solution was then pipetted at the rate of 0.2 mL min^{-1} until the pH of the TEMPO-oxidised BC suspension reached a value of 11. Throughout the NaOH titration process, the conductivity of the suspension was recorded using a multiparameter (HI-2550, Hanna Instruments, UK) and the carboxylate content of the TEMPO-oxidised BC was calculated based on the conductivity of the weak acid groups. All measurements were duplicated.

5.3.2 Porosity of (TEMPO-oxidised) BC films

The absolute density (ρ_A) of the TEMPO-oxidised BC was determined using He pycnometry (Accupyc II 1340, Micromeritics Ltd., Hexton, UK). To evaluate the envelope density of the (TEMPO-oxidised) BC films (ρ_E), a micrometre was used to first measure the thickness of the films. With the thickness known, the envelope volume was determined and ρ_E was calculated by taking the ratio between the mass and envelope volume of the films. The porosity (P) of the film was then obtained using the following equation:

$$P = 1 - \frac{\rho_E}{\rho_A} \tag{5.1}$$

5.3.3 Tensile Properties of (TEMPO-oxidised) BC films

Tensile testing of the films was conducted in accordance with ASTM D632-14. Rectangular shaped test specimens were cut from the (TEMPO-oxidised) BC films using a manual cutting press (ZCP 020, Zwick Roell Ltd., Herefordshire, UK). The test specimens had an overall length of 40 mm and a width of 5 mm. The tensile test was conducted using a micro-tensile tester (model MT-200, Deben UK Ltd., Woolpit, UK) equipped with a 200 N load cell. After mounting the test specimen onto the micro tensile tester, the exposed specimen length was 25 mm. Prior to loading the specimen under uniaxial tension, a speckle pattern was marked on the surface of the test specimen; the strain of the test specimens was evaluated by monitoring the movement of this pattern using a non-contact video extensometer (iMetrum Ltd., Bristol, UK). All test specimens were loaded with a crosshead displacement speed of 0.5 mm min^{-1}, which corresponded to a strain rate of 3×10^{-4} % s^{-1}. A total of 5 specimens were tested for each sample.

5.3.4 Film Transmittance

The transmittance and haze of films was measured using a UV/vis spectrophotometer (PerkinElmer Lambda 365, Akron, Ohio, United States). The spectral region chose to study was between 200 and 700 nm. All transmittance measurements were triplicated.

5.3.5 Morphology of self-standing TOBC films

Scanning electron microscopy (SEM) (Tescan Mira, Tescan-UK Ltd., Cambridge, UK) was used to evaluate the internal morphology of selected TOBC films. It was

conducted using at an accelerating voltage of 1 keV. Prior to SEM, the films were freeze-dried (Alpha 1-2 LDplus, Martin Christ, Osterode, DE), mounted onto aluminium SEM stubs using carbon tabs and coated with Cr (Q150T ES, Quorum, East Sussex, UK) using a coating current of 40 mA for 3.5 min. (Due to COVID-19 lab access restrictions, the SEM were conducted by Ms Joanne Li).

5.4 Results and discussion

As previously shown (and for completeness here in this chapter), the press-drying of the BC pellicle (Figure 5-1a) produces a dried and well-consolidated network of BC nanopaper (Figure 5-1b). When the BC nanopaper was subjected to TEMPO-mediated oxidation, the BC nanopaper swelled into a hydrogel (Figure 5-1c). The TEMPO-oxidised BC hydrogel was found to be robust and water stable. Both the evaporative drying of neat TOBC hydrogel and PVA-doped TOBC hydrogel produces flat TOBC films (Figure 5-1f and g). However, the evaporative drying of TOBC-in-water suspension directly without the use of PVA additive leads to high film shrinkage (Figure 5-1h). This issue was circumvented through the use of PVA as the additive (Figure 5-1i). Herein, we only characterised neat BC nanopaper, self-standing TOBC film produced from TOBC hydrogel, as well as self-standing TOBC films produced from PVA-doped TOBC hydrogel and PVA-doped TOBC suspension.

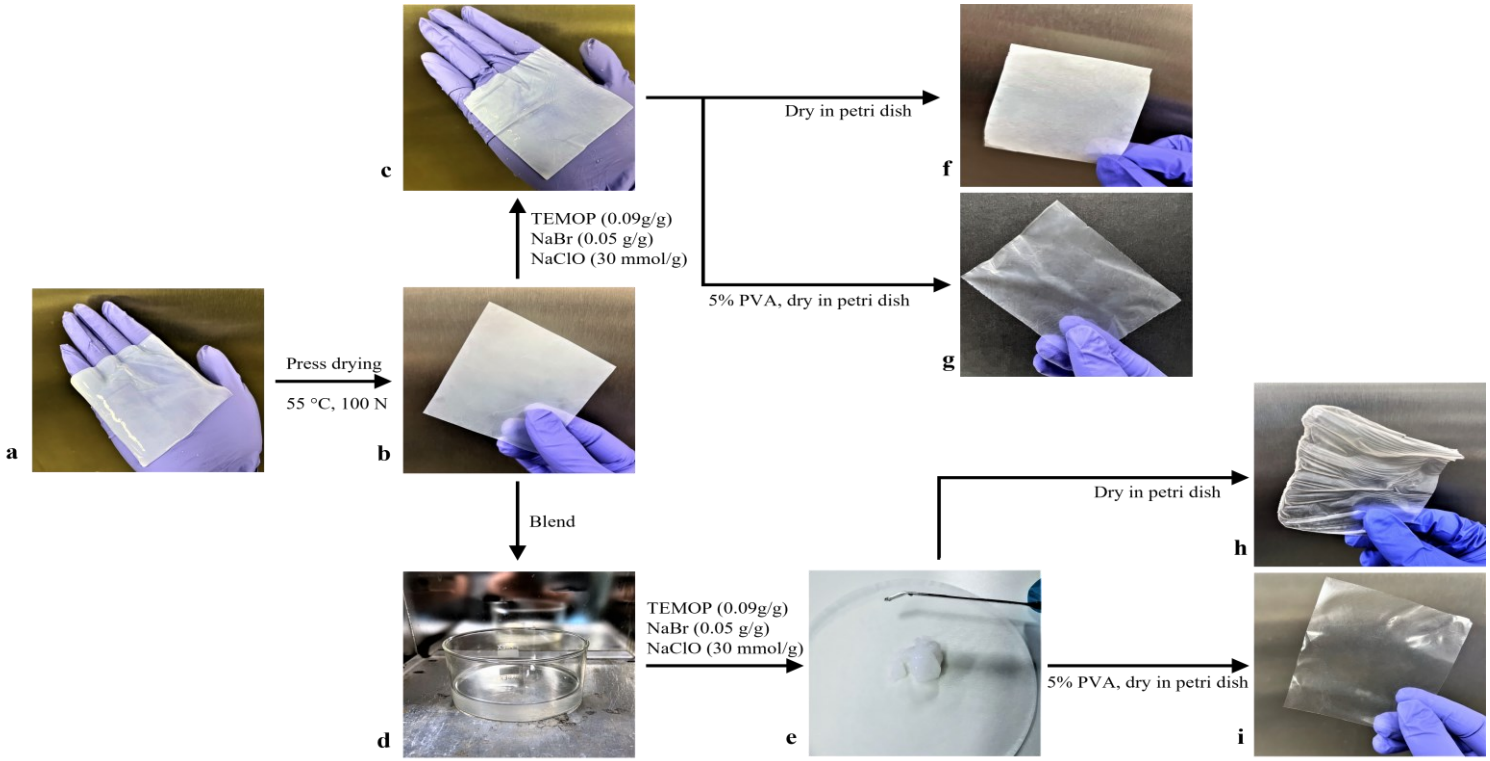


Figure 5-1 (a) BC pellicle containing ca. 99 wt% water; (b) a dried and well-consolidated BC nanopaper; (c) The visual appearance of TEMPO-oxidised BC hydrogels produced from the oxidation of the BC nanopaper; (d) BC slurry made by blending the BC nanopaper; (e) TEMPO-oxidised BC hydrogels produced from the oxidation of the BC slurry; (f) TOBC film from TOBC hydrogel; (g) PVA-doped TOBC film from TOBC hydrogel; (h); TOBC film from TOBC suspension (i) PVA-doped TOBC film from TOBC suspension.

5.4.1 Carboxylate content, internal morphology and porosity of TOBC films

The carboxylate content of the TOBC hydrogel was found to be slightly lower (1.20 mmol g^{-1}) compared to TOBC made from BC-in-water suspension (see Table 5-1). TEMPO-oxidised BC nanopaper, oxidised with 30 mmol g^{-1} NaClO resulted in a carboxylate content of 1.20 mmol g^{-1}. This can be attributed to the higher accessibility of C6 hydroxyl groups in the starting BC suspension compared to BC nanopaper. Figure 5-2 shows the morphology of the PVA-doped TOBC films. Both types of TOBC films possessed similar layered structure and are identical to neat BC nanopaper shown in Figure 3-2a.

Table 5-1 Carboxylate content of the various (TEMPO-oxidised) BC films. ρ_A and P denote the absolute density and porosity respectively.

Nanopaper	Carboxylate Content [mmol g^{-1}]	ρ_A [g cm^{-3}]	P [%]
Neat BC	-	1.62 ± 0.02	36.7 ± 3.1
TOBC hydrogel	1.20 ± 0.03	1.63 ± 0.01	28.2 ± 1.4
TOBC suspension	1.40 ± 0.01	-	-
PVA-doped TOBC hydrogel	-	1.51 ± 0.01	11.9 ± 1.5
PVA-doped TOBC from suspension	-	1.49± 0.01	10.6± 1.7

The TOBC film made from TOBC hydrogel was found to possess a porosity of 28.2% (Table 5-1). This is lower than that of neat BC nanopaper of 36.7%. The porosity of the PVA-doped TOBC films was even lower, *ca.* 10%. These results stem from the hydrogen bonding between PVA hydroxyl groups and the cellulose

carboxylate groups, creating a tighter (denser) network. Furthermore, the PVA also filled in some of the pores in the network. Similar results were also observed by Ozkan *et al.* [101]

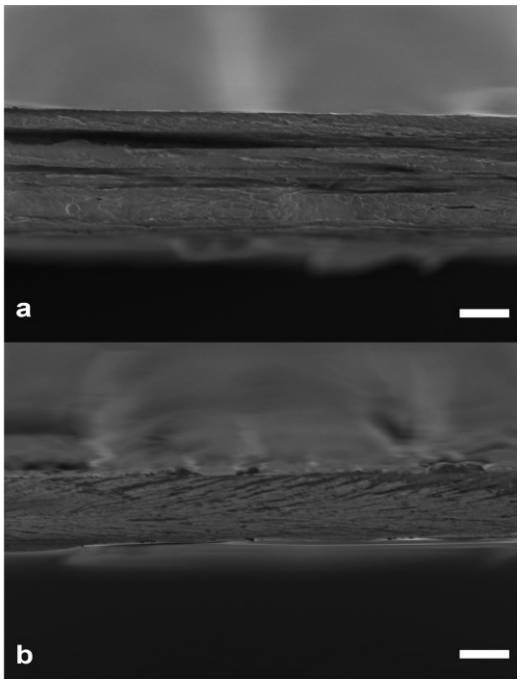


Figure 5-2 SEM micrographs of (a) PVA-doped TOBC film from TOBC hydrogel; (b)PVA-doped TOBC film from TOBC suspension. Scale bar = 10 μm.

5.4.2 Tensile properties of (PVA-doped) TOBC films.

Figure 5-3 displays the stress-strain curves of the (TEMPO-oxidised) BC films tested under uniaxial tension. After the initial elastic response, all samples yielded prior to catastrophic failure, characterised by a sudden load drop to zero once peak stress was reached. Neat BC nanopaper had a tensile modulus of 15.1 GPa (Table 5-2). This is remarkable considering the fact that the grammage of this BC nanopaper was only 16 g m^{-2}. The tensile modulus of neat BC nanopaper at a grammage of 80 g m^{-2} was also similar at 15.4 GPa (see chapter 3). More remarkable, the tensile modulus raised to 17.2 GPa in TOBC film produced from

TOBC hydrogel. As discussed in chapter 3, a pair of carboxyl moieties forms two hydrogen bonds with each other between TOBC; however, a pair of hydroxyl groups in neat BC nanofibrils can only form one hydrogen bond with each other. As a result, the tensile modulus of the TEMPO-oxidised BC films is higher than that of neat BC film and increases with increasing carboxylate content. This also reduces the plasticity of the (TEMPO-oxidised) BC films, increasing their brittleness and reduces their tensile strength. It was found that this effect is particularly severe in low grammage TOBC film, with a tensile strength of only 42 MPa compared to low grammage neat BC nanopaper of 107 MPa.

Table 5-2: Tensile properties and transmittance of the various (TEMPO-oxidised) BC films. E, σ, ε and T denote the Young's modulus, tensile strength, strain-at-failure and transmittance of the films, respectively.

Film	E [GPa]	σ [MPa]	ε [%]	T [%] at 700 nm
Neat BC	15.12 ±0.41	107.15 ± 3.83	1.67 ± 0.26	23.20
TOBC hydrogel	17.23 ± 1.26	41.58 ± 7.91	0.29 ± 0.06	37.37
PVA	1.065†	49†	200†	88.92†
PVA-doped TOBC hydrogel	14.05 ± 2.53	47.45 ± 3.94	0.43 ± 0.16	73.70
PVA-doped TOBC from suspension	9.95 ± 2.55	32.75 ± 9.00	0.36 ± 0.12	81.25

†Data obtained from Lee *et al*. [102], Tang *et al*. [103] and Yahia *et al*. [104]

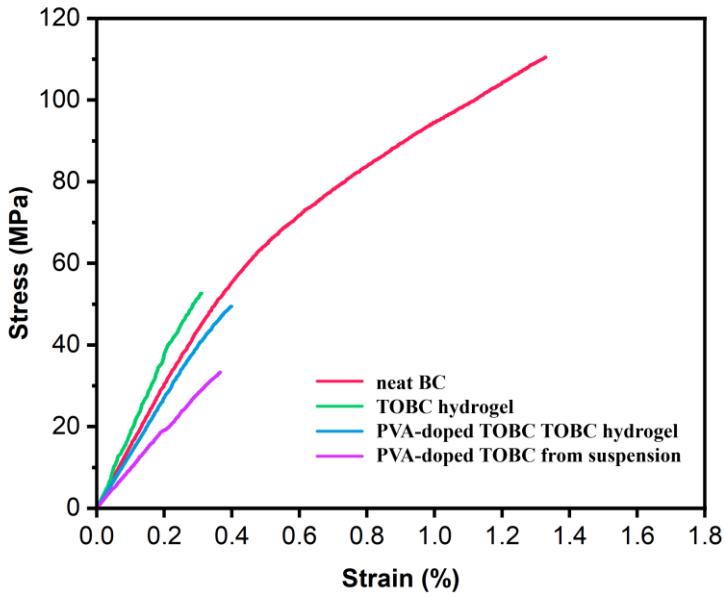


Figure 5-3: Representative tensile stress-strain curves of neat BC, TOBC film from TOBC hydrogel, PVA-doped TOBC film from TOBC hydrogel, and PVA-doped TOBC film from TOBC suspension.

The tensile modulus and strength of PVA-doped TOBC film made from TOBC hydrogel was found to be similar to the self-standing TOBC film made directly from the TOBC hydrogel. However, the tensile properties of the PVA-doped TOBC film made from TOBC suspension were lower. The tensile modulus of this film was only 10 GPa and the tensile strength of only 33 MPa. This decrease in tensile properties is hypothesised to be due to the use of a homogenous BC suspension as the feedstock. In such a suspension, the pseudo continuous network of BC nanofibrils in the BC pellicle is lost, leading to poorer mechanical performance.

5.4.3 Transmittance of (PVA-doped) TOBC films

Neat BC nanopaper, TOBC film made from TOBC hydrogel and the "wavy" TOBC film made from TOBC suspension without PVA doping were not transparent (Figure 5-4a-c) whilst the PVA-doped TOBC films were found to be optically transparent (Figure 5-4d-e). The transmittance is inversely related to the haze. To compare, the transmittance of the pure PVA film is reported as 88.920 % (Table 5-2) at 700 nm [104]. Light transmittance measurements summarised in Figure 5-5a showed that within neat BC has a light transmittance of 3%-23% between 300-700 nm, TOBC film made from TOBC hydrogel has a light transmittance of 2%-37% between 300-700 nm, PVA-doped TOBC film made from TOBC hydrogel has a light transmittance of 35%-74% between 300-700 nm and PVA-doped TOBC film made from TOBC suspension has a light transmittance of 63%-81% between 300-700 nm. Finally, the light transmission of the PVA-doped TOBC films decreased by less than 10% compared to the neat PVA films. This shows a minimal transmission degradation due to the nanofiber network in the PVA-doped TOBC films.

Once the TOBC was doped with PVA, the porosity decreased (see Table 5-1) and the air/fiber interfaces were replaced with PVA/fiber interfaces. This interfacial change enhances the light transmittance of the PVA-doped TOBC films. This is because the amount of light reflection at the interface is highly dependent on the refractive index of the two materials forming the interface. Generally, multiphase materials suffer from reduced transparency due to increased light scattering due to differences in the refractive indices of the materials that make up the composites. The formula for this relationship is given below:

$$r = \left(\frac{n_R - n_F}{n_R + n_F}\right)^2 \tag{5.2}$$

Where r is the reflective coefficient, and n_R and n_F are refractive indices (RIs) of the resin and fiber, respectively. Thus, the reflective coefficient increases as the difference between the RIs of the resin and fiber increase. A greater amount of light is reflected as a result. The RI of air, cellulose nanofiber, PVA and TOCN films from TOBC hydrogel are 1 [103], 1.62 [105],1.52 [103] and 1.55 [1, 106] at room temperature respectively. As such, PVA-doped TOBC films have a substantially higher light transmittance than either the neat BC nanopaper or the TOBC film made directly from TOBC hydrogel without PVA doping. It is further hypothesised that due to the variances in their refractive indices and the potential for some unfilled capillaries [103], the loss of transparency for the PVA-doped TOBC films is minimal (less than 10%). The PVA doped into the TOBC film flows from the two ends of a fiber capillary, trapping air. The air is trapped because of the layered fiber structure and the existence of non-exposed nanofibrils of TOBC film. Therefore, unfilled capillaries exist in the resulting PVA-doped TOBC film. When light is transmitted through these films, light reflects and refracts along the fiber/PVA interfaces and the unfilled capillary interfaces. Therefore, more light loss is expected as compared to fully filled pore-free composite films.



Figure 5-4: The visual appearance of (a) BC nanopaper; (b) TOBC film from TOBC hydrogel; (c) TOBC film from TOBC suspension; (d) PVA-doped TOBC film from TOBC hydrogel; (e) PVA-doped TOBC film from TOBC suspension.

In addition, the transmittance of PVA-doped TOBC film made from TOBC hydrogel is 10% lower than that of PVA-doped TOBC film made from TOBC suspension. This may be due to the difference in the carboxylate content of TOBC hydrogel *versus* TOBC made from BC suspension. Both the carboxylate groups of the TOBC and the hydroxyl groups of PVA interacts through hydrogen bonding.

Hence, the higher carboxylate content TOBC made from BC suspension is postulated to have more intimate contact, resulting in fewer light scattering events in the corresponding film.

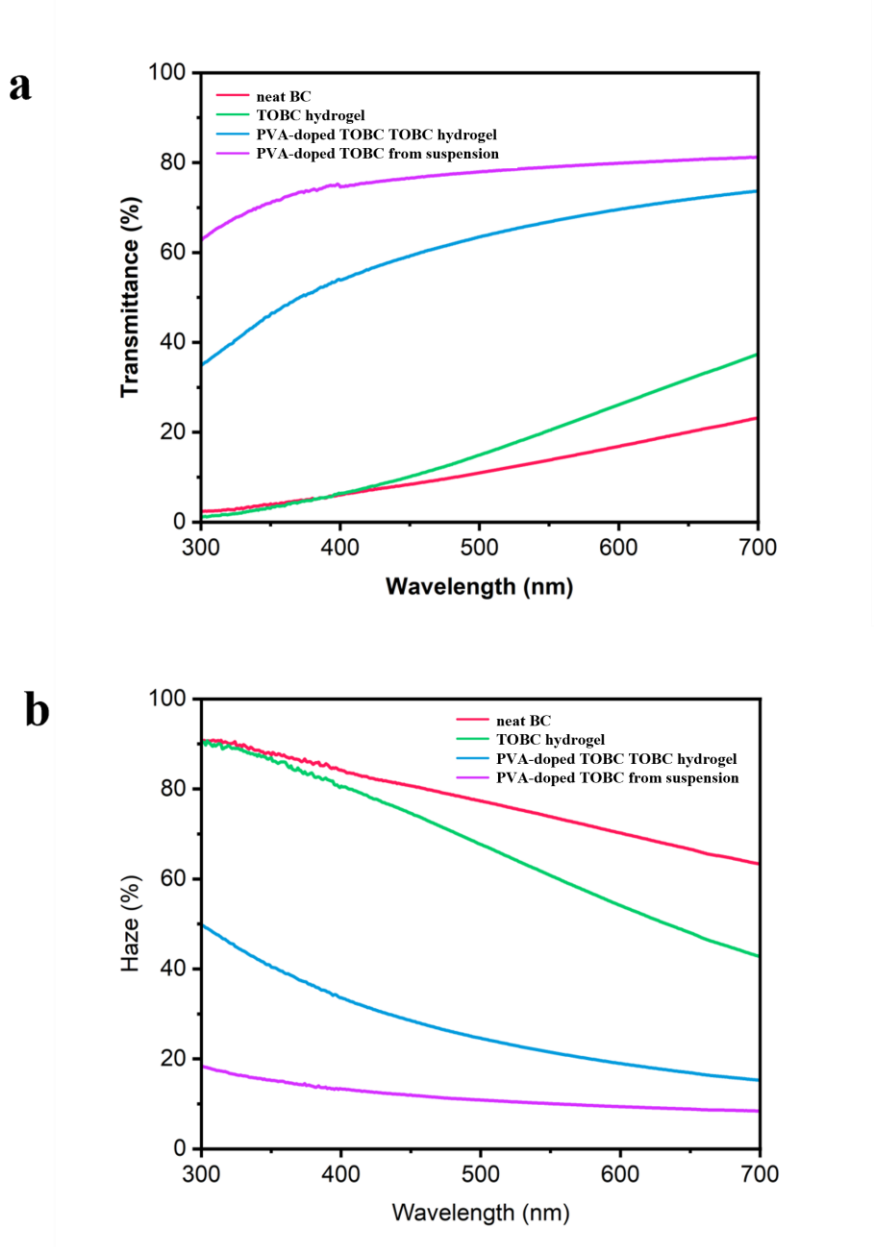


Figure 5-5: (a) transmittance and (b) haze of the BC nanopaper; TOBC film from TOBC hydrogel; PVA-doped TOBC film from TOBC hydrogel and PVA-doped TOBC film from TOBC suspension as a function of wavelength.

5.5 Conclusions

This work further demonstrated that the simple method to fabricate robust and water stable TEMPO-oxidised BC hydrogels and TOCN films derived from dried and well-consolidated BC nanopaper in chapter 3 is also effective even from a 20% initial grammage of BC nanopaper. TOBC films made from TOBC hydrogel and PVA-doped TOBC films made from TOBC hydrogel could be fabricated with simple and efficient method, while TOBC films made from TOBC hydrogel suspension were hard to make and PVA-doped TOBC films made from TOBC suspension needed a time-consuming evaporation step. In addition, films made by well-consolidated BC nanopapers had better mechanical performance than that of blending BC nanopapers with just a slight loss of transparency. The relatively lower transmittance of the PVA-doped TOBC film made from TOBC hydrogel is due to light scattering by unfilled pores/capillaries.

Impregnating low light transmittance TEMPO oxidised BC with PVA creates films with high visible light transmittance. Transmittances as high as 80% was achieved in the PVA-doped TOBC films made from TOBC suspension with PVA contents as low as 25 wt%, this contrasts favourably with other PVA films that require PVA contents in 40—75 wt% range [32, 107]. At high fiber contents of ~75 wt%, the Young's modulus increased more than 1200%. This is largely due to the intimate contact and strong interfacial adhesion between the ultrafine TEMPO-oxidised BC fibers and the PVA. From these results, this chapter finds that the self-standing TEMPO-oxidised nanocellulose film produced from press-drying a TOBC hydrogel perform better mechanical properties than those made from the vacuum filtration of a suspension of TEMPO-oxidised nanocellulose.

Chapter 6 – Conclusions and future work

The investigations discussed in this thesis looked into how BC nanopapers were affected by TEMPO-mediated oxidation. Based on the TEMPO-mediated oxidation of dried and well-consolidated BC nanopaper, a straightforward approach for fabricating strong and water-stable TOCN hydrogels was presented in Chapter 3. This work discovered that the TEMPO-mediated oxidation of BC nanopaper was kinetically limited initially. Tensile strength and strain-at-failure are reduced because of TEMPO-mediated oxidation on BC nanopapers, which also increases tensile modulus. This is a result of the existence of carboxyl functionalities, which enhance hydrogen bonds inside the TEMPO-oxidised BC films. Chapter 4 demonstrated that BC nanopaper that had been heat-pressed at a lower temperature from pristine BC pellicle was more vulnerable to TEMPO-mediated oxidation. Several hypotheses are discussed, including the impact of any residual moisture in the BC nanopaper, the capillary force's intensity during the production of the BC nanopaper, the exposed BC nanofibril surface area, and the strength of interfibril bonding. Chapter 5 compared the properties of films made by well-consolidated BC nanopapers and blending BC nanopapers. The films made by well-consolidated BC nanopapers could be manufactured with a more efficient method and had better mechanical performance than that of blending BC nanopapers. Additionally, an optically transparent PVA-doped TOBC film was successfully produced with great promise.

The first part of future work is to investigate how heat-pressing temperature affect the strength inter-fibril bonding of BC nanopaper. Further engineering and quantification of the structure changed inside BC nanopapers with press-drying will

be worth to investigate. Since current research reported that there was no influence of drying temperature, final drying time and drying constraint history on the tensile properties of paper [108, 109]. However, it was also stated that the rate and temperature of drying can influence the overall extent of hornification and rapid drying results in a higher degree of honification than slow drying in moderate environment [110]. Significantly, these deliberations are grounded in the realm of paper drying, and it is plausible that investigations into the impact of drying conditions on bacterial cellulose have not yet been undertaken—a prospect that holds great promise and scholarly value.

Scanning Electron Microscopy (SEM) is valuable for studying fracture surfaces of cellulose-based materials, offering insights into fracture behavior and microstructural details. It's been used to examine fracture surface morphology in cellulose composites, analyse crack initiation, and provide detailed imaging of fracture surfaces, aiding in understanding the material's fracture mechanisms and properties [111-113]. Hence, SEM could be more instrumental in future work on cellulose-based materials for fracture surface analysis and other characteristic measurements.

Due to the explosive growth of technologies such as computer and smartphone displays, mechanically reinforced, optically functional materials have garnered increasing interest. The lack of light scattering in nanocomposite materials whose components' thicknesses are less than one-tenth of the wavelength of a typical photon of light makes them suitable for a range of optical applications [114, 115]. The results from this thesis exactly find that TEMPO-oxidised fibers are promising reinforcing fibers for composite materials with high fiber content and high light

transmittance. It is a possible contender for use in flexible displays, precision optical device components, train and vehicle windows, transparent armour, and other applications. Therefore, the second part of future work should focus on optimizing optically transparent composites reinforced with TEMPO oxidised bacterial cellulose nanofibers to further enhance their performances.

Future work should be using TOBC(s) as reinforcement in PVA, acrylic and epoxy respectively. Because fibers could give optically functional materials the needed mechanical reinforcement, the use of electrospun nylon-4,6 nanofiber reinforcement has been researched. At a 3.9% fiber content, an optically clear composite was produced [107]. The challenge, therefore, is to increase the fiber-volume of composite without compromising transparency. A transparent (80% transmission at wavelength range of 500-800 nm) composite reinforced using bacterial nanofibers was reported by H. Yano et al.[32] with 60% fiber content, the composite is optically transparent. It is because the hydroxyl groups in BC help to have a good interfacial adhesion with polymer resin. Hence, TOBC should also have improvements on reinforcement polymer composite or even better than that of BC due to its advantages illustrated in this thesis.

In conclusion, future research endeavors ought to center their attention on the refinement of oxidised processing parameters, including but not limited to the concentration of chemicals, reaction time and temperature. And more characteristics of TOBC should be determined to help optimal the performance of itself for further applications.

References

[1] A. Isogai, T. Saito, H. Fukuzumi, TEMPO-oxidized cellulose nanofibers, Nanoscale 3(1) (2011) 71-85.

[2] T. Saito, A. Isogai, TEMPO-mediated oxidation of native cellulose. The effect of oxidation conditions on chemical and crystal structures of the water-insoluble fractions, Biomacromolecules 5(5) (2004) 1983-9.

[3] T. Saito, S. Kimura, Y. Nishiyama, A. Isogai, Cellulose nanofibers prepared by TEMPO-mediated oxidation of native cellulose, Biomacromolecules 8(8) (2007) 2485-91.

[4] H. Fukuzumi, T. Saito, T. Iwata, Y. Kumamoto, A. Isogai, Transparent and high gas barrier films of cellulose nanofibers prepared by TEMPO-mediated oxidation, Biomacromolecules 10(1) (2009) 162-5.

[5] S.S. Ahankari, A.R. Subhedar, S.S. Bhadauria, A. Dufresne, Nanocellulose in food packaging: A review, Carbohydr Polym 255 (2021) 117479.

[6] R. Curvello, V.S. Raghuwanshi, G. Garnier, Engineering nanocellulose hydrogels for biomedical applications, Adv Colloid Interface Sci 267 (2019) 47-61.

[7] K. Heise, E. Kontturi, Y. Allahverdiyeva, T. Tammelin, M.B. Linder, Nonappa, O. Ikkala, Nanocellulose: Recent Fundamental Advances and Emerging Biological and Biomimicking Applications, Adv Mater 33(3) (2021) e2004349.

[8] S. Liu, Z.X. Low, Z. Xie, H. Wang, TEMPO‐Oxidized Cellulose Nanofibers: A Renewable Nanomaterial for Environmental and Energy Applications, Advanced Materials Technologies 6(7) (2021).

[9] A. Mautner, Nanocellulose water treatment membranes and filters: a review, Polymer International 69(9) (2020) 741-751.

[10] T. Hänninen, A. Isogai, Oxidative Chemistry in Preparation and Modification on Cellulose Nanoparticles, Nanocellulose and Sustainability, CRC Press2018, pp. 45-65.

[11] M. Hirota, N. Tamura, T. Saito, A. Isogai, Oxidation of regenerated cellulose with NaClO2 catalyzed by TEMPO and NaClO under acid-neutral conditions, Carbohydrate Polymers 78(2) (2009) 330-335.

[12] A. Isogai, Y. Kato, Preparation of Polyuronic Acid from Cellulose by TEMPO-mediated Oxidation, Cellulose 5(3) (1998) 153-164.

[13] B. Sun, C. Gu, J. Ma, B. Liang, Kinetic study on TEMPO-mediated selective oxidation of regenerated cellulose, Cellulose 12(1) (2005) 59-66.

[14] T. Isogai, M. Yanagisawa, A. Isogai, Degrees of polymerization (DP) and DP distribution of cellouronic acids prepared from alkali-treated celluloses and ball-milled native celluloses by TEMPO-mediated oxidation, Cellulose 16(1) (2009) 117-127.

[15] M. Florea, H. Hagemann, G. Santosa, J. Abbott, C.N. Micklem, X. Spencer-Milnes, L. de Arroyo Garcia, D. Paschou, C. Lazenbatt, D. Kong, H. Chughtai, K. Jensen, P.S. Freemont, R. Kitney, B. Reeve, T. Ellis, Engineering control of bacterial cellulose production using a genetic toolkit and a new cellulose-producing strain, Proc Natl Acad Sci U S A 113(24) (2016) E3431-40.

[16] C. Tokoh, K. Takabe, M. Fujita, H. Saiki, Cellulose Synthesized by Acetobacter Xylinum in the Presence of Acetyl Glucomannan, Cellulose 5(4) (1998) 249-261.

[17] D. Wloch, N. Herrera, K.-Y. Lee, Optically transparent laminated acrylic composites reinforced with mercerised bacterial cellulose nanopaper, Composites Part A: Applied Science and Manufacturing 172 (2023) 107583.

[18] J. Sugiyama, J. Persson, H. Chanzy, Combined infrared and electron diffraction study of the polymorphism of native celluloses, Macromolecules 24(9) (1991) 2461-2466.

[19] S.H. Jun, S.G. Park, N.G. Kang, One-Pot Method of Synthesizing TEMPO-Oxidized Bacterial Cellulose Nanofibers Using Immobilized TEMPO for Skincare Applications, Polymers (Basel) 11(6) (2019).

[20] T.T. Nge, M. Nogi, H. Yano, J. Sugiyama, Microstructure and mechanical properties of bacterial cellulose/chitosan porous scaffold, Cellulose 17(2) (2010) 349-363.

[21] C.-N. Wu, K.-C. Cheng, Strong, thermal-stable, flexible, and transparent films by self-assembled TEMPO-oxidized bacterial cellulose nanofibers, Cellulose 24(1) (2017) 269-283.

[22] A. Payen, Mémoire sur la composition du tissu propre des plantes et du ligneux, Comptes rendus 7(lu 17 décembre 1838) (1838) 1052-1056.

[23] I. Siró, D. Plackett, Microfibrillated cellulose and new nanocomposite materials: a review, Cellulose 17(3) (2010) 459-494.

[24] R.J. Moon, A. Martini, J. Nairn, J. Simonsen, J. Youngblood, Cellulose nanomaterials review: structure, properties and nanocomposites, Chemical Society Reviews 40(7) (2011) 3941-3994.

[25] J.I. Morán, V.A. Alvarez, V.P. Cyras, A. Vázquez, Extraction of cellulose and preparation of nanocellulose from sisal fibers, Cellulose 15 (2008) 149-159.

[26] J.H. Lee, B. Subhadra, Y.J. Son, D.H. Kim, H.S. Park, J.M. Kim, S.H. Koo, M.H. Oh, H.J. Kim, C.H. Choi, Phylogenetic group distributions, virulence factors and antimicrobial resistance properties of uropathogenic Escherichia coli strains isolated from patients with urinary tract infections in South Korea, Lett Appl Microbiol 62(1) (2016) 84-90.

[27] D. Dai, M. Fan, P. Collins, Fabrication of nanocelluloses from hemp fibers and their application for the reinforcement of hemp fibers, Industrial Crops and Products 44 (2013) 192-199.

[28] A. Hirai, M. Tsuji, H. Yamamoto, F. Horii, In Situ Crystallization of Bacterial Cellulose III. Influences of Different Polymeric Additives on the Formation of Microfibrils as Revealed by Transmission Electron Microscopy, Cellulose 5(3) (1998) 201-213.

[29] C. Tokoh, K.J. Takabe, M. Fujita, Cellulose synthesized by Acetobacter xylinum in the presence of plant cell wall polysaccharides, Cellulose 9(1) (2002) 65-74.

[30] M. Nogi, K. Handa, A.N. Nakagaito, H. Yano, Optically transparent bionanofiber composites with low sensitivity to refractive index of the polymer matrix, Applied Physics Letters 87(24) (2005).

[31] A.N. Nakagaito, S. Iwamoto, H. Yano, Bacterial cellulose: the ultimate nano-scalar cellulose morphology for the production of high-strength composites, Applied Physics A 80(1) (2005) 93-97.

[32] H. Yano, J. Sugiyama, A.N. Nakagaito, M. Nogi, T. Matsuura, M. Hikita, K. Handa, Optically Transparent Composites Reinforced with Networks of Bacterial Nanofibers, Advanced Materials 17(2) (2005) 153-155.

[33] M. Iguchi, S. Yamanaka, A. Budhiono, Bacterial cellulose—a masterpiece of nature's arts, Journal of Materials Science 35(2) (2000) 261-270.

[34] S. Kalia, A. Dufresne, B.M. Cherian, B.S. Kaith, L. Avérous, J. Njuguna, E. Nassiopoulos, Cellulose-based bio-and nanocomposites: a review, International journal of polymer science 2011 (2011).

[35] A.C. O'sullivan, Cellulose: the structure slowly unravels, Cellulose 4 (1997) 173-207.

[36] A. Ishikawa, T. Okano, J. Sugiyama, Fine structure and tensile properties of ramie fibres in the crystalline form of cellulose I, II, IIII and IVI, Polymer 38(2) (1997) 463-468.

[37] S. Swingler, A. Gupta, H. Gibson, M. Kowalczuk, W. Heaselgrave, I. Radecka, Recent Advances and Applications of Bacterial Cellulose in Biomedicine, Polymers 13(3) (2021) 412.

[38] S.M.A. Ojagh, F. Vahabzadeh, N. Fallah, T.G.M. van de Ven, E. Hamzehpoor, S. Cranmer-Smith, X. Lan, Hairy bacterial nanocellulose: preparation and bioconjugation with an antibacterial agent, Cellulose (2023).

[39] R.M. Brown Jr, J. Willison, C.L. Richardson, Cellulose biosynthesis in Acetobacter xylinum: visualization of the site of synthesis and direct measurement of the in vivo process, Proceedings of the National Academy of Sciences 73(12) (1976) 4565-4569.

[40] F. Rol, B. Karakashov, O. Nechyporchuk, M. Terrien, V. Meyer, A. Dufresne, M.N. Belgacem, J. Bras, Pilot-Scale Twin Screw Extrusion and Chemical Pretreatment as an Energy-Efficient Method for the Production of Nanofibrillated

Cellulose at High Solid Content, ACS Sustainable Chemistry & Engineering 5(8) (2017) 6524-6531.

[41] A. Isogai, Development of completely dispersed cellulose nanofibers, Proc Jpn Acad Ser B Phys Biol Sci 94(4) (2018) 161-179.

[42] D. da Silva Perez, S. Montanari, M.R. Vignon, TEMPO-Mediated Oxidation of Cellulose III, Biomacromolecules 4(5) (2003) 1417-1425.

[43] T. Isogai, T. Saito, A. Isogai, TEMPO Electromediated Oxidation of Some Polysaccharides Including Regenerated Cellulose Fiber, Biomacromolecules 11(6) (2010) 1593-1599.

[44] V.M. Marx, Viskosimetrische molekulargewichtsbestimmung von cellulose in kupfer-äethylendiamin, Die Makromolekulare Chemie 16(1) (1955) 157-176.

[45] Y. Okita, T. Saito, A. Isogai, Entire Surface Oxidation of Various Cellulose Microfibrils by TEMPO-Mediated Oxidation, Biomacromolecules 11(6) (2010) 1696-1700.

[46] Y. Okita, T. Saito, A. Isogai, TEMPO-mediated oxidation of softwood thermomechanical pulp, hfsg 63(5) (2009) 529-535.

[47] T. Saito, M. Hirota, N. Tamura, S. Kimura, H. Fukuzumi, L. Heux, A. Isogai, Individualization of nano-sized plant cellulose fibrils by direct surface carboxylation using TEMPO catalyst under neutral conditions, Biomacromolecules 10(7) (2009) 1992-6.

[48] L. Mao, P. Ma, K. Law, C. Daneault, F. Brouillette, Studies on Kinetics and Reuse of Spent Liquor in the TEMPO-Mediated Selective Oxidation of Mechanical Pulp, Industrial & Engineering Chemistry Research 49(1) (2010) 113-116.

[49] H. Luo, G. Xiong, D. Hu, K. Ren, F. Yao, Y. Zhu, C. Gao, Y. Wan, Characterization of TEMPO-oxidized bacterial cellulose scaffolds for tissue engineering applications, Materials Chemistry and Physics 143(1) (2013) 373-379.

[50] Y. Jia, X. Zhai, W. Fu, Y. Liu, F. Li, C. Zhong, Surfactant-free emulsions stabilized by tempo-oxidized bacterial cellulose, Carbohydrate Polymers 151 (2016) 907-915.

[51] C.N. Wu, S.C. Fuh, S.P. Lin, Y.Y. Lin, H.Y. Chen, J.M. Liu, K.C. Cheng, TEMPO-Oxidized Bacterial Cellulose Pellicle with Silver Nanoparticles for Wound Dressing, Biomacromolecules 19(2) (2018) 544-554.

[52] S.-S. Kim, J.-H. Jeon, H.-I. Kim, C.D. Kee, I.-K. Oh, High-Fidelity Bioelectronic Muscular Actuator Based on Graphene-Mediated and TEMPO-Oxidized Bacterial Cellulose, Advanced Functional Materials 25(23) (2015) 3560-3570.

[53] A. Santmarti, J.W. Teh, K.Y. Lee, Transparent Poly(methyl methacrylate) Composites Based on Bacterial Cellulose Nanofiber Networks with Improved Fracture Resistance and Impact Strength, ACS Omega 4(6) (2019) 9896-9903.

[54] S. Takaichi, T. Saito, R. Tanaka, A. Isogai, Improvement of nanodispersibility of oven-dried TEMPO-oxidized celluloses in water, Cellulose 21(6) (2014) 4093-4103.

[55] S. Fujisawa, Y. Okita, H. Fukuzumi, T. Saito, A. Isogai, Preparation and characterization of TEMPO-oxidized cellulose nanofibril films with free carboxyl groups, Carbohydrate Polymers 84(1) (2011) 579-583.

[56] S. Katz, R.P. Beatson, The determination of strong and weak acidic groups in sulfite pulps, Svensk papperstidning 87(6) (1984) 48-53.

[57] A. Santmarti, H. Zhang, T. Lappalainen, K.-Y. Lee, Cellulose nanocomposites reinforced with bacterial cellulose sheets prepared from pristine and disintegrated pellicle, Composites Part A: Applied Science and Manufacturing 130 (2020) 105766.

[58] K.-Y. Lee, H. Qian, F.H. Tay, J.J. Blaker, S.G. Kazarian, A. Bismarck, Bacterial cellulose as source for activated nanosized carbon for electric double layer capacitors, Journal of Materials Science 48(1) (2013) 367-376.

[59] K.-Y. Lee, A. Bismarck, Susceptibility of never-dried and freeze-dried bacterial cellulose towards esterification with organic acid, Cellulose 19(3) (2012) 891-900.

[60] J.M.B. Fernandes Diniz, M.H. Gil, J.A.A.M. Castro, Hornification—its origin and interpretation in wood pulps, Wood Science and Technology 37(6) (2004) 489-494.

[61] O. Nechyporchuk, M.N. Belgacem, J. Bras, Production of cellulose nanofibrils: A review of recent advances, Industrial Crops and Products 93 (2016) 2-25.

[62] K.-Y. Lee, F. Quero, J.J. Blaker, C.A.S. Hill, S.J. Eichhorn, A. Bismarck, Surface only modification of bacterial cellulose nanofibres with organic acids, Cellulose 18(3) (2011) 595-605.

[63] K.S. Kontturi, K.-Y. Lee, M.P. Jones, W.W. Sampson, A. Bismarck, E. Kontturi, Influence of biological origin on the tensile properties of cellulose nanopapers, Cellulose 28(10) (2021) 6619-6628.

[64] M. Hervy, F. Bock, K.-Y. Lee, Thinner and better: (Ultra-)low grammage bacterial cellulose nanopaper-reinforced polylactide composite laminates, Composites Science and Technology 167 (2018) 126-133.

[65] M. Hervy, J.J. Blaker, A.L. Braz, K.-Y. Lee, Mechanical response of multi-layer bacterial cellulose nanopaper reinforced polylactide laminated composites, Composites Part A: Applied Science and Manufacturing 107 (2018) 155-163.

[66] S. Gea, F.G. Torres, O.P. Troncoso, C.T. Reynolds, F. Vilasecca, M. Iguchi, T. Peijs, Biocomposites Based on Bacterial Cellulose and Apple and Radish Pulp, International Polymer Processing 22(5) (2007) 497-501.

[67] F. Quero, S.J. Eichhorn, M. Nogi, H. Yano, K.-Y. Lee, A. Bismarck, Interfaces in Cross-Linked and Grafted Bacterial Cellulose/Poly(Lactic Acid) Resin Composites, Journal of Polymers and the Environment 20(4) (2012) 916-925.

[68] A.N. Papadopoulos, C.A.S. Hill, A. Gkaraveli, Determination of surface area and pore volume of holocellulose and chemically modified wood flour using the nitrogen adsorption technique, Holz als Roh- und Werkstoff 61(6) (2003) 453-456.

[69] L.A. Goetz, J.R. Sladky, A.J. Ragauskas, Preparation of microwave-assisted polymer-grafted softwood kraft pulp fibers. Enhanced water absorbency, Journal of Applied Polymer Science 119(1) (2011) 387-395.

[70] J. Laine, T. Lindstrom, C. Brernberg, G. Glad-Nordrnark, Studies on topochemical modification of cellulosic fibres, Part 4. Toposelectivity of carboxymethylation and its effects on the swelling of fibres 18(3) (2003) 316-324.

[71] R.M. Brown, Jr., J.H. Willison, C.L. Richardson, Cellulose biosynthesis in Acetobacter xylinum: visualization of the site of synthesis and direct measurement of the in vivo process, The Proceedings of the National Academy of Sciences 73(12) (1976) 4565-9.

[72] S. Yamanaka, K. Watanabe, N. Kitamura, M. Iguchi, S. Mitsuhashi, Y. Nishi, M. Uryu, The structure and mechanical properties of sheets prepared from bacterial cellulose, Journal of Materials Science 24(9) (1989) 3141-3145.

[73] S.-S. Wang, Y.-H. Han, Y.-X. Ye, X.-X. Shi, P. Xiang, D.-L. Chen, M. Li, Physicochemical characterization of high-quality bacterial cellulose produced by Komagataeibacter sp. strain W1 and identification of the associated genes in bacterial cellulose production, RSC Advances 7(71) (2017) 45145-45155.

[74] T. Saito, I. Shibata, A. Isogai, N. Suguri, N. Sumikawa, Distribution of carboxylate groups introduced into cotton linters by the TEMPO-mediated oxidation, Carbohydrate Polymers 61(4) (2005) 414-419.

[75] A.D. French, Idealized powder diffraction patterns for cellulose polymorphs, Cellulose 21(2) (2014) 885-896.

[76] A. Mautner, K.-Y. Lee, T. Tammelin, A.P. Mathew, A.J. Nedoma, K. Li, A. Bismarck, Cellulose nanopapers as tight aqueous ultra-filtration membranes, Reactive and Functional Polymers 86 (2015) 209-214.

[77] M. Wakabayashi, S. Fujisawa, T. Saito, A. Isogai, Nanocellulose Film Properties Tunable by Controlling Degree of Fibrillation of TEMPO-Oxidized Cellulose, Front Chem 8 (2020) 37.

[78] J.M. Indias, R. Guerrero, M. Scarpa, P. Bettotti, Functional nanocellulose films as fluorescent media, SPIE2018.

[79] A. Mautner, K.Y. Lee, P. Lahtinen, M. Hakalahti, T. Tammelin, K. Li, A. Bismarck, Nanopapers for organic solvent nanofiltration, Chemical Communications 50(43) (2014) 5778-5781.

[80] H. Fukuzumi, T. Saito, A. Isogai, Influence of TEMPO-oxidized cellulose nanofibril length on film properties, Carbohydr Polym 93(1) (2013) 172-7.

[81] G. Rodionova, Ø. Eriksen, Ø. Gregersen, TEMPO-oxidized cellulose nanofiber films: effect of surface morphology on water resistance, Cellulose 19(4) (2012) 1115-1123.

[82] K.Y. Yang, D. Wloch, K.-Y. Lee, TEMPO-oxidised nanocellulose hydrogels and self-standing films derived from bacterial cellulose nanopaper, RSC Advances 11(45) (2021) 28352-28360.

[83] M. Wohlert, T. Benselfelt, L. Wågberg, I. Furó, L.A. Berglund, J. Wohlert, Cellulose and the role of hydrogen bonds: not in charge of everything, Cellulose 29(1) (2022) 1-23.

[84] U. Hirn, R. Schennach, Comprehensive analysis of individual pulp fiber bonds quantifies the mechanisms of fiber bonding in paper, Scientific Reports 5(1) (2015) 10503.

[85] M. Henriksson, L.A. Berglund, P. Isaksson, T. Lindström, T. Nishino, Cellulose Nanopaper Structures of High Toughness, Biomacromolecules 9(6) (2008) 1579-1585.

[86] G.J. Gittens, Variation of surface tension of water with temperature, Journal of Colloid and Interface Science 30(3) (1969) 406-412.

[87] N.B. Vargaftik, B.N. Volkov, L.D. Voljak, International Tables of the Surface Tension of Water, Journal of Physical and Chemical Reference Data 12(3) (1983) 817-820.

[88] J. Kalová, R. Mareš, The temperature dependence of the surface tension of water, AIP Conference Proceedings 2047(1) (2018) 020007.

[89] M. Thommes, K. Kaneko, A.V. Neimark, J.P. Olivier, F. Rodriguez-Reinoso, J. Rouquerol, K.S.W. Sing, Physisorption of gases, with special reference to the evaluation of surface area and pore size distribution (IUPAC Technical Report), Pure and Applied Chemistry 87(9-10) (2015) 1051-1069.

[90] S. Brunauer, P.H. Emmett, E. Teller, Adsorption of Gases in Multimolecular Layers, Journal of the American Chemical Society 60(2) (1938) 309-319.

[91] A. Kondor, A. Santmarti, A. Mautner, D. Williams, A. Bismarck, K.-Y. Lee, On the BET Surface Area of Nanocellulose Determined Using Volumetric, Gravimetric and Chromatographic Adsorption Methods, Frontiers in Chemical Engineering 3 (2021).

[92] J. Rouquerol, P. Llewellyn, F. Rouquerol, Is the BET Equation Applicable to Microporous Adsorbents?, Studies in Surface Science and Catalysis 160 (2007) 49-56.

[93] N. Herrera, J. Li, K.-Y. Lee, Tough poly(ethylene glycol)-sized bacterial cellulose sheet for high impact strength laminated acrylic composites, Composites Part A: Applied Science and Manufacturing 156 (2022) 106845.

[94] D. Page, A theory for the tensile strength of paper, Tappi 52 (1969) 674-681.

[95] D. Page, A theory for the elastic modulus of paper, British Journal of Applied Physics 16(2) (1965) 253.

[96] D.E. Giacomozzi, O. Joutsimo, Drying temperature and hornification of industrial never-dried pinus radiata pulps. 1. Strength, optical, and water holding properties, BioResources 10(3) (2015) 5791-5808.

[97] T. Wahlström, The Influence of Drying Time and Temperature Revisited, Miami University Oxford, OH, USA, 2006.

[98] L. Salmén, J.S. Stevanic, Effect of drying conditions on cellulose microfibril aggregation and “hornification”, Cellulose 25 (2018) 6333-6344.

[99] D. Rahmadiawan, H. Abral, M.K. Ilham, P. Puspitasari, R.A. Nabawi, S.-C. Shi, E. Sugiarti, A.N. Muslimin, D. Chandra, R.A. Ilyas, R. Zainul, Enhanced UV blocking, tensile and thermal properties of bendable TEMPO-oxidized bacterial cellulose powder-based films immersed in PVA/Uncaria gambir/ZnO solution, Journal of Materials Research and Technology 26 (2023) 5566-5575.

[100] K. Wang, R. Hazra, Q. Ma, L. Jiang, Z. Liu, Y. Zhang, S. Wang, G. Han, Multifunctional silk fibroin/PVA bio-nanocomposite films containing TEMPO-oxidized bacterial cellulose nanofibers and silver nanoparticles, Cellulose 29 (2022) 1-20.

[101] M. Ozkan, M. Borghei, A. Karakoc, O.J. Rojas, J. Paltakari, Films based on crosslinked TEMPO-oxidized cellulose and predictive analysis via machine learning, Sci Rep 8(1) (2018) 4748.

[102] S.-Y. Lee, D.J. Mohan, I.-A. Kang, G.-H. Doh, S. Lee, S.O. Han, Nanocellulose reinforced PVA composite films: Effects of acid treatment and filler loading, Fibers and Polymers 10(1) (2009) 77-82.

[103] C. Tang, H. Liu, Cellulose nanofiber reinforced poly(vinyl alcohol) composite film with high visible light transmittance, Composites Part A: Applied Science and Manufacturing 39(10) (2008) 1638-1643.

[104] I.S. Yahia, S.M.A.S. Keshk, Preparation and characterization of PVA/Congo red polymeric composite films for a wide scale laser filters, Optics & Laser Technology 90 (2017) 197-200.

[105] J. Brandrup, E.H. Immergut, E.A. Grulke, A. Abe, D.R. Bloch, Polymer handbook, Wiley New York1999.

[106] M. Nogi, H. Yano, Optically transparent nanofiber sheets by deposition of transparent materials: A concept for a roll-to-roll processing, Applied Physics Letters 94(23) (2009) 233117.

[107] M.M. Bergshoef, G.J. Vancso, Transparent Nanocomposites with Ultrathin, Electrospun Nylon-4,6 Fiber Reinforcement, Advanced Materials 11(16) (1999) 1362-1365.

[108] J. Stone, A. Scallan, The Influence of Drying on the Pore Structure of the Cell Wall, Pulp and Paper Research Institute of Canada1965.

[109] P. Mäkelä, Effect of drying conditions on the tensile properties of paper, Proceedings of 14th Pulp and Paper Fundamental Research Symposium, Oxford, 2009, pp. 1079-1094.

[110] E. Letková, M. Letko, M. Vrška, Influence of recycling and temperature on the swelling ability of paper, Chemical Papers 65(6) (2011) 822-828.

[111] H.-S. Yang, D.J. Gardner, J.W. Nader, Morphological properties of impact fracture surfaces and essential work of fracture analysis of cellulose nanofibril-filled polypropylene composites, Journal of Applied Polymer Science 128(5) (2013) 3064-3076.

[112] H. Gao, T. Qiang, Fracture Surface Morphology and Impact Strength of Cellulose/PLA Composites, Materials (Basel) 10(6) (2017).

[113] L. Afolabi, P. Megat-Yusoff, M. Hamizol, Fabrication and Characterization of Cellulose Microfibrils from Pandanus tectorius(Screw Pine) for Polymer

Composite Application, Research & Reviews Journal of Material Sciences 06 (2018).

[114] B.M. Novak, Hybrid Nanocomposite Materials—between inorganic glasses and organic polymers, Advanced Materials 5(6) (1993) 422-433.

[115] L.L. Beecroft, C.K. Ober, Nanocomposite Materials for Optical Applications, Chemistry of Materials 9(6) (1997) 1302-1317.